Chapter 4

Docetaxel and erlotinib–loaded folic acid functionalized solid lipid nanoparticles

4. Introduction of solid lipid nanoparticles

Solid lipid nanoparticles (SLNs) represent a class of lipid–based nano–delivery systems that emerged in the early 1990s. Their development aimed to capitalize on the advantages of previous colloidal carriers, such as liposomes, emulsions, and polymeric nanoparticles, while mitigating their limitations. SLNs are heterogeneous systems consisting of a solid lipid inner phase dispersed in an aqueous surfactant solution. These carriers exhibit biocompatibility and biodegradability due to their composition from physiological lipids. Notably, SLNs can entrap a substantial payload of lipophilic and hydrophilic drug molecules. Furthermore, they enable precise control over the release profile of the entrapped drug through formulation and preparation adjustments. Additionally, SLNs offer protection against enzymatic degradation and boast ease of scalability.

4.1. Methods

4.1.1. Synergy analysis

Synergy analysis was performed to identify the molar ratio of the drugs combination that signifies the synergism. For that, the cell viability of DOC and ERL was analyzed individually in two different TNBC cell lines (MDA–MB–231, and 4T1) using MTT assay. Briefly, 1 x 10^4 cells/well were seeded in a 96 well plate and incubated overnight, followed by replacing each well with fresh media containing different doses of DOC, and ERL for 24, 48, and 72 h. After a respective time, the culture media was aspirated and each well was treated with MTT solution (100 µl, 0.5 mg/ml) and incubated for 4 h, followed by the addition of DMSO to dissolve the formazan crystals. The absorbance was then measured at 570 nm. The IC_{50} was calculated by curve fitting the cell viability data. All the studies were performed in triplicate. The percentage cell viability was calculated using the formula (1):

$$\% \text{ Viability} = \frac{(\text{Abs of sample well})X100}{\text{Abs of control well}} \qquad (1)$$

Wherein, Abs of control is the absorbance of the control group, and Abs of the sample is the absorbance of the sample (treated with DOC, and ERL) [92]. Based on the IC_{50} value of the DOC, and ERL, the drugs were mixed in different molar ratios, namely 1:4, 1:3, 1:2, 1:1, 2:1, 3:1, and 4:1. They were then serially diluted and subjected to MTT assay for 24 h, from where the IC_{50} of the combination was obtained, which was further employed for identification of combination indices (CI). The CompuSyn program (ComboSyn, Inc.,

Paramus, NJ, USA) analyzed the data. The CI was plotted as a function of the fractional inhibition (Fa), where, CI>1, is antagonism; CI=1, is additive, and CI<1, is synergism [93].

4.1.2. Preformulation

4.1.2.1. Screening of solid lipid

Solid lipids are screened based on the solubility of DOC and ERL in lipids. Excess amounts (~10–15 mg) of DOC and ERL were added in 500 mg of each solid lipid, followed by stepwise incorporation of 2 mg of drugs with continuous stirring for 1 h at 10°C above each solid lipid's melting point. The solid lipid was visually analyzed for the transparent mixture's formation without any drug crystals [94].

4.1.2.2. Screening of surfactant

The surfactants were screened based on their emulsification ability. Briefly, 100 mg of selected solid lipid was dissolved in 3 ml methylene chloride, followed by the addition of 10 ml of surfactant solutions (5 % w/v). The mixture was stirred at 40°C to remove the methylene chloride. One ml of the mixture was diluted with distilled water, and % transmittance was determined using a UV–VIS spectrophotometer at 638.2 nm [95].

4.1.2.3. Drug–excipient compatibility study

Compatibility between the drugs and the excipients was analyzed by Fourier Transform Infrared (FTIR) spectroscopy (Shimadzu FTIR 8300 Spectrophotometer, Shimadzu, Tokyo, Japan). In FTIR, the KBr pellet press technique was used, and the obtained pellet was placed in a pan and screened within the wavenumber range of 400–4000 cm^{-1} [96].

4.1.3. Preparation and optimization of SLNs

4.1.3.1. Preparation of SLNs

DOC–SLNs and ERL–SLNs were prepared by the high–shear homogenization–ultrasound dispersion method with slight modification [97]. Briefly, the selected solid lipid was melted at 70°C and accurately weighed drugs were added to the melted lipid. Simultaneously, the aqueous phase was prepared by adding selected surfactant in distilled water at 70°C. After complete solubilization of drugs into the molten solid lipid, the aqueous phase was added dropwise with continuous stirring in a magnetic stirrer for 1 h, at 750 rpm and 70°C. The resultant coarse emulsion was then subjected to high–shear homogenization (IKA T–25 digital ultra Turrax, Germany) for 1 min at 5000 rpm, followed by probe sonication (UP 200H, Hielscher, Germany) for a specific time at 60% amplitude and cooled at ambient

temperature for solidification of solid lipid and formation of SLNs. The SLNs prepared were then stored at 4°C until use.

4.1.3.2. Optimization using Quality by Design approach

To assess the pivotal material variables and process variables required for the fabrication of quality formulations with optimum attributes, a Quality by Design (QbD) approach was employed. Figure 4. 1 shows the Ishikawa diagram used as a visualization tool for the QbD approach.

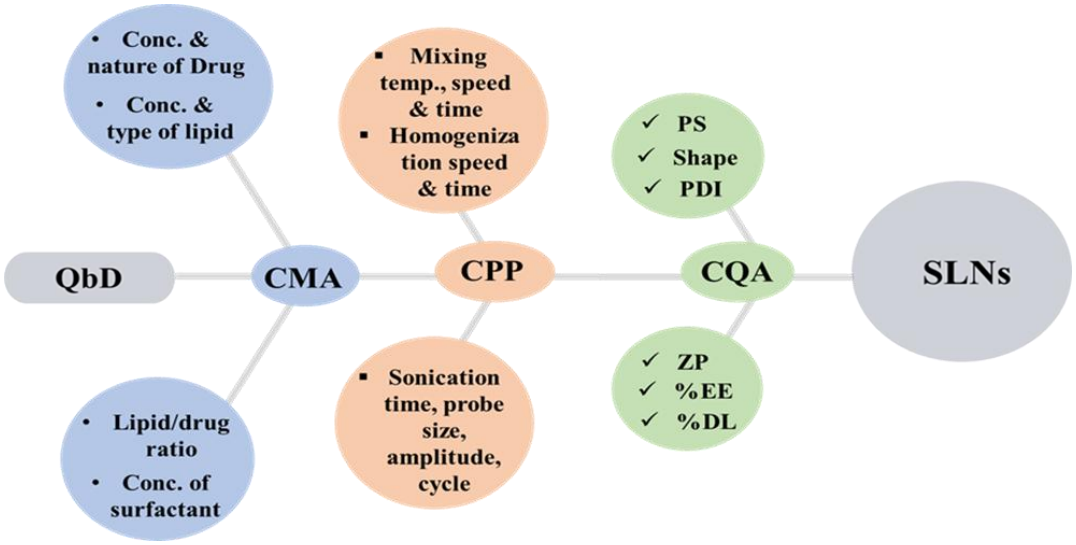

Figure 4. 1: Ishikawa fishbone diagram displaying the interaction between CMA (critical material attribute) and CPP (critical process parameters) to optimize CQA (critical quality attributes)

Screening model using Plackett Burman Design

Plackett Burman design (PBD) was employed with 7–factor and 18 runs using SAS JMP® Pro 14 (Trial version). The generated data was then fitted into the quadratic model and analyzed for the effect of each factor on the quality attributes by evaluating the Pareto plots and the actual vs. predicted plot. The details of experimental batches of SLNs in PBD are given in Table 4. 1.

Table 4. 1: Detailed experimental batches of SLNs in PBD

S.No.	Conc. SL (%w/v)	Conc. Surf (%w/v)	Mixing Speed (rpm)	Homo. Time (min)	Homo. Speed (rpm)	Sonication Time (min)	Sonication Amplitude (%)
1	3	5	500	3	5000	5	60

2	3	5	750	1	1000	5	40
3	2	1	750	3	5000	3.5	40
4	3	3	250	5	1000	3.5	40
5	3	1	750	1	3000	2	80
6	1	1	500	5	3000	5	40
7	1	5	750	5	5000	3.5	80
8	2	1	500	1	1000	3.5	60
9	1	3	500	1	5000	2	40
10	1	1	250	3	1000	5	80
11	1	3	750	3	1000	2	60
12	3	1	250	5	5000	2	60
13	2	5	500	5	1000	2	80
14	2	3	750	5	3000	5	60
15	2	5	250	3	3000	2	40
16	1	5	250	1	3000	3.5	60
17	3	3	500	3	3000	3.5	80
18	2	3	250	1	5000	5	80

Conc.= Concentration; SL=Solid Lipid; Surf=Surfactant; Homo.=Homogenization; PDI=Polydispersity Index

Optimizing model using Box Behnken Design

Box Behnken Design (BBD) using 3–factor and 3–level was employed to optimize the response variables using SAS JMP® Pro 14 (Trial version). Each factor was designated three different levels: low (-1), intermediate (0), and high (+1). The data were then fitted into the quadratic equation, and based on maximum desirability, various plots were evaluated, such

as Pareto plots, actual by predicted plots, prediction profilers, and 3D surface profilers. The independent variables in PBD and BBD are given in Table 4. 2.

Table 4. 2: Independent variables with the assigned values at different levels in the PBD and BBD

Plackett Burman Design (PBD)		
Factors	**Levels**	
	Level 1	**Level 2**
Solid lipid (% w/v)	1	3
Surfactant concentration (% w/v)	1	5
Mixing speed (rpm)	250	750
Homogenization time (min)	1	5
Homogenization speed (rpm)	1000	5000
Sonication time (min)	2	5
Sonication amplitude (%)	40	80
Responses	**Constraints**	
Particle size (nm)	< 200	
Polydispersity index (PDI)	< 0.35	

Box Behnken Design (BBD)			
Factors	**Levels**		
	Low (-1)	**Intermediate (0)**	**High (+1)**
Solid lipid concentration (% w/v)	1	2	3
Surfactant concentration (% w/v)	1	3	5
Sonication time (min)	2	3.5	5
Responses	**Constraints**		
Particle size (nm)	< 200		
Polydispersity index (PDI)	< 0.35		
Entrapment efficiency (% EE)	Maximum		

Drug loading (% DL)	Maximum

Model validation

The designated levels were incorporated within the design space, where the experimental values were compared with the predicted values of the responses, giving each response a prediction error.

4.1.3.3. Surface functionalization of SLNs with folic acid

Synthesis of folic acid–stearic acid (FA–SA) conjugate using EDC coupling reaction

The FA–SA was prepared per the previous report with slight modifications [98, 99]. Briefly, 300 mg stearic acid and 300 mg EDC were added to 5 ml of DMF with continuous stirring for 1 h at ambient temperature. Folic acid solution (450 mg in 1.5 ml of pyridine) was then added to the above mixture and stirred overnight, followed by the addition of distilled water into the reaction mixture to precipitate the formed conjugate. Later, the water–soluble products, EDC, and unreacted folic acid were removed via dialysis (MWCO–12kDa, Sigma Aldrich) for 72 h in distilled water, wherein the water was changed after every 6 h with fresh distilled water, followed by filtration through 0.45 μm Millipore filter, and lyophilization to procure yellow colored FA–SA which was further confirmed by using FTIR.

Functionalization of SLNs with FA

Folic acid conjugated SLNs (FA–SLNs) were prepared by using the high–shear homogenization–ultrasound dispersion method, as described in section 4.1.3.1, with a slight modification of displacing 6 mg of solid lipid with 6 mg of FA–SA in the lipid phase. The surface functionalization was then confirmed by FTIR.

4.1.4. Characterization of the optimized formulations

4.1.4.1. Particle size (PS), polydispersity index (PDI), and zeta potential (ZP)

The PS, PDI, and ZP of the developed DOC–SLNs, ERL–SLNs, FA–DOC–SLNs, and FA–ERL–SLNs were analyzed using DLS (DelsaTMNano, Beckman colter, Brea, CA, USA). Briefly, small aliquots of different formulations were suitably diluted with distilled water and analyzed for the above parameters [100].

4.1.4.2. Morphology analysis

Transmission electron microscopy (TEM) and atomic force microscopy (AFM) were employed to visualize the shape and morphology of the different SLNs dispersions. For

TEM, the SLNs were first diluted with distilled water, followed by the addition of a drop of different SLNs dispersions on the carbon coated grid, air–dried, and then analyzed by TEM (Tecnai G2 20 TWIN, FEI Company of USA (SEA) PTE, LTD) operated at 120 kV [101]. Similarly, for AFM, the different SLNs dispersions were first suitably diluted using distilled water, and a drop of each dispersion was placed onto a clean glass slide, air–dried, and then analyzed by AFM (NTEGRA Prima, NT–MDT Service & Logistics Ltd. Amsterdam, Netherlands), at 15.0 KV [100].

4.1.4.3. Entrapment efficiency & drug loading efficiency

The entrapment and drug loading efficiency were determined indirectly by measuring the concentration of free drugs in the supernatant [102]. Briefly, SLNs dispersion (2 ml) was ultracentrifuged at 45,000 rpm for 30 min at 4°C, followed by collection of the supernatant, and suitably diluted with methanol. The DOC and ERL concentrations were measured using the validated HPLC method (Agilent 1260 Infinity II; Santa Clara, CA, United States) by employing the following formulas (2), and (3);

$$\%\ \text{Entrapment efficiency (\%EE)} = \frac{\text{Total amount of drug} - \text{amount of drug in the supernatant}}{\text{Total amount of drug}} \text{ x } 100 \qquad (2)$$

$$\%\ \text{Drug loading (\%DL)} = \frac{\text{Total amount of drug} - \text{amount of drug in the supernatant}}{\text{Total weight of the SLNs}} \text{ x } 100 \qquad (3)$$

The quantity of DOC and ERL were measured by Agilent 1260 Infinity II HPLC system (Santa Clara, CA, United States), with C18 analytic column (Inertsil® ODS3: 15 cm × 0.46 cm, 5 µm, GL Sciences Inc., Japan), and the methanol and acetic water (80:20, volume ratio), as mobile phase. The effluent was monitored at a UV absorption wavelength of 230 and 335 nm for DOC and ERL respectively at a 1.0 ml/min flow rate with the 10 µl injection volume (*See Appendix*).

4.1.4.4. Lyophilization studies

Different SLNs were lyophilized as per the previous protocol [103]. Briefly, the SLNs were frozen at -60°C for 8 h, followed by primary drying at -60 to 20°C for 42 h, and secondary drying at 25°C for 2 h. A preliminary screening of the cryoprotectants was performed at 5% w/v of different cryoprotectants blended with the SLNs. After selecting the optimized cryoprotectant, a range of the different concentrations (2.5–10 % w/v) of the optimized cryoprotectant was tested. The lyophilized SLNs were analyzed for the re–dispersibility index and re–dispersibility score.

4.1.4.5. Stability studies

Lyophilized SLNs were evaluated for stability as per ICH guidelines Q1A (R2), where the lyophilized SLNs were stored for six months in different storage conditions of 4±3°C, 25±2 °C/60±5 % RH, and 40±2°C/75±5 % RH. The samples were withdrawn after 1, 3, and 6 months and tested for the effect on the PS, PDI, ZP, and % EE [104].

4.1.4.6. *In vitro* drug release study

An *in vitro* release study was performed to analyze the release profile of drugs from the nanoformulations in the media, mimicking the physiological condition when administered orally. The release media includes simulated gastric fluid (pH 1.2), simulated intestinal fluid (pH 6.8), and phosphate buffer saline (pH 7.4); mimicking the physiological condition of the systemic circulation. The release media also include phosphate buffer saline (pH 5.5); mimicking the tumor microenvironment. The sink condition was maintained by 0.1 % w/v tween 80. The SLNs dispersion (equivalent to 2 mg of drug) was filled in the activated dialysis bag (MWCO: 12 kDa), tied at both ends, and suspended in 50 ml of different release media, with continuous stirring at 100 rpm and 37±0.5°C. Eventually, 1 ml aliquots were withdrawn at different time intervals (0.5, 0.75, 1, 1.5, and 2 h for pH 1.2; 0.5, 1, 1.5, 2, 3, 4, 5, and 6 h for pH 6.8; 0.5, 1, 1.5, 2, 3, 4, 5, 6, 12, 24 h for pH 7.4, and pH 5.5) and replaced with equal volume of fresh media. The withdrawn samples were then analyzed using the validated HPLC method (Agilent 1260 Infinity II, Santa Clara, CA, USA) to estimate % cumulative drugs released from SLNs [96, 105].

Kinetic mechanism of drug release

To evaluate the release kinetics and release pattern of the drugs from the carrier, the data obtained from the *in vitro* drug release study was fitted into five mathematical kinetics models, namely, zero order, first order, Higuchi model, Hixon–Crowell model, and Korsmeyer–Peppas model. The drug release kinetics was determined by finding the best–fit model, as obtained from the highest correlation coefficient (R^2), and the drug release mechanism was studied using the Korsmeyer–Peppas model, as obtained from the diffusion–release exponent (n) [106].

4.1.4.7. *In vitro* lipolysis study using pH–stat model

In vitro lipolysis study was performed to analyze the stability or the integrity of the developed SLNs in the intestinal pH conditions. It was performed according to Wijaya *et*

al., 2020 with slight modifications [107]. A lipolysis buffer was prepared with 50 mM tris maleate, 150 mM sodium chloride, 5 mM calcium chloride, 20 mM sodium taurodeoxycholate, and 5 mM phosphatidylcholine. Also, pancreatin was freshly prepared by mixing 1 g of pancreatin powder in 5 ml of lipolysis buffer. The pancreatin powder should have amylase, lipase, and protease activity not less than 25 USP, 2 USP, and 25 USP, respectively. The pancreatin solution was centrifuged at 2000 rpm for 10 min, and the supernatant was collected and stored at 4°C.

The SLNs were mixed with 9 ml lipolysis buffer during the lipolysis study and stirred at 200 rpm, 37±1°C, for 10 min. At the same time, its pH was maintained at 6.80±0.2 using 1.0 M NaOH or 1.0 N HCl, followed by adding 1 ml of chilled pancreatin to initiate the enzymatic digestion of the LNPs. At this time, the pH of the media was maintained at 6.8±0.2 using 0.2 M NaOH solution. The volume of 0.2 M NaOH consumed to maintain the pH at 6.8±0.2 was recorded because the liberation of free fatty acids decreases the pH of the media, which the NaOH further neutralized. The experiment was continued for 2 h, and free fatty acid liberated was calculated using the formula (4);

$$\% \text{ FFA} = \frac{\text{VNaoH x mNaOH x Mwlipid x 100}}{\text{Wlipid x 2}} \quad (4)$$

where, V_{NaOH} = volume of NaOH in liters, m_{NaOH} = molarity of NaOH, Mw_{lipid} = apparent molecular weight of the lipid, and W_{lipid} = weight of lipid in the media in grams.

For control, a drug–loaded suspension was prepared and subjected to *in vitro* lipolysis, as mentioned above.

After completion of the study, the final digestion media was treated with 1 M 4–bromophenylboronic acid in methanol to inhibit further digestion, followed by ultracentrifugation (Type 90 Ti rotor, Beckman Coulter) at 40,000 rpm for 40 min at 4°C. The middle aqueous phase was collected, mixed with methanol, and centrifuged for 15 min at 4000 rpm. The top methanol phase was collected in which the drugs were solubilized, which was then analyzed using HPLC (Agilent 1260 Infinity II, Santa Clara, CA, USA). The bioaccessibility (%) of DOC and ERL was calculated using formula (5):

$$\text{Bioaccessibility (BA) \%} = \frac{\text{Total mass of solubilized drug (g) x 100}}{\text{Total mass of drug in original lipid sample (g)}} \quad (5)$$

4.1.5. *In vitro* cell culture studies

MDA–MB–231 cell lines were purchased from the National Center for Cell Science (NCCS), Pune, India, and 4T1 cell lines were generously provided by Dr. Virander S.

Chauhan, Arturo Falaschi Emeritus Scientist, International Centre for Genetic Engineering & Biotechnology, New Delhi, India. Cells were cultured in DMEM (Dulbecco's modified eagle's medium), supplemented with 10 % FBS (Gibco, Thermo Scientific, Waltham, MA, USA) and 1 % antibiotic, anti–mitotic solution (Himedia, Mumbai, India) (10,000 U Penicillin, 10 mg streptomycin, 25 µg Amphotericin B per ml) and grown at 37°C temperature in a humidified incubator (Heracell VIOS 160i, Thermo fisher. MA, USA).

4.1.5.1. Cell viability assay of SLNs using MTT

The cell viability was analyzed in different TNBC cell lines using MTT assay. Briefly, $1x10^4$ cells/well were seeded in a 96 well plate and incubated overnight, followed by replacing each well with fresh media containing different SLNs for 24, 48, and 72 h. After a respective time, the culture media was aspirated and each well was treated with MTT (100 µl, 0.5 mg/ml) and incubated for 4 h, followed by the addition of DMSO to dissolve the formazan crystals. The absorbance was then measured at 570 nm. The IC_{50} was calculated by curve fitting the cell viability data. All the studies were performed in triplicate. The percentage cell viability (% Viability) was calculated using equation 1 [92].

4.1.5.2. Cellular uptake assay

Drug–loaded SLNs in cancer cells were analyzed for their intracellular accumulation capacity into the cancer cells using a qualitative and quantitative cellular uptake assay. In qualitative cellular uptake, Coumarin 6 (C6) was utilized as a model dye since it replicates the lipophilic properties of the drugs. C6–loaded SLNs and C6–loaded FA–SLNs were prepared similarly to drug–loaded SLNs, with the only difference being the replacement of drugs with C6 (equivalent to 3 µg). The cells were seeded in a 6 well plate with a density of 3×10^5 cells/well and incubated overnight followed by aspiration of the media, and the addition of fresh media containing C6, C6–loaded SLNs, and C6–loaded FA–SLNs and incubated for 4 h. After incubation, the cells were washed with cold PBS, treated with DAPI (10 µg/ml) for staining the nuclei, and incubated for 10 min. The cells were then observed under a fluorescence microscope (Olympus BX53, Tokyo, Japan) [108].

A quantitative cell uptake assay measured the amount of drugs uptake by the cells. Briefly, the cells were seeded in 12 well plates at the density of $5x10^5$ cells/well, and incubated overnight, followed by aspiration of the media and addition of fresh media containing DOC, ERL, and different SLNs formulations (equivalent concentration of 2 µM, and 20 µM of DOC, and ERL, respectively). The cells were again incubated for different periods *viz*., 0.5,

1, 2, and 4 h. After the respective period, the media were aspirated and the cells were washed with cold PBS to remove the extracellular drugs, followed by trypsinization. The treated cell suspension was collected and centrifuged at 1600 rpm for 5 min. The pellets obtained were treated with methanol for the lysis of the cells and release of the absorbed nanoparticles by the cells followed by centrifugation at 10,000 rpm for 10 min. The supernatant obtained was then analyzed in a HPLC (Agilent 1260 Infinity II HPLC system) to quantify DOC and ERL [109].

4.1.5.3. Colony formation assay

The colony formation assay was performed to analyze the effectiveness of the developed formulations in preventing a single adherent cell from forming colonies. The cells were seeded at 500 cells/well density in 35 mm petri plates and incubated overnight. The media were aspirated and fresh media was added containing drugs and different SLNs dispersions (equivalent to 0.5 and 8 µM of DOC and ERL, respectively when administered individually, and equivalent to 0.5 and 1.5 µM of DOC and ERL respectively in combination). The study was continued for 10 days, and the media was replaced with fresh media every alternate day. After completion of the study, the cell colonies were stained with 0.5 % crystal violet in methanol for 10–12 min. The colonies were manually counted under a microscope and images by a digital camera [110].

4.1.5.4. Mitochondrial membrane potential (MMP) assay

Prohibition of MMP is one of the characteristics of early apoptosis. Therefore, to identify whether mitochondria were involved in DOC and ERL–induced apoptosis, we performed an MMP assay. The MMP was analyzed using JC–1 dye (Invitrogen, Thermo Scientific, San Diego, MA, USA), a lipophilic cationic dye that accumulates within the mitochondria depending on their membrane potential ($\Delta\Psi_m$). Briefly, cells were seeded at $1x10^5$ cells/well density in a 35 mm petri plate and incubated overnight, followed by aspiration of media and addition of fresh media containing drugs and different SLNs dispersion (for single delivery: equivalent to 2 µM DOC, and 20 µM ERL; whereas for combination delivery: equivalent to 2 µM DOC and 6 µM ERL), and incubated for 24 h. After the treatment period, cells were washed with cold PBS and incubated with JC–1 dye (10 µM) for 45 min, followed by washing with cold PBS three times, to remove the unbound JC–1 dye. The cells were then imaged by a fluorescence microscope (Olympus BX53, Tokyo, Japan) [111].

4.1.5.5. Reactive oxygen species (ROS) assay

H_2DCFDA dye was employed to analyze the generation of intracellular reactive oxygen species (ROS). In brief, the cells were seeded in 35 mm petri dishes at a density of $5x10^5$ cells/well and incubated overnight, followed by aspiration of media, and replenishment with fresh culture media comprising of different treatments, as mentioned in MMP assay, and incubated for 24 h. Here, 0.05% v/v H_2O_2 was employed as positive control and added to the cells 2 h before termination of the study. For fluorescence microscopy, after completion of the 24 h incubation period, H_2DCFDA dye (10 µM) was added and incubated for 30 min, washed with cold PBS, and analyzed using a fluorescence microscope (Olympus BX53, Tokyo, Japan) [112]. For flow cytometry, the cells treated with different treatments were trypsinized, and collected, to which 500 µl H_2DCFDA dye (10 µM) was added and incubated for 30 min, followed by washing with cold PBS and analysis using flow cytometry (CytoFlex LX, Beckman coulter, MA, USA) [113].

4.1.5.6. Annexin V apoptosis assay

The anticancer properties of DOC and ERL were assessed by inducing apoptosis in MDA–MB–231 and 4T1 cells using an annexin V binding assay. Briefly, the cells were seeded in 8 well chambered cell culture slides (Mat Tek, Asland, MA, USA) at the cell density of $3x10^4$ cells/well and incubated overnight, followed by treatments with different SLNs formulation, as mentioned in the MMP assay and incubated for 24 h. The media was aspirated, followed by washing with cold PBS and staining the cells with Annexin V–Cy3.18 conjugate (AnnCy3) and 6–carboxyfluorescein diacetate (6–CFDA) using the Annexin V–Cy3^{TM} Apoptosis Detection Kit from Sigma in St. Louis, MO, USA. After 10 min incubation, the cells were washed with cold PBS and observed using a fluorescence microscope (Olympus BX53, Tokyo, Japan). Further, the apoptosis index was calculated as the ratio of the red fluorescence intensity to the green fluorescence intensity [100].

4.1.5.7. Wound healing assay

A wound healing assay was performed to analyze the developed nanoformulations' anti-metastatic potential. Culture–insert 2 well (Ibidi, Lochhamer Schlag, Gräfelfing, Germany) was employed for seeding 200 µl of cells at the cell density of $3x10^4$ cells/100 µl, and incubated for 24 h. After the attachments of the cells onto the well, sterile forceps were employed to form the wounds by gently removing the culture inserts. The cells were then subjected to different SLNs formulations (for single delivery equivalent to 1 µM DOC, and

10 µM ERL; whereas for combination delivery equivalent to 1 µM DOC, and 3 µM ERL), and images were taken immediately (t=0 h), followed by incubation for 24 h. The wound healing images were also taken after 24 h under an inverted microscope (Dewinter, New Delhi, India). ImageJ software was employed for calculating the rate of wound closure (formula 6, and 7). A decrease in the rate of wound closure was taken as an indication of a decrease in the metastatic property of the TNBC cells [114].

$$Distance\ of\ wound\ clsoing = Initial\ wound\ distance - Final\ wound\ distance \quad (6)$$

$$Rate\ of\ wound\ closure = {Distance\ of\ wound\ closing\ (\mu m)}/{Time\ (h)} \quad (7)$$

4.1.5.8. Transwell migration assay

Transwell migration assay was also performed to analyze the developed formulations' anti–metastatic potential. Briefly, cells were pretreated with different SLNs formulations, as mentioned in the wound healing assay for 1 h. The cells were trypsinized and collected in serum–free media. 500 µl of these serum–free cell suspensions were seeded in six transwell upper chamber (Sigma–Aldrich, MA, USA) at the cell density of $4x10^2$ cells/100 µl while the lower chambers were filled with complete media containing 10% FBS, which acts as chemoattractant. The cells were then incubated for 24 h. The cells in the upper chamber were fixed and stained by 4 % formaldehyde and 0.5 % toluidine blue respectively. The migrating cells were observed using an inverted microscope (Dewinter, New Delhi, India) [115].

4.1.6. *In vivo* anticancer studies

The institutional Animal Ethics Committee, Depart. Pharm. Engg. & Tech. IIT (BHU), approved all animal research (IIT (BHU)/IAEC/2023/II/064), and CCSEA (formerly known as CPCSEA) standards were followed for animal handling. Female Sprague Dawley rats aged 9–11 weeks were purchased from the IMS Animal House at Banaras Hindu University (BHU), Varanasi, India, and female BALB/c mice aged 6–8 weeks were procured from Central Animal House, CSIR–CDRI, Lucknow. The rats and mice were housed at 22±2°C with a 12/12 h light/dark cycle and were given basic amenities.

4.1.6.1. Pharmacokinetic study

A pharmacokinetic study was performed to measure the plasma–drug concentrations from the developed formulations compared to the control. Experiments involving female Sprague

Dawley rats were randomly divided into nine groups, five animals in each group (n=5), as outlined in the table 4. 3 below:

Table 4. 3: Groups for the pharmacokinetic study

Groups	Formulation	Dose
1	DOC susp.	DOC equivalent to 10 mg/Kg; ERL equivalent to 30 mg/Kg. Suspension (susp.) was prepared by suspending drugs in 0.5% w/v carboxymethyl cellulose (CMC)
2	ERL susp.	
3	DOC–SLNs	
4	ERL–SLNs	
5	FA–DOC–SLNs	
6	FA–ERL–SLNs	

The animals were fasted for 12 h before the experiment. Then the doses were administered orally to each group and at predetermined time intervals (0.5, 1, 2, 4, 6, 8, 10, 12, and 24 h) following the administration of a single dosage, 200 µl blood was collected from a retro–orbital vein in heparinized centrifuge tube while being anesthetized. The blood was centrifuged at 10,000 rpm for 10 min at 4°C to procure plasma. Methanol was then employed for extracting the drug before the plasma was filtered by 0.22 µm nylon membrane filters (Merck, Bangalore, India). The filtered plasma samples were analyzed for drug content using validated HPLC methods (Infinity 1200, Agilent, USA) (*See Appendix*). The pharmacokinetic parameters, including AUC, Tmax, Cmax, elimination half–life, etc., were computed using PK solver software [116].

4.1.6.2. Quantitative biodistribution study

The quantitative biodistribution study was performed to analyze the distribution profile of drugs to the various vital organs. Female Balb/c mice aged 6–8 weeks were fasted for 12 h before the experiment. The animals were segregated into six groups: Group 1 received DOC susp., Group 2 received ERL susp., Group 3 received DOC–SLNs, Group 4 received ERL–SLNs, Group 5 received FA–DOC–SLNs, and Group 6 received FA–ERL–SLNs; with n=3 in each group. The animals were given oral dose at DOC equivalent to 10 mg/kg, and ERL equivalent to 30 mg/kg. The animals were sacrificed at 12 h after the single administration

and different organs (brain, lungs, heart, liver, spleen, and kidney) were carefully excised and washed with normal saline. The organ samples were minced and homogenized in normal saline to form tissue homogenate. A 0.2 ml portion was then extracted with 0.5 ml methanol, vortexed, and centrifuged. The supernatant was filtered and analyzed for DOC and ERL using a validated HPLC method (Infinity 1200, Agilent, USA) [117].

4.1.6.3. *In vivo* anticancer efficacy study

Female Balb/c mice aged 6–8 weeks were used to analyze the *in vivo* anticancer efficacy of different formulations and free drugs [118]. When the 4T1 cells attained 90% confluency, they were trypsinized and collected. The cells were adjusted to 5×10^5 cells/100 µl cell media (1:1 PBS: Matrigel) and subcutaneously inoculated into the fourth mammary pad of each animal. Every alternate day, the tumor size was measured with a digital Vernier caliper using the formula (8), as shown below:

$$Tumor\ volume\ (V) = \frac{a \times b^2}{2} \qquad (8)$$

where (a) is the diameter of the long side, and (b) is the diameter of the perpendicular. The tumor was then allowed to grow for seven days, and when the tumor volume reached ~80 mm^3, the animals were segregated into various groups (n=5), as indicated in table 4. 4;

Table 4. 4: Groups for the anticancer efficacy study

Groups	Formulation	Dose
1	Tumor Control	DOC equivalent to 10 mg/Kg; ERL equivalent to 30 mg/Kg. Suspension (susp.) was prepared by suspending drugs in 0.5% w/v carboxymethyl cellulose (CMC)
2	DOC susp.	
3	ERL susp.	
4	DOC susp. + ERL susp.	
5	DOC–SLNs + ERL–SLNs	
6	FA–DOC–SLNs + FA–ERL–SLNs	

The doses were administered orally thrice a week for 21 days, with a total of 9 doses, and anticancer efficacy was evaluated by various parameters namely, tumor volume, tumor weight, body weight of the tumor–bearing animal, and % tumor inhibition rate [119].

4.1.6.4. Hematological, biochemical, and histopathological study

After completing the *in vivo* anticancer efficacy study, blood was taken from retro–orbital vein for hematological and biochemical analysis. Following a gentle cervical dislocation, the vital organs (heart, lungs, liver, spleen, and kidney) were excised for histopathology analysis. The hematological, and biochemical parameters were analyzed for evaluating the toxicity profile of the formulation. Briefly, blood was withdrawn from the retro–orbital veins into the heparinized tubes. Hematological parameters, such as RBCs count, WBCs count, platelets count, haemoglobin content etc., were estimated using an automated hemato analyzer (Microbion, Life Sciences, New Delhi, India). Plasma samples from blood were taken for analysis of biochemical parameters namely, ALT, AST, ALB, urea, and creatinine using ELISA kits (ARKAY healthcare PVT, LTD in Gujarat, India) in a biochemical analyzer (CHEM–5–Plus v2, Erba Mannheim, Germany) [120]. For histopathological analysis, the organs were excised from the tumor–bearing mice and immersed in a 10% formaldehyde solution, which was then cut and embedded in white paraffin wax blocks. Then cryostat microtome (TNR, TN60, Florida, USA) was employed to divide the blocks into tiny sections (4–5 μm). Hematoxylin & eosin (H&E) dye was used to stain the slides to demonstrate histological alterations after the treatment. After that, slides were analyzed using a microscope [121].

4.2. Statistical analysis

All the data are expressed as mean±standard deviation (SD). The *in vitro* data was analyzed using the GraphPad Prism statistical program (Version 8.0; San Diego, CA, USA) and ImageJ software (Bethesda, Maryland, USA). To find out if there are any statistically significant differences between the means of three or more different experiments, analysis of variance (ANOVA) was employed followed by the Tukey–Kramer multiple comparison test. Statistics were deemed significant at p values less than 0.05.

4.3. Results & discussions

4.3.1. Synergy analysis

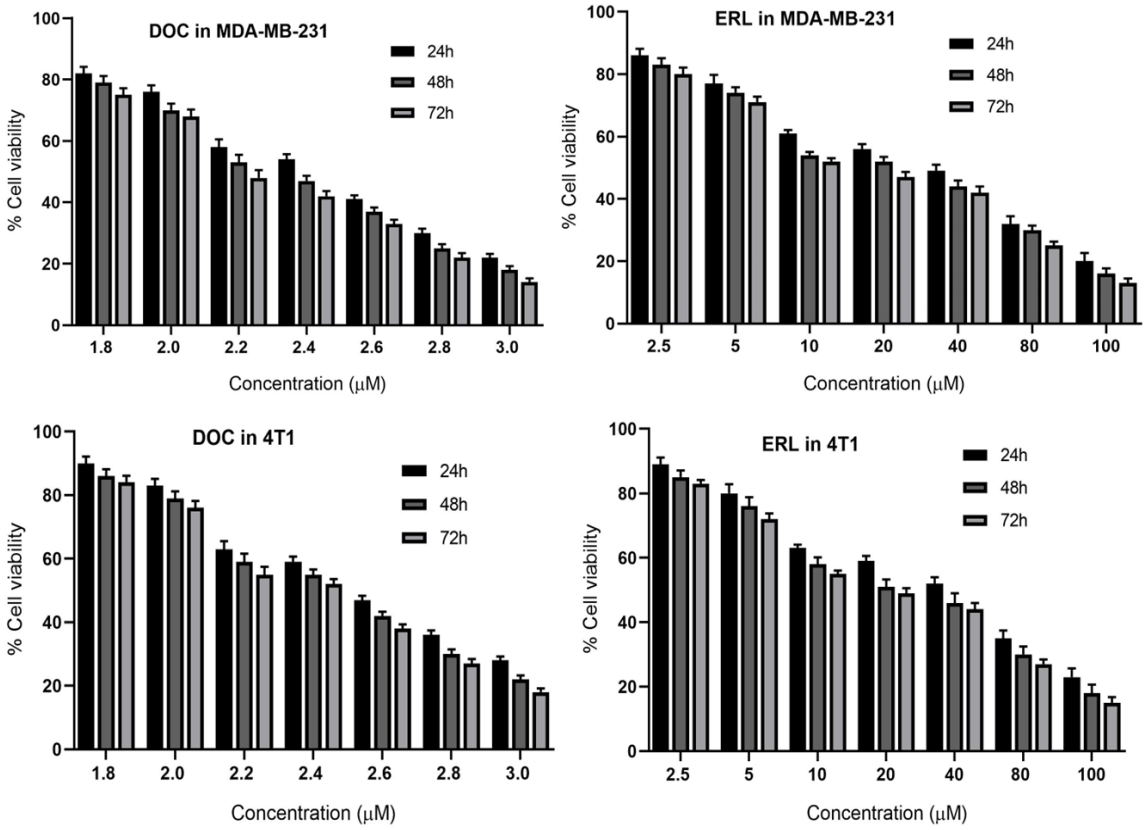

Figure 4. 2: Synergy analysis by using MTT assay for DOC, and ERL in MDA–MB–231, and 4T1 cell lines. Data are presented as mean±SD (n=3)

The cell cytotoxicity was first analyzed for free DOC and ERL, as shown in figure 4. 2, followed by their combination at different molar ratios in two TNBC cell lines (Table 4. 5). The CI was meticulously examined to pinpoint the ideal ratio of DOC to ERL for their encapsulation into FA–SLNs. It was found that at a 1:3 molar ratio of DOC to ERL, an increased cytotoxicity was observed (Figure 4. 3). This was demonstrated by combination indexes of 0.35 for MDA–MB–231 and 0.37 for 4 T1, indicating synergism.

Table 4. 5: Cytotoxicity of DOC and ERL used to treat TNBC cells as single drugs and in combination (as the mixtures of these drugs)

IC_{50} (μM) at 24 h	Free Drugs		Combination of free drugs (DOC: ERL) in molar ratios						
	DOC	ERL	1:4	1:3	1:2	1:1	2:1	3:1	4:1
MDA–MB–231	2.54± 0.04	25.72± 0.35	15.21± 0.23	7.42± 0.05	11.27± 0.56	14.28± 0.45	13.21± 0.43	12.12± 0.56	10.52± 0.41

4T1	3.22± 0.08	29.74± 0.38	16.75± 0.27	8.41± 0.04	13.52± 0.72	16.85± 0.24	14.56± 0.73	12.52± 0.62	11.12± 0.42

Values are presented as mean±SD (n=3)

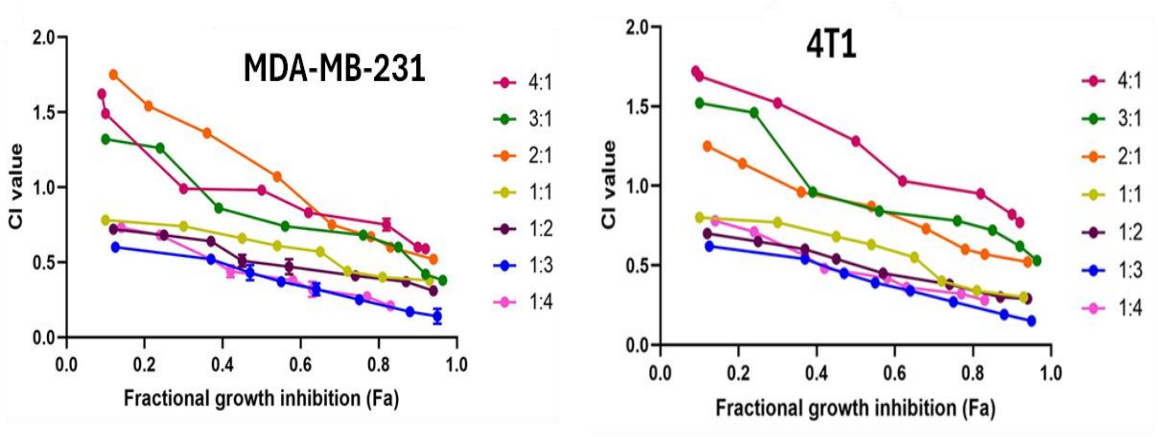

Figure 4. 3: Comparison of CI values of different molar ratios of DOC and ERL

It was inferred that a 1:3 molar ratio of DOC to ERL likely provides the best balance of their complementary actions on cancer cell proliferation. While increasing the dose of DOC, the cytotoxic effect of DOC might dominate, providing an additive effect and increasing the chances of dose–related toxicity related to DOC. However, a lower concentration of docetaxel showed less synergism.

4.3.2. Preformulation

4.3.2.1. Screening of solid lipid and surfactant

Precirol ATO 5 has been selected as the solid lipid, as both DOC, and ERL showed maximum solubility in Precirol ATO 5. Further, Tween 20 was selected as the surfactant, as it showed increased emulsification ability, as observed from the highest % transmittance, compared to other surfactants (Figure 4. 4).

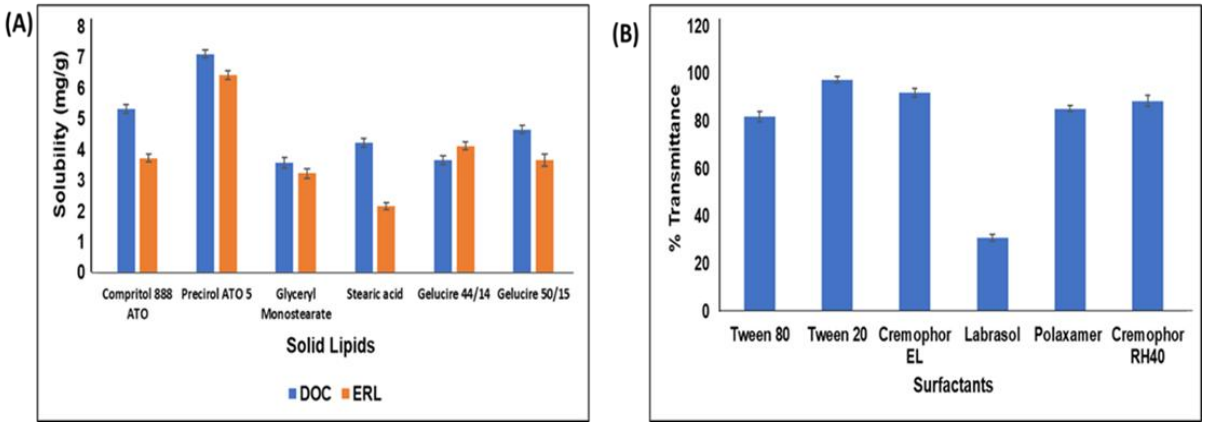

Figure 4. 4: Solubility profile of DOC and ERL in solid lipids (A), and % transmittance of selected solid lipid in different surfactants (B). Data are presented as mean±SD (n=3)

The solubility of the drugs within the lipid core has an immense influence over the loading capacity of the SLNs, as evident that an enhanced solubility reflects increased loading of the drugs within the lipid core. A total of six solid lipids were selected, out of which Precirol ATO 5 exhibited maximum solubility, due to the presence of more glycerides (mono –, di – , and tri –), providing a loose, and highly porous structure, allowing enhanced and easy drug accommodation and improved solubility. Hence, it was inferred that proper screening of the solid lipid is crucial as it significantly influences entrapment efficiency and drug loading [122]. Surfactants also play an important role in stabilizing the SLNs by preventing the coalescence of highly unstable surfaces. During particle size reduction of SLNs, new surfaces are formed, which is supposed to increase the force of attraction between the particles, thereby increasing the interfacial tension and destabilizing the system. The hydrophilic nature of Tween 20 (HLB=16.7) imparts a repulsive force at the interfacial surface, and decreases the surface energy of the system, thereby stabilizing the system. Hence, it was inferred that the proper selection of surfactant is crucial for maintaining the long–term stability of the SLNs [123].

4.3.2.2. Drug–excipient compatibility study

The characteristic peaks were observed in excipients namely Precirol ATO 5, and Tween 20 using FTIR. The physical mixtures of DOC–excipients and ERL–excipients exhibited the characteristic peaks of the respective drugs and the excipients, with no relevant changes in the individual peaks (Figure 4. 5).

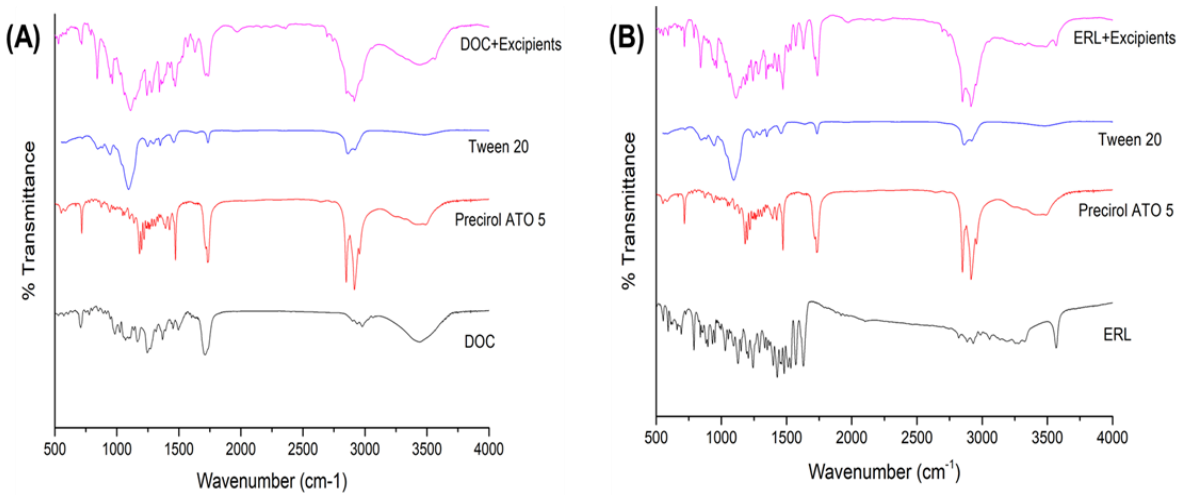

Figure 4. 5: FTIR spectra indicating the compatibility profile of various excipients of SLNs with DOC (A), and ERL (B)

The drugs and the excipients are considered compatible as in the FTIR spectra, no new peaks were observed, and no existing peaks disappeared.

4.3.3. Preparation and optimization of SLNs

4.3.3.1. Preparation of SLNs

In this study, we employed a "nano + nano approach" for combination therapy by preparing separate SLNs for DOC and ERL, which are co–administered to enhance therapeutic efficacy. Such an approach offers more flexibility in dosing and formulation [124]. During the co–encapsulation approach, there arose a discrepancy in the %EE, as DOC and ERL showed 20% and 80% EE respectively. The higher lipophilicity of ERL (Log P=2.7) may have displaced the DOC (Log P=2.4) from the lipidic core, reducing DOC's % EE and compromising its therapeutic efficacy. Such circumstances prompted us to proceed with "nano + nano" combination type, where the % EE of DOC and ERL in their respective SLNs was between 70–80 %, maintaining the therapeutic efficiency of both drugs. Our findings concord with the findings of Chen *et al*., 2017 stating that co–loading multiple drugs in one nanocarrier at the predetermined dose or dose ratio is problematic because of their different physicochemical properties and the varied carrier–drug affinity [125]. Based on the synergy analysis, as a 1:3 molar ratio was selected for improved synergism, the DOC and ERL were loaded as 0.1 % w/v and 0.3 % w/v, respectively.

4.3.3.2. Optimization using Quality by Design approach

Screening model

From the PBD, 18 runs were obtained as shown in table 4. 6. The runs further generated Pareto plots (figure 4. 6), from where it was found that three out of seven independent variables i.e., conc. of surfactant, conc. of solid lipid and sonication time, showed a significant effect on critical quality attributes i.e., particle size and PDI ($p < 0.05$), as shown in figure 4. 6. For optimization of the screened variables, BBD was employed where certain independent variables were kept constant based on the result of the PBD.

Table 4. 6: Experimental batches of SLNs in PBD

Formulations	Particle size (nm)	PDI
1	175	0.181
2	221	0.211
3	132	0.202
4	228	0.239
5	241	0.242
6	182	0.195
7	140	0.134
8	181	0.152
9	152	0.168
10	138	0.138
11	179	0.159
12	172	0.264
13	198	0.198
14	213	0.213
15	256	0.256
16	227	0.157
17	231	0.231
18	158	0.158

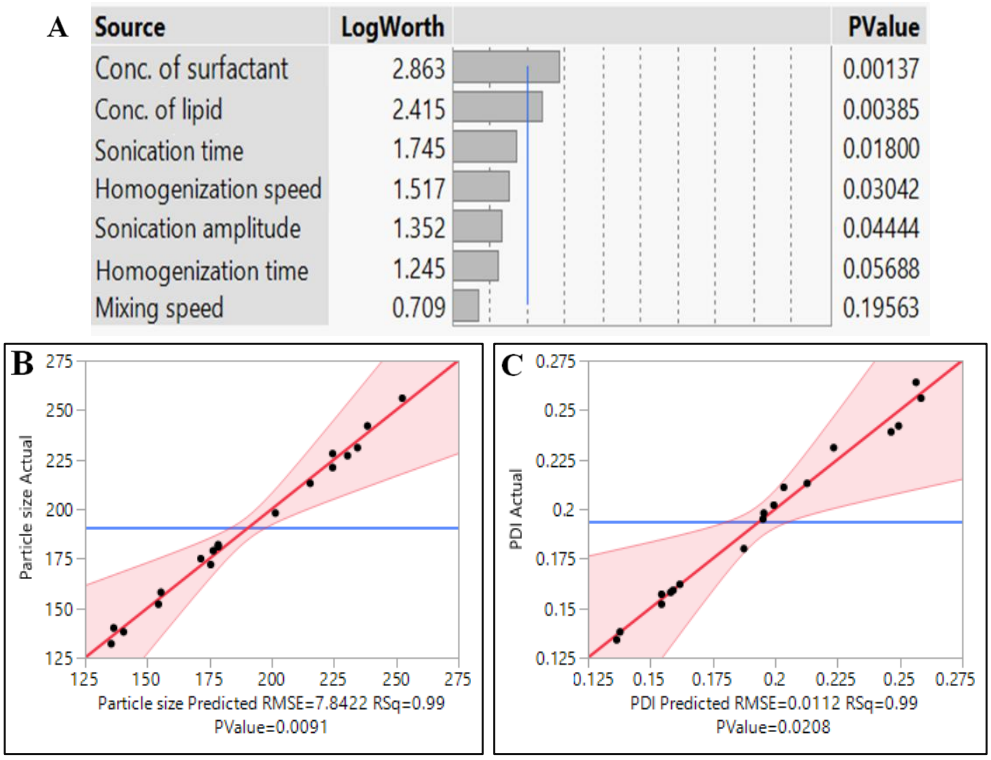

Figure 4. 6: Pareto plot analysis (A). Actual by predicted plots for particle size (B) and PDI (C).

From the screening design, three factors (concentration of solid lipids, concentration of surfactant, and sonication time) having a significant effect on the responses were screened, while others were fixed at a constant value due to their insignificant influence over the responses. PS and PDI are considered essential characteristics in formulation, as PS affects the release profile and absorption. PDI demonstrates the dispersed nature of the nanoparticles, i.e., monodisperse or polydisperse.

Optimizing model

BBD was used to optimize the DOC–SLNs and ERL–SLNs, where the interaction between the factors and the responses/dependent variables was analyzed, as shown in table 4. 7, and 4. 8. From the actual by predicted plot (Figure 4. 7(A–D), 4. 8(A–D)), we have defined the p values, which were found to be <0.05, and revealed the significance of the model.

Further, Pareto plots were analyzed, indicating the interaction between the independent and dependent variables (Figure 4. 7(E–H), 4. 8(E–H)). It was revealed that the positive value indicates synergistic interaction, whereas the negative value indicates the antagonistic interaction between the variables and the responses. Moreover, the Pareto chart arranged the variables in their higher–order interactions with the respective responses.

Further, to derive the maximum desirability, the prediction profiler was analyzed (Figure 4. 9(A), (B)). Solid lipids and surfactant concentration exhibited a parabolic effect on all the

given responses at lower and higher values. On the contrary, sonication time showed a parabolic effect on particle size and PDI, while an insignificant effect on % EE and % DL.

The maximum desirability was obtained at a 95 % confidence level from the prediction profiler, which stated that for preparation of DOC–SLNs, 1 % w/v solid lipid, 3 % w/v surfactant, and 5 min sonication time was required, and for ERL–SLNs, 2 % w/v solid lipid, 3 % w/v surfactant, and 5 min sonication time was required.

The response surface plots were employed to analyze the interaction between the two variables and the responses while keeping the other variable constant (Figure 4. 10(A–L) and 4. 11(A–L)).

In model validation, three factors with three levels were selected within the design space for analyzing the quadratic model, where the actual values of the responses were compared with that of the predicted ones, as provided by the design, and were found to be within the range of 10% prediction error (Table 4. 9).

Table 4. 7: Experimental batches of DOC–SLNs in BBD

S. No.	Conc. SL (%w/v)	Conc. Surf (%w/v)	Sonication Time (min)	Particle Size (nm)	PDI	EE (%)	DL (%)
1	1	1	3.5	230.21±2.55	0.357±0.004	43.33±2.11	3.87±0.03
2	2	1	5	73.87±3.62	0.233±0.002	81.36±1.45	3.63±0.01
3	1	3	2	94.22±2.75	0.243±0.003	54.11±1.22	1.50±0.02
4	2	3	3.5	196.07±3.31	0.267±0.005	48.63±2.04	1.95±0.03
5	3	5	3.5	353.16±3.68	0.348±0.001	74.11±1.54	1.91±0.01
6	2	5	5	109.18±2.36	0.147±0.004	77.78±1.29	2.10±0.02
7	3	3	2	354.89±4.13	0.215±0.008	69.94±1.42	2.15±0.05
8	2	5	2	110.23±3.11	0.148±0.006	77.76±1.53	2.12±0.04
9	2	3	3.5	75.09±2.65	0.199±0.002	63.30±2.15	1.93±0.06
10	2	3	3.5	90.57±2.53	0.210±0.001	64.20±2.24	1.95±0.04

11	3	3	5	221.12±2.30	0.283±0.004	77.86±2.33	2.28±0.07
12	2	1	2	325.63±3.64	0.305±0.003	49.13±1.52	2.58±0.02
13	3	1	3.5	384.23±4.18	0.348±0.003	55.63±1.82	2.36±0.08
14	**1**	**3**	**5**	**118.42±2.36**	**0.212±0.006**	**73.47±1.11**	**3.15±0.06**
15	1	5	3.5	53.71±2.07	0.135±0.009	65.76±1.43	2.08±0.05

Values are presented as mean±SD (n=3).

Table 4. 8: Experimental batches of ERL–SLNs in BBD

S. No.	**Conc. SL (%w/v)**	**Conc. Surf (%w/v)**	**Sonication Time (min)**	**Particle Size (nm)**	**PDI**	**EE (%)**	**DL (%)**
1	1	3	5	50.12±2.32	0.134±0.002	76.81±1.32	3.88±0.02
2	2	1	2	380.43±1.24	0.307±0.003	46.43±1.62	2.50±0.04
3	3	5	3.5	367.41±2.54	0.349±0.004	71.11±1.11	3.18±0.01
4	3	3	2	365.62±3.65	0.219±0.001	78.84±1.52	3.29±0.05
5	2	3	3.5	164.32±2.37	0.266±0.002	65.58±1.06	3.02±0.06
6	2	5	2	113.14±2.75	0.142±0.003	78.72±1.72	3.11±0.03
7	1	1	3.5	345.06±3.68	0.345±0.002	41.73±1.55	2.55±0.06
8	3	1	3.5	387.27±4.12	0.335±0.007	52.46±2.12	3.29±0.02
9	1	5	3.5	50.24±1.43	0.132±0.004	63.07±2.18	3.05±0.07
10	**2**	**3**	**5**	**102.66±1.45**	**0.217±0.002**	**77.53±1.06**	**4.20±0.02**
11	3	3	5	220.66±2.35	0.287±0.006	82.41±1.49	3.35±0.06
12	1	3	2	84.52±1.53	0.223±0.007	55.65±1.23	2.48±0.08
13	2	1	5	76.60±1.82	0.207±0.002	80.43±1.93	4.59±0.10

14	2	3	3.5	75.27±1.29	0.198±0.005	66.12±1.15	3.08±0.08
15	2	3	3.5	88.12±2.40	0.212±0.004	64.40±1.25	3.05±0.06

Values are presented as mean±SD (n=3).

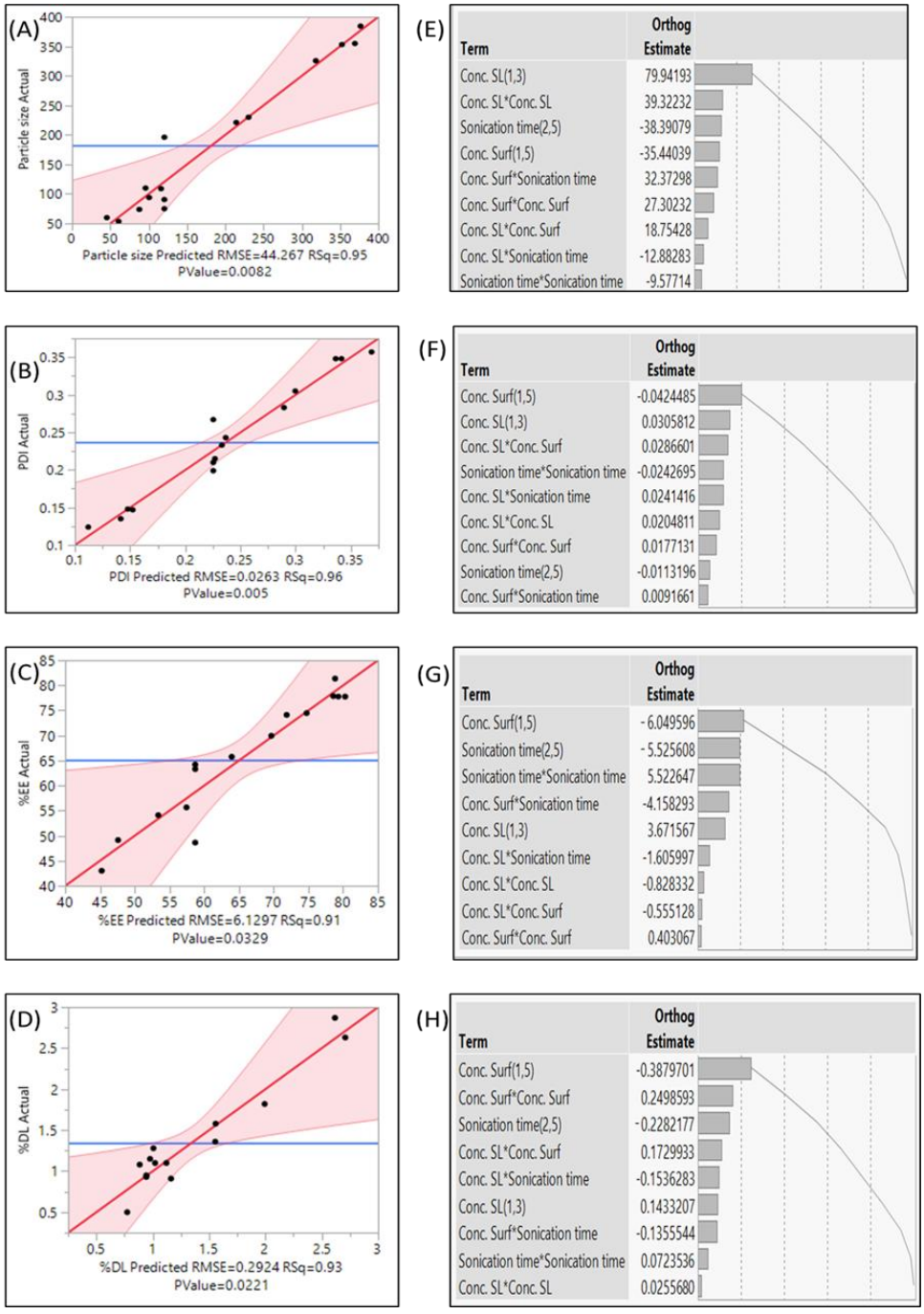

Figure 4. 7: Actual by predicted plot for (A) PS (B) PDI (C) % EE and (D) % DL of DOC–SLNs and Pareto plot analysis based on their influence on (E) PS (F) PDI (G) % EE and (H) % DL

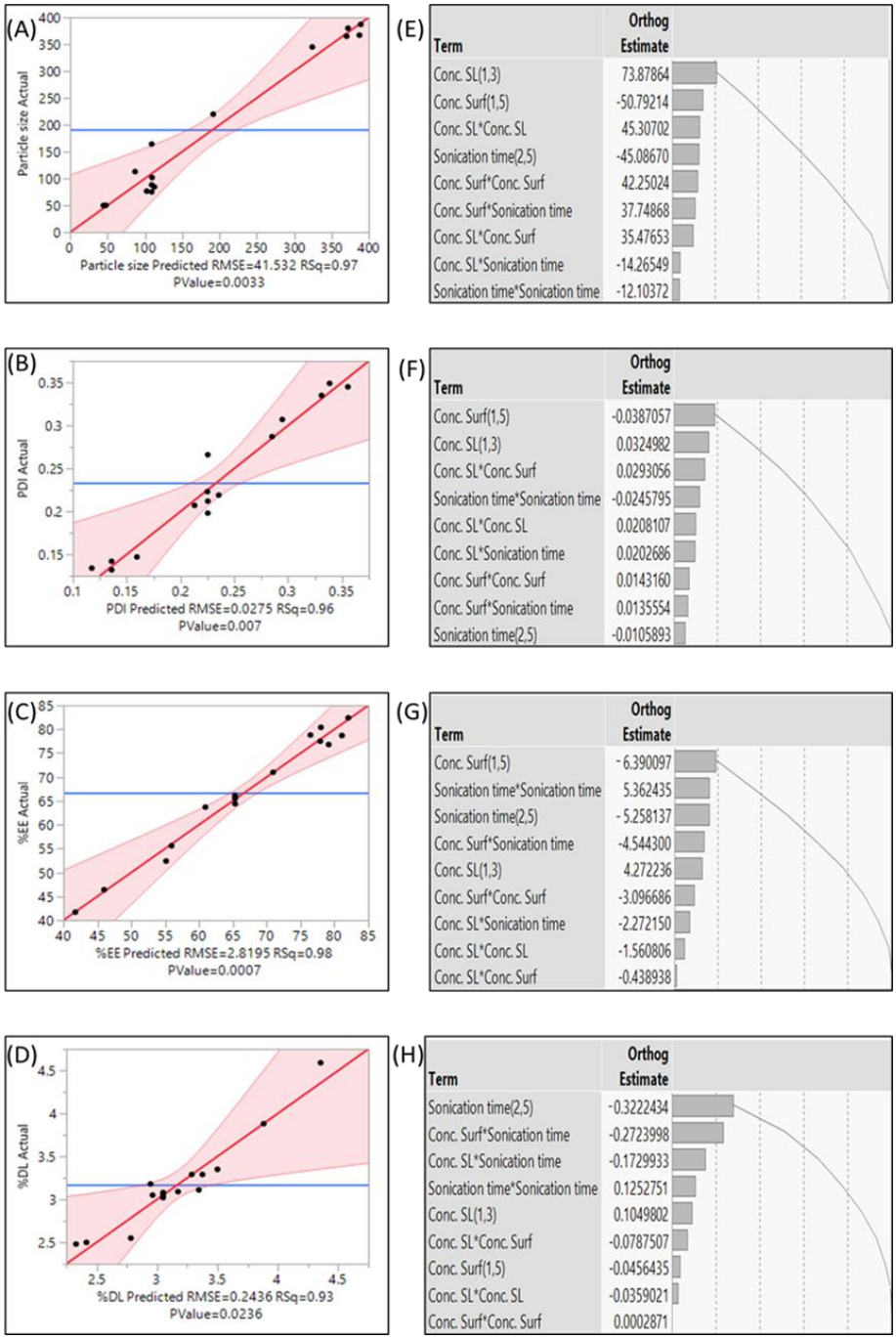

Figure 4. 8: Actual by predicted plot for (A) PS (B) PDI (C) % EE and (D) % DL of ERL–SLNs and Pareto plot analysis based on their influence on (E) PS (F) PDI (G) % EE and (H) % DL

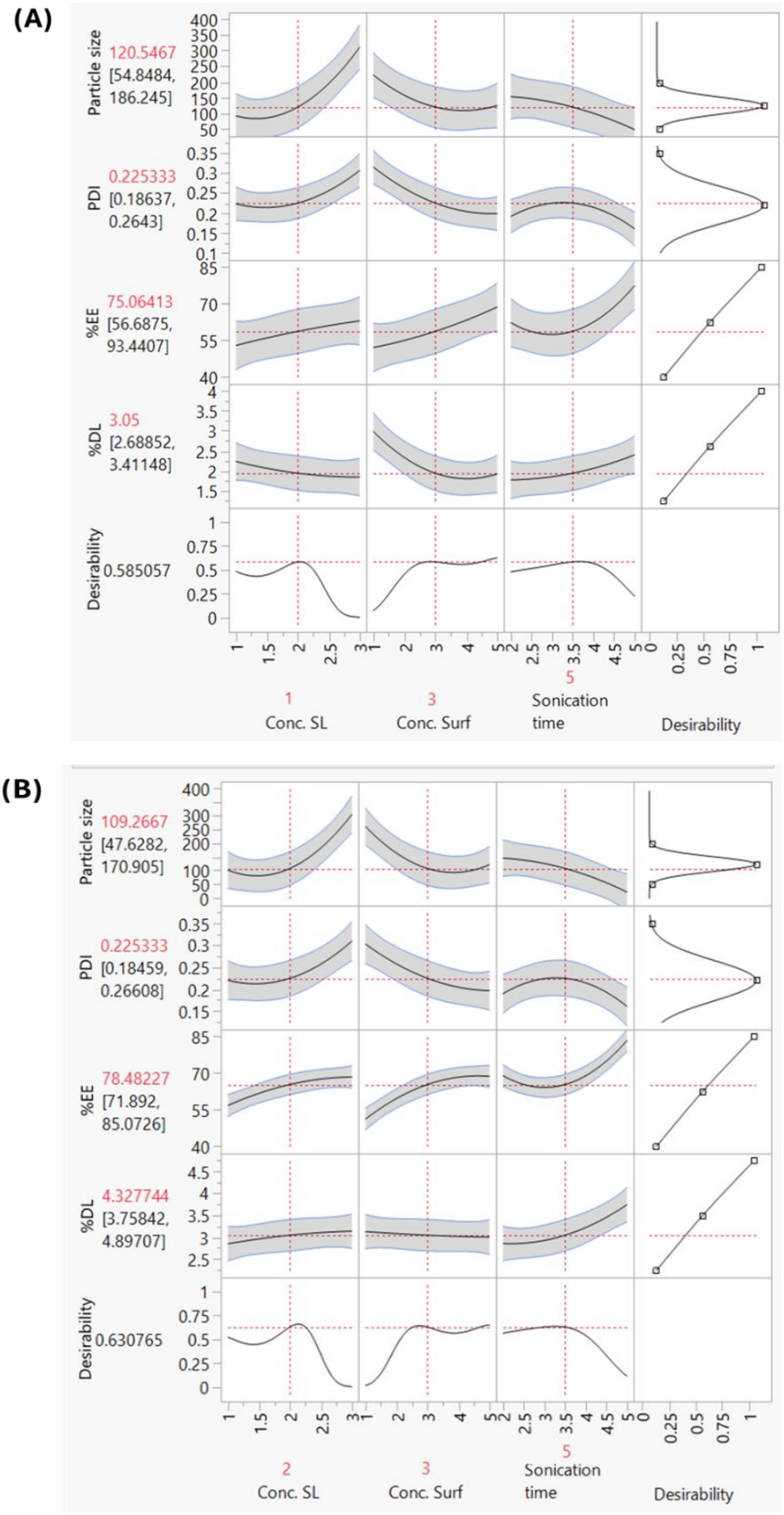

Figure 4. 9: Prediction profiler depicting the maximum desirability at 95 % confidence level for DOC–SLNs (A), and ERL–SLNs (B) revealing the influence of selected factors on responses

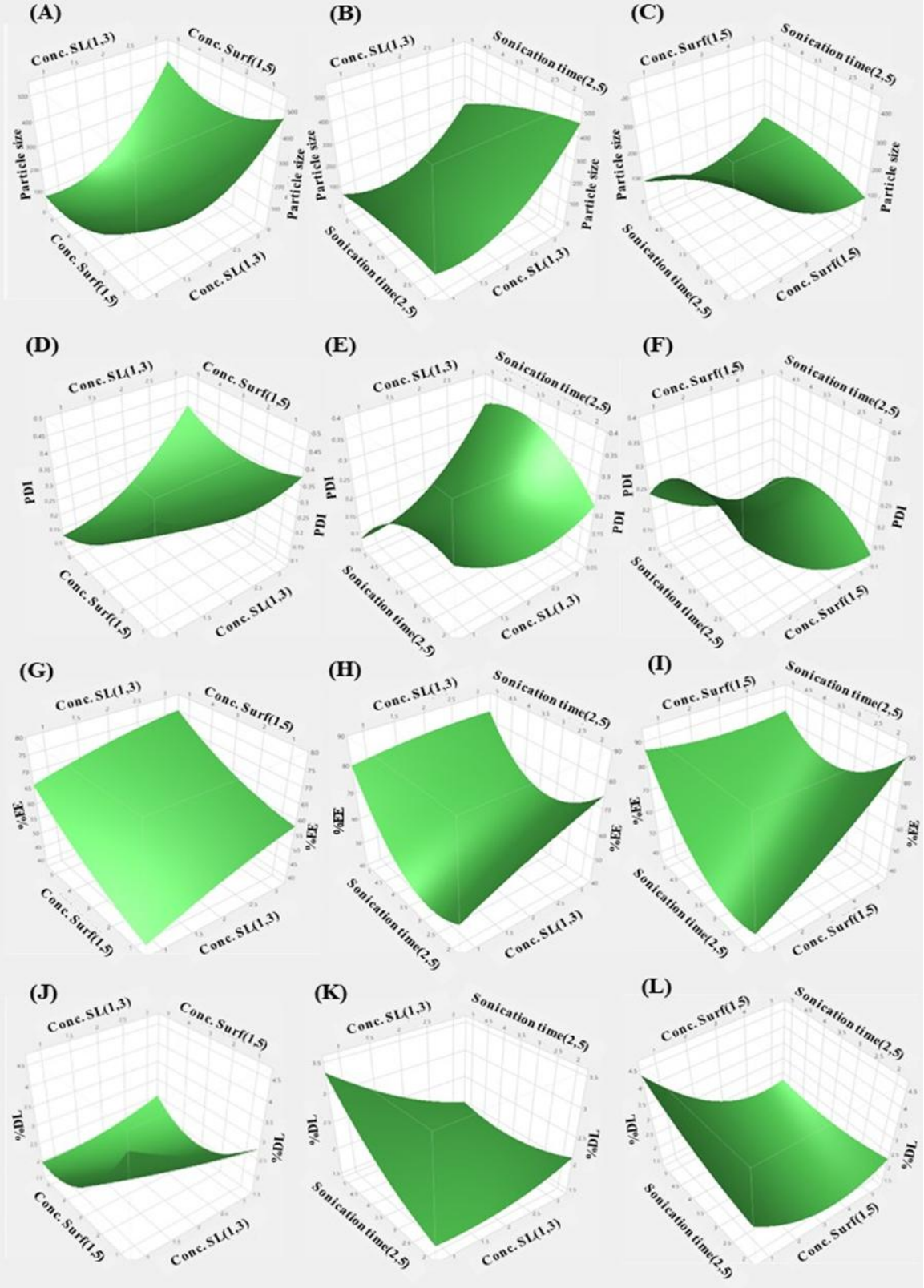

Figure 4. 10: 3D response surface plot representing the influence of factors on PS (A–C), PDI (D–F), % EE (G–I), and % DL (J–L) for DOC–SLNs

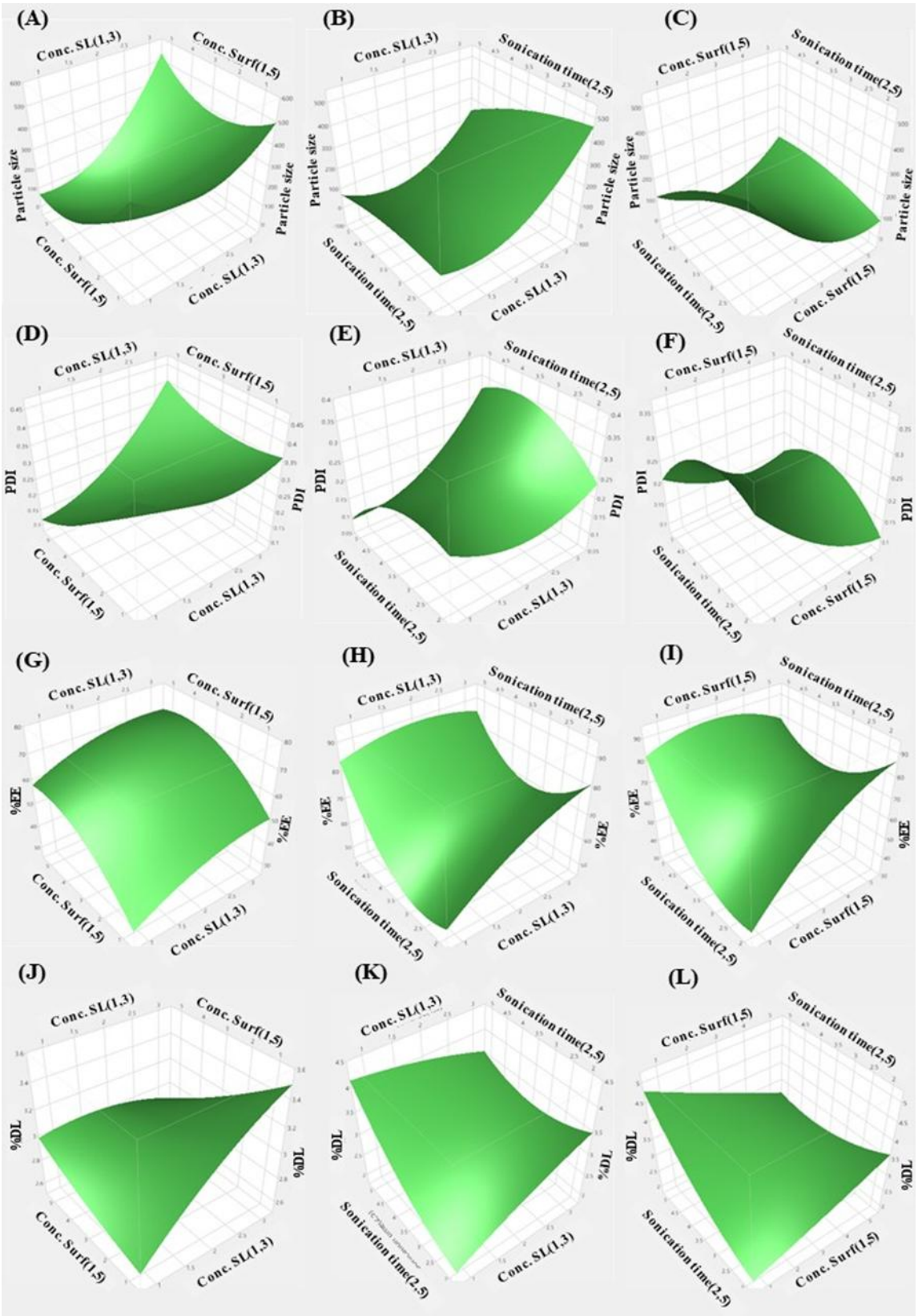

Figure 4. 11: 3D response surface plot representing the influence of factors on PS (A–C), PDI (D–F), % EE (G–I), and % DL (J–L) for ERL–SLNs

Table 4. 9: Model validation of Box Behnken Design

Formulation	Conc. SL (%w/v)	Conc. Surf (%w/v)	Sonication time (min)	Actual by predicted	Particle size (nm)	PDI	EE (%)	DL (%)
DOC–SLNs	1	3	5	Predicted	120.55	0.225	75.06	3.05
				Actual	118.42	0.212	73.47	3.15
				Pred. error	1.76	5.77	2.12	3.17
ERL–SLNs	2	3	5	Predicted	109.26	0.225	78.48	4.32
				Actual	102.66	0.217	77.50	4.20
				Pred. error	6.02	3.55	1.25	2.78

From the Pareto plots, and response surface plots obtained from the BBD, it was observed that as solid lipid conc. increases, the PS of SLNs also increases. It was inferred that high solid lipid contents enhance the chances of particle contact and subsequent aggregation. The lower conc. of surfactant failed to cover the surface of SLNs, as a result, the interfacial tension gets higher resulting in particle aggregation. However, higher concentration leads to bridging between nanoparticles and can cause toxicity. In addition, an increase in sonication time reduces the PS due to increased mechanical stress within the particles. A similar analysis was found while evaluating the effect of solid lipid concentration, surfactant concentration, and sonication time over PDI. A higher concentration of solid lipids offers a spare space within the lipid core to accommodate an excess amount of drugs during the preparation of SLN. This results in a decreased diffusion rate of the drugs from the internal phase to the external phase as the viscosity of the lipid phase is higher, thus exhibiting a higher EE and DL. However, an increase in surfactant concentration results in increased partitioning of drugs into the external phase leading to a decrease in EE and DL. Similarly, an increase in sonication time increases the kinetic energy which may force the drugs out into the aqueous media, thereby decreasing the EE and DL. Also, the increase in sonication time decreases the PS, which eventually limits the space within the lipid core, thereby

decreasing the EE and DL. The results agreed with the studies performed by Badawi *et al*., 2020 [126].

4.3.3.3. Surface functionalization of SLNs with folic acid

The folic acid–stearic acid conjugate (FA–SA) was formed which was further confirmed by FTIR (Figure 4. 12), with the presence of an amide bond in the FA–SA conjugate, which was absent in the physical mixture of folic acid and stearic acid (FA+SA).

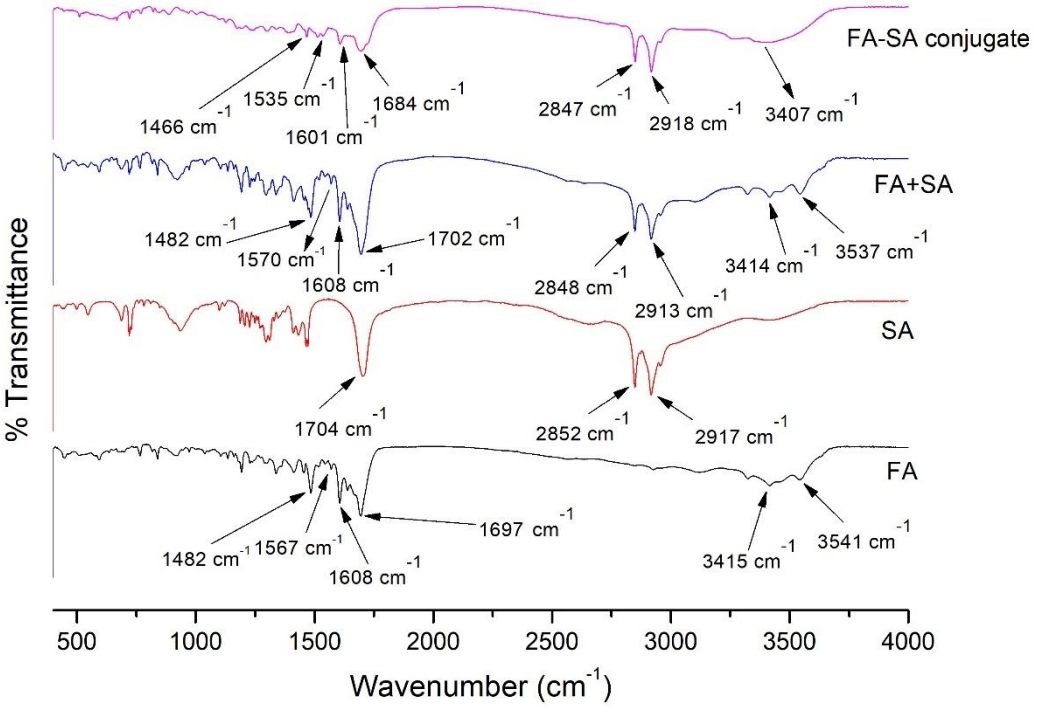

Figure 4. 12: FTIR spectra of folic acid (FA), stearic acid (SA), physical mixture of FA, and SA (FA+SA), and conjugated FA, and SA (FA–SA)

Further, the FTIR spectra of FA–SA, different SLN dispersions, and FA–conjugated SLN dispersions were obtained. FA–SA exhibited C=O stretching vibrations (amide I band), C–N stretching and N–H bending vibrations (2° amide II band), and NH stretching vibrations (amide A band) at 1684, 1535, and 3407 cm^{-1}, respectively. The stated bands of amide linkage appeared in FA–DOC–SLNs, and FA–ERL–SLNs, but were absent in DOC–SLNs, and ERL–SLNs, which suggested the successful conjugation of FA onto the surface of SLNs (Figure 4. 13).

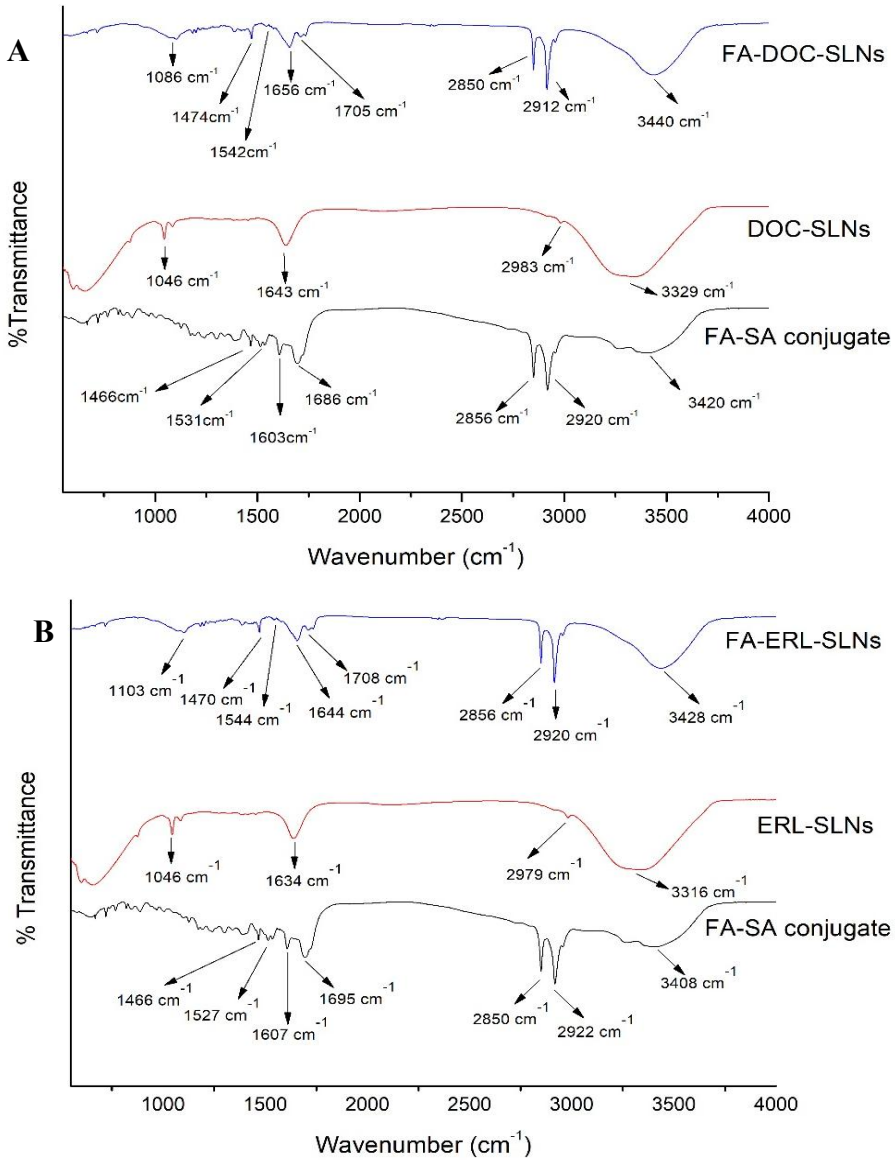

Figure 4. 13: FTIR spectra of folic acid functionalized DOC–SLNs (A), and ERL–SLNs (B)

4.3.4. Characterization of the optimized SLNs

4.3.4.1. Particle size, polydispersity index, zeta potential, morphology, % entrapment efficiency, and % drug loading

The PS, PDI, ZP, % EE, and % DL of different SLNs formulations are shown in Table 4. 10. Morphology was further determined by TEM (Figure 4. 14. II (A–D)), and AFM (Figure 4. 14. III (A–D)), which revealed that the particles formed are spherical, and were found to be in good correlation with the size obtained by DLS (Figure 4. 14. I (A–D)).

Table 4. 10: Critical quality attributes of the optimized nanoformulations

Parameters	PS (nm)	PDI	ZP (mV)	EE (%)	DL (%)
DOC–SLNs	118.42±2.20	0.212±0.006	-15.33±0.59	73.47±1.11	3.15±0.06
FA–DOC–SLNs	128.33±2.65	0.250±0.005	-12.26±0.22	73.16±1.45	3.17±0.05
ERL– SLNs	102.66±1.45	0.217±0.002	-14.57±0.32	77.53±1.06	4.20±0.02
FA–ERL–SLNs	125.40±3.22	0.245±0.001	-11.44±0.15	78.84±1.53	4.16±0.04

Values are presented as mean±SD (n=3).

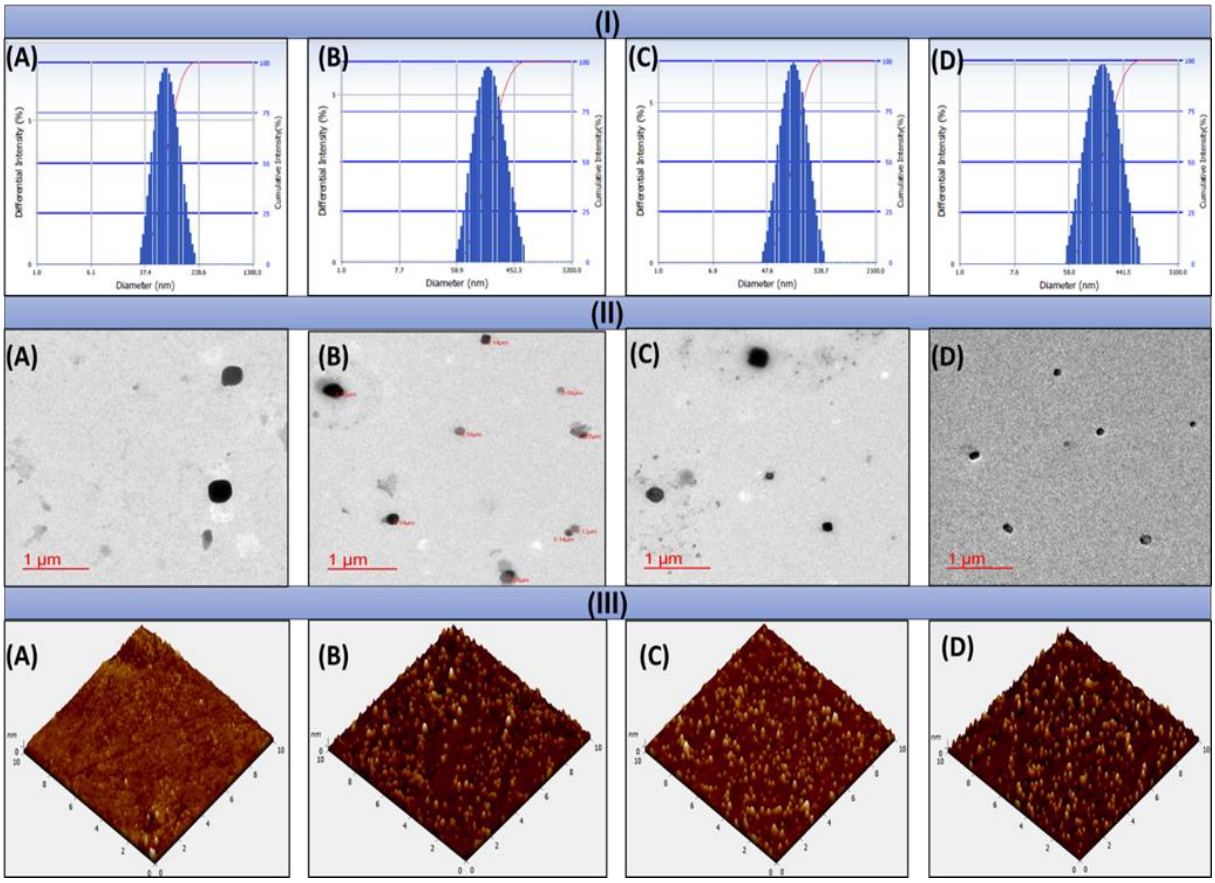

Figure 4. 14: Size and morphology determination using (I) Zeta sizer, (II) TEM, and (III) AFM of DOC–SLNs (A), FA–DOC–SLNs (B), ERL–SLNs (C), and FA–ERL–SLNs (D)

Tween 20 is a non–ionic surfactant, the lipid matrices used in the SLNs might be the source of the negative surface charges. The ionization of the long alkyl chain fatty acids of the various glycerides of the solid lipids explains the negative surface charges of SLNs. A similar result was observed by Banerjee *et al*., 2018 [127]. On conjugating the SLNs with FA, the ZP is slightly reduced, because, during conjugation, a long alkyl chain of the fatty

acids (ionized form) on the end of different glycerides of the solid lipids was consumed by FA [128]. A slight increase in the PS of the FA–SLNs occurs due to the rearrangement of the outer surface of the SLNs, because of the FA conjugation, which eventually resulted in a slightly broader particle size distribution, as compared to the unconjugated SLNs. The TEM images showed the monodispersed and spherical SLNs, and FA–SLNs, which were found to be per DLS results. The results obtained agreed with the study performed by De *et al*., 2023 [129].

4.3.4.2. Lyophilization studies

To maintain the long–term storage stability of the nanoformulations, they were lyophilized using cryoprotectants. The effect of lyophilization on the quality attributes of the SLNs is shown in Table 4. 11. It was found that based on the re–dispersity index and re–dispersity score, trehalose was selected as the cryoprotectant. On further optimizing the different concentrations of trehalose, it was found that 7.5% w/v showed a re–dispersity index close to 1. It was further observed that at lower concentrations, the re–dispersity index was increased ($p<0.05$), whereas, at higher concentrations, an insignificant difference was observed in the particle size between the freshly prepared and the lyophilized ones ($p>0.05$) (Table 4. 12).

Table 4. 11: Preliminary screening of different cryoprotectants based on re–dispersity index, and re–dispersity score for lyophilization of different SLNs

	DOC–SLNs			**FA–DOC–SLNs**			**ERL–SLNs**			**FA–ERL–SLNs**		
	PS (nm)	Ri = (Sf/Si)	RS	PS (nm)	Ri = (Sf/Si)	RS	PS (nm)	Ri = (Sf/Si)	RS	PS (nm)	Ri = (Sf/Si)	RS
Ini. Size	118.42 ±2.36	-	-	128.33 ±2.65	-	-	102.66 ±1.45	-	-	125.40 ±3.32	-	-
D	241.73 ±2.43	2.04 ±0.13	**	318.28 ±4.10	2.48 ±0.20	**	271.31 ±2.16	2.64 ±0.19	**	348.74 ±3.28	2.78 ±0.16	**
S	312.14 ±3.24	2.63 ±0.17	**	328.34 ±1.25	2.56 ±0.12	**	302.81 ±2.14	2.94 ±0.21	**	351.63 ±2.52	2.80 ±0.05	**
T	**162.42 ±2.06**	**1.37 ±0.21**	***	**195.15 ±2.42**	**1.52 ±0.23**	***	**184.13 ±2.21**	**1.79 ±0.27**	***	**204.33 ±3.17**	**1.63 ±0.17**	***
M	211.14 ±3.21	1.78 ±0.15	**	252.34 ±2.27	1.96 ±0.16	**	282.21 ±3.27	2.75 ±1.29	**	318.38 ±3.51	2.54 ±0.06	**

F	224.21 ±2.68	1.89 ±0.18	**	251.36 ±2.17	1.95 ±0.27	**	241.73 ±2.49	2.35 ±0.17	**	267.34 ±2.42	2.13 ±0.14	**

Ri: re–dispersibility index; RS: re–dispersity score; D: Dextrose; S: Sucrose; T: Trehalose; M: Mannitol; F: Fructose. ***re-dispersible within 20 s with mild mixing, **re–dispersible within 1 min, *re–dispersion requires vortexing for 2 min. Bold indicates the optimized one. Values are presented as mean±SD (n=3).

Table 4. 12: Optimization of Trehalose concentration based on re–dispersity index and re–dispersity score for lyophilization of different SLNs

	DOC–SLNs			**FA–DOC–SLNs**			**ERL–SLNs**			**FA–ERL–SLNs**		
	PS (nm)	Ri = (Sf/Si)	RS	PS (nm)	Ri = (Sf/Si)	RS	PS (nm)	Ri = (Sf/Si)	RS	PS (nm)	Ri = (Sf/Si)	RS
Ini. Size	118.42 ±2.36	-	-	128.33 ±2.65	-	-	102.66 ±1.45	-	-	125.40 ±3.32	-	-
2.5 %	213.55 ±2.20	1.80 ±0.15	**	234.42 ±3.44	1.83 ±0.12	**	228.38 ±2.54	2.22 ±0.10	**	256.17 ±2.16	2.09 ±0.24	**
5%	162.42 ±2.06	1.37 ±0.21	***	195.15 ±2.42	1.52 ±0.23	***	184.13 ±2.21	1.79 ±0.27	***	202.42 ±2.24	1.61 ±0.15	***
7.5 %	**145.24 ±2.14**	**1.23 ±0.17**	***	**172.52 ±2.34**	**1.34 ±0.11**	***	**153.48 ±1.11**	**1.49 ±0.08**	***	**164.53 ±2.27**	**1.31 ±0.12**	***
10 %	146.62 ±2.18	1.24 ±0.22	***	174.26 ±2.37	1.36 ±0.17	***	154.62 ±1.31	1.51 ±0.16	***	165.89 ±2.47	1.32 ±0.14	***

Ri: re–dispersibility index; RS: re–dispersibility score; ***re–dispersible within 20 s with mild mixing, **re–dispersible within 1 min, *re–dispersion requires vortexing for 2 min. Bold indicates the optimized one. Values are presented as mean±SD (n=3).

Lyophilization creates a protective network around the SLNs and ameliorates their storage stability. However, during lyophilization, the SLNs experience an increase in their PS, which might be due to the change in the surfactant's property, experienced by removing the water molecules, thus leading to slight aggregation. Such amendments can be downplayed in this case by incorporating a suitable cryoprotectant, 7.5 % w/v. Similar observations were found in our previous report [103]. The cryoprotectants are sugars that persist in the amorphous form during lyophilization and get converted to pseudo–hydrated form when dehydrated, thus forming a shield in the form of a network around the SLNs and protecting them against ice crystals [130].

4.3.4.3. Stability studies

The stability of the lyophilized formulations was analyzed following ICH guidelines for providing knowledge regarding the shelf–life of the formulations. The influence of different SLNs over their quality attributes for different storage conditions (temperature and humidity) was analyzed and shown in Table 4. 13. No significant changes ($p>0.05$) were observed in the quality attributes of different SLNs at 4±3°C. However, significant changes ($p<0.05$) were observed in 25±2°C/60±5 % RH and 40±2°C/75±5 % RH.

Table 4. 13: Stability profile of different SLNs in accordance with ICH guidelines

Parameters	Months	DOC–SLNs	FA–DOC–SLNs	ERL–SLNs	FA–ERL–SLNs
4±3°C					
PS (nm)	0	118.42±2.60	128.33±2.65	102.66±1.45	125.40±3.32
	1	119.34±2.15	129.12±2.52	103.54±2.33	125.92±2.61
	3	119.87±2.20	129.63±2.28	104.25±2.15	126.11±2.18
	6	120.65±2.21	130.41±2.16	105.05±2.55	126.32±2.52
PDI	0	0.212±0.006	0.250±0.005	0.217±0.002	0.245±0.001
	1	0.213±0.005	0.251±0.003	0.218±0.003	0.245±0.002
	3	0.214±0.001	0.252±0.007	0.219±0.005	0.246±0.008
	6	0.215±0.003	0.252±0.006	0.219±0.004	0.247±0.002
%EE	0	73.47±1.11	73.16±1.45	77.53±1.06	78.84±1.53
	1	72.67±1.45	72.76±1.64	77.12±1.32	78.58±1.72
	3	72.12±1.58	72.02±1.83	76.83±1.27	77.21±1.42
	6	71.54±1.65	71.66±1.53	75.21±1.47	76.73±1.26
ZP (mV)	0	-15.33±0.59	-12.26±0.22	-14.57±0.81	-11.16±0.76
	1	-15.43±0.24	-12.15±0.21	-13.87±0.15	-10.78±0.15
	3	-15.12±0.11	-11.76±0.24	-13.45±0.21	-10.21±0.26
	6	-14.78±0.23	-11.14±0.31	-13.10±0.28	-9.61±0.30

25±2°C; 60±5 % RH					
PS (nm)	0	118.42±2.60	128.33±2.65	102.66±1.45	125.40±3.32
	1	120.23±3.27	130.43±3.15	110.48±3.59	130.36±3.87
	3	123.13±3.28	132.38±3.64	113.75±4.27	134.11±4.21
	6	125.28±3.43	134.57±3.38	116.53±4.55	137.38±4.58
PDI	0	0.212±0.006	0.250±0.005	0.217±0.002	0.245±0.001
	1	0.215±0.004	0.252±0.002	0.221±0.004	0.249±0.002
	3	0.218±0.006	0.255±0.007	0.225±0.003	0.253±0.007
	6	0.220±0.002	0.258±0.003	0.229±0.006	0.255±0.006
%EE	0	73.47±1.11	73.16±1.45	77.53±1.06	78.84±1.53
	1	71.71±1.53	72.15±1.62	76.55±1.63	77.45±1.68
	3	68.23±1.51	70.44±1.41	75.35±1.52	75.17±1.25
	6	65.34±1.28	67.45±1.37	73.56±1.61	72.41±1.26
ZP (mV)	0	-15.33±0.59	-12.26±0.22	-14.57±0.81	-11.16±0.76
	1	-14.03±0.29	-11.34±0.37	-13.55±0.23	-10.75±0.12
	3	-12.76±0.26	-10.66±0.42	-11.26±0.28	-9.34±0.76
	6	-11.12±0.38	-9.31±0.36	-10.74±0.32	-8.51±0.62
40±2°C; 75±5 % RH					
PS (nm)	0	118.42±2.60	128.33±2.65	102.66±1.45	125.40±3.32
	1	136.14±4.22	140.55±4.18	120.26±4.15	143.53±4.26
	3	142.66±4.68	147.64±4.53	138.65±4.12	151.43±4.48
	6	155.54±4.31	159.48±4.75	145.75±4.38	160.56±4.37
PDI	0	0.212±0.006	0.250±0.005	0.217±0.002	0.245±0.001
	1	0.235±0.004	0.258±0.002	0.235±0.003	0.267±0.002
	3	0.255±0.005	0.279±0.003	0.245±0.007	0.288±0.004

	6	0.275±0.007	0.295±0.006	0.267±0.008	0.298±0.003
%EE	0	73.47±1.11	73.16±1.45	77.53±1.06	78.84±1.53
	1	70.45±1.27	68.45±1.62	72.37±1.16	71.88±1.52
	3	62.27±1.54	60.56±1.21	63.04±1.27	61.55±1.33
	6	56.67±1.75	52.46±1.18	51.22±1.31	54.92±1.25
ZP (mV)	0	-15.33±0.59	-12.26±0.22	-14.57±0.81	-11.16±0.76
	1	-12.65±0.25	-10.58±0.72	-11.47±0.18	-9.66±0.20
	3	-9.16±0.15	-8.47±0.62	-9.55±0.36	-7.15±0.34
	6	-6.53±0.53	-6.58±0.51	-7.62±0.40	-5.73±0.55

Values are presented as mean±SD (n=3)

The lipids in SLNs are a mixture of α and β′ polymorphs. By virtue of kinetic energy (e.g. temperature), the lipids can be converted to β polymorph accompanied by gel formation leading to instability as evaluated by discrepancies in particle size, PDI, and ZP [131]. Thus, at 40±2°C/75±5%RH, SLNs demonstrated poor stability. The SLNs were found stable at 4±3°C and 25±2°C/60±5 %RH for at least six months without compromising the product quality. The observations were found consistent with that of Thiruchenthooran *et al.,* 2022 [132].

4.3.4.4. *In vitro* drug release study

The *in vitro* release profile from different SLNs is demonstrated in figure 4. 15. Maximum drugs were released at pH 5.5, representing tumor microenvironment (~80 %), whereas, ~60 % of drugs were released at pH 7.4, representing the systemic circulation. Further, it was observed that not more than 20 % of drugs were released in gastric pH (pH 1.2). Moreover, the surface functionalization of SLNs with FA showed a decreased release profile at pH 1.2, 6.8, and 7.4, as compared to non–conjugated SLNs, however, the conjugated SLNs showed increased release at pH 5.5, compared to non–conjugated SLNs.

Further, the kinetic model revealed that SLNs follow Higuchi kinetic model, while FA–SLNs follow the Korsemeyer–Peppas model. From the Korsmeyer–Peppas model, it was observed that all the SLNs deliver Fickian drug transport mechanism, whereas FA–SLNs follow non–Fickian transport mechanism (Table 4. 14).

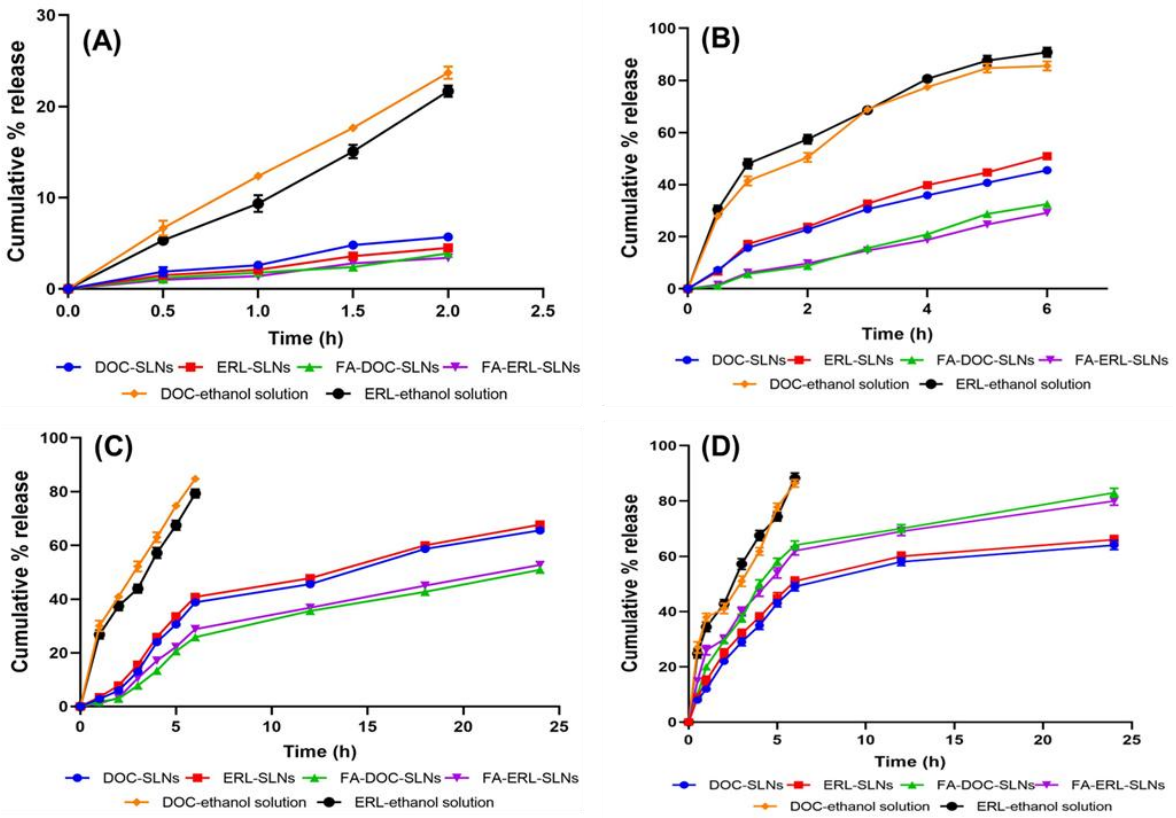

Figure 4. 15: Comparative release profile of DOC–SLNs, ERL–SLNs, FA–DOC–SLNs, FA–ERL–SLNs, DOC–ethanol solution, and ERL–ethanol solution in different simulated biological media: (A) SGF (pH 1.2), (B) SIF (pH 6.8), (C) PBS (pH 7.4), and (D) PBS (pH 5.5). Data are presented as mean±SD (n=3)

Table 4. 14: Kinetic Models for the analysis of release profile

Models	Correlation Coefficient (R^2)			
	DOC–SLNs	ERL–SLNs	FA–DOC–SLNs	FA–ERL–SLNs
Zero order	0.9259	0.9028	0.9191	0.9025
First order	0.9433	0.9348	0.9447	0.9258
Higuchi	**0.9811**	**0.9807**	0.9729	0.9632
Hixon–Crowell	0.9476	0.9311	0.9477	0.9565
Korsmeyer–Peppas (n)	0.9598 (0.3214)	0.9475 (0.3752)	**0.9797** (0.7638)	**0.9772** (0.7641)

The *in vitro* release studies of DOC/ERL loaded SLNs, and FA–DOC/ERL–SLNs were performed at various physiological conditions and tumor microenvironment. The drug release pattern was probably associated with the distribution of drugs in SLNs. SLNs fabricated by hot–melt homogenization method display a uniform distribution of lipids

within the matrix, thereby facilitating a uniform distribution of drugs within SLN's core. It was observed that ~10 % release occurred at pH 1.2 for all formulations, which might be attributed to unentrapped drugs over the SLNs' surface. Moreover, at pH 6.8 and 7.4, the SLNs demonstrated a biphasic release profile where an initial burst release was followed by a sustained release of drugs from the lipid matrix into the release media. Hence, it was revealed that a sustained release profile was observed due to the drug diffusion or matrix erosion for a prolonged period irrespective of the pH of the dissolution media. The results were found in accordance with the studies performed by Velmurugan *et al.,* 2016 [127, 133]. The release study was also performed at pH 5.5 to mimic the tumor microenvironment. The higher drug release at acidic pH was attributed to their basic nature. Further, conjugation decreases the release profile at all pH due to the formation of ligand corona around the nanoparticles. However, a slightly higher release profile was observed from FA–SLNs at pH 5.5, compared to SLNs due to the slight dissociation of folic acid in an acidic environment, attributed to the partial deprotonation of the -COOH group, causing its degradation. The kinetic study demonstrated that the DOC/ERL–SLNs follow the Higuchi model, suggesting that the drugs release from SLNs involve a diffusion process. The study agreed with the findings of Elmowafy *et al.,* 2017 [134]. In contrast, FA–DOC/ERL–SLNs follow the Korsemeyer–Peppas model, which indicates surface erosion–based drug release from the system. A similar model was observed by Sahrayi *et al*., 2022 [135]. Further, the n diffusional exponent of the Korsemeyer–Peppas model revealed that the release mechanism of SLNs is Fickian diffusion, whereas FA–SLNs follow an anomalous (non–Fickian transport). It can be inferred that there is more than one mechanism that controls the release which makes sense considering that surface gatekeepers (functionalization) disassembly impacts drug–matrix interaction. Thus, it was revealed that the release of the drugs predominantly depends on the matrix drug load.

4.3.4.5. *In vitro* lipolysis study

The extent of lipolysis is calculated by the % liberated free fatty acids (% FFA), as shown in figure 4. 16(A). It was found that non–conjugated SLNs showed rapid lipolysis within the first 25 min (67.2±2.8 %), as compared to conjugated SLNs (42.6±3.5 %), followed by slow lipolysis for both the formulations, which extended to 84.2±3.6 %, and 77.6±3.1 % for SLNs, and FA–SLNs respectively within 120 min. Simultaneously, the bioaccessibility of the drugs after the lipolysis was also studied as shown in figure 4. 16(B). It was observed that the bioaccessibility of DOC, and ERL were lowest from the suspension due to their

lipophilic nature, and highest from SLNs. However, surface functionalization was observed to decrease the bioaccessibility of the drugs from the FA–SLNs in the intestinal pH, which was found to be in accordance with their % FFA.

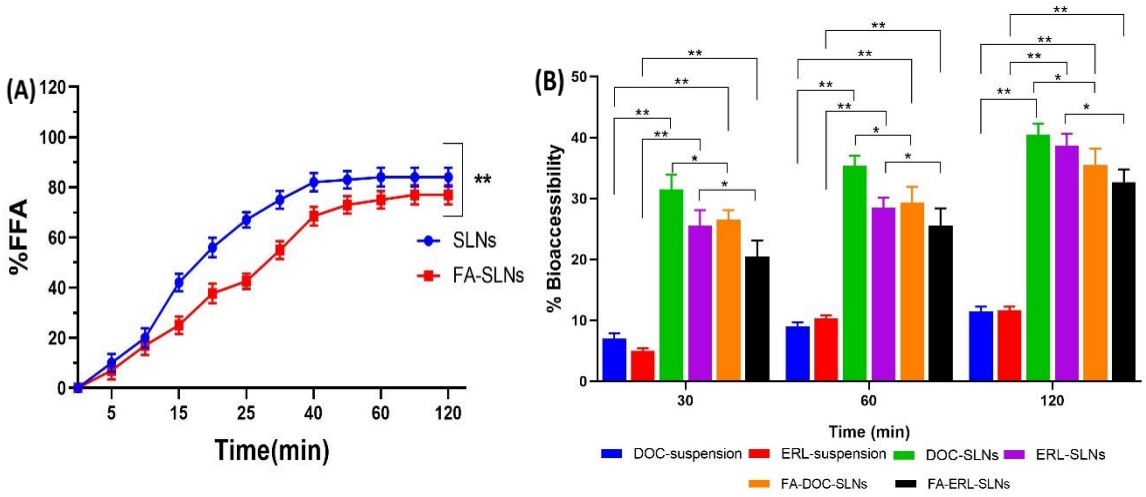

Figure 4. 16: (A) Lipid digestion kinetics from SLNs and FA–SLNs expressed as the % FFA as a function of time. Statistical analysis was performed by a two–tailed paired t–test, and the significance level ** $p<0.01$ (B) Bioaccessibility of DOC, and ERL from different formulations after *in vitro* lipolysis. Data are presented as mean±SD (n=3). Statistical analysis was performed by one–way ANOVA followed by the Tukey P test with multiple comparisons and the significance level *$p<0.05$, and **$p<0.01$

The free fatty acids are released during the digestion of the lipidic preparations, which decreases the pH. These are then maintained by adding NaOH to monitor the kinetics of lipid digestion. The bile salts and phospholipids within the GIT convert the free fatty acids into micelles. Theoretically, these micelles act as a container for lipids and therapeutic agents, which are then collectively transported to epithelium cells for absorption. The SLNs contain Precirol ATO 5 as a solid lipid, a mixture of long–chain triglycerides (C>12). Long chain triglycerides (LCTs) take more time to lipolyze than medium chain triglycerides (MCTs). After digestion, these long chain triglyceride forms a long chain–free fatty acids which will accumulate in the oil–water interface, inhibiting the lipase activity, and slowing the bioaccessibility as evidenced by the data which showed that approximately 30–40 % of the drugs were made bioaccessible. In addition, the lipids within the SLNs are more densely arranged, restricting the access of lipase, and resulting in a decreased rate of lipolysis. However, compared to suspensions, the nanoparticles showed increased bioaccessibility due to improved emulsification and an increase in surface area to volume ratio, which ultimately improved the lipid digestion rate and drug diffusion rate into the micelles formed by bile salts and phospholipids. Less drugs were found bioaccessible from FA–SLNs, as contributed

by the lower availability of the drugs in the aqueous phase due to decreased lipolysis caused by the limited contact of lipidic matrices with the digestive media [136].

4.3.5. *In vitro* cell culture studies

4.3.5.1. MTT assay

Cell viability assay was performed to evaluate the cytotoxicity of different SLNs dispersions in TNBC cells. It was found that in all the incubation periods, the drugs–loaded FA–SLNs showed higher cytotoxicity, compared to drugs–loaded SLNs, followed by free drugs. Furthermore, a significant reduction in IC_{50} ($p<0.01$) of drugs–loaded FA–SLNs, was observed as compared to drugs–loaded SLNs, and free drugs (Figure 4. 17, and 4. 18).

Further, the IC_{50} of the different combinations at 24 h were indicated in table 4. 15

Table 4. 15: IC_{50} values of the combinations in MDA–MB–231, and 4T1 cells

Combinations	IC_{50} values (μM) for 24 h	
	MDA–MB–231	4T1
DOC + ERL	7.46±0.78	8.41±0.42
DOC–SLNs + ERL–SLNs	1.71±0.31	2.01±0.27
FA–DOC–SLNs + FA–ERL–SLNs	0.84±0.07	0.96±0.02

Data are presented as mean±SD (n=3)

Treatment of TNBC cells with DOC, and ERL–loaded nanoformulations showed time and concentration–dependent anticancer effects. The IC_{50} values at respective time frames were found to be in the order of FA–SLNs<SLNs<free drugs, demonstrating the importance of FA conjugation on the SLNs. The cell cytotoxicity assay revealed that surface functionalization of SLNs with FA improved the targetability which resulted in elevated drug concentration within the cells as observed by the significant increase in cell cytotoxicity compared to free drugs and their combination. This was even more obvious when cells were treated with the combination of FA–DOC–SLNs + FA–ERL–SLNs.

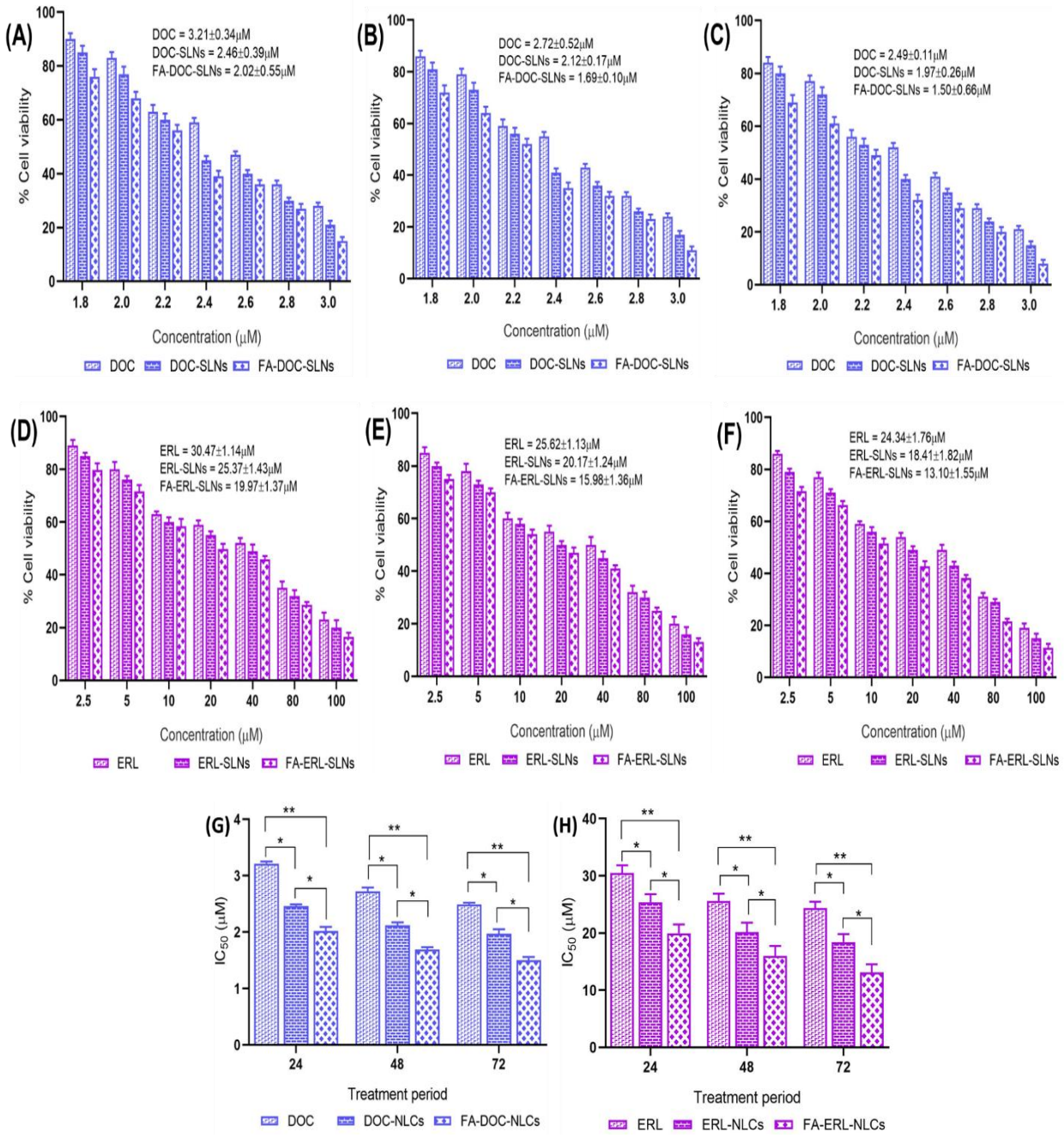

Figure 4. 17: Cell cytotoxicity assay of DOC, DOC–SLNs, and FA–DOC–SLNs in the MDA–MB–231 cell line at 24 h (A), 48 h (B), and 72 h (C), and ERL, ERL–SLNs, and FA–ERL–SLNs at 24 h (D), 48 h (E), and 72 h (F). IC_{50} values of DOC–loaded SLNs (G), and ERL–loaded SLNs (H). Data are presented as mean±SD (n=3). Statistical analysis was performed by one–way ANOVA followed by the Tukey P test with multiple comparisons and the significance level *p<0.05, and **p<0.01

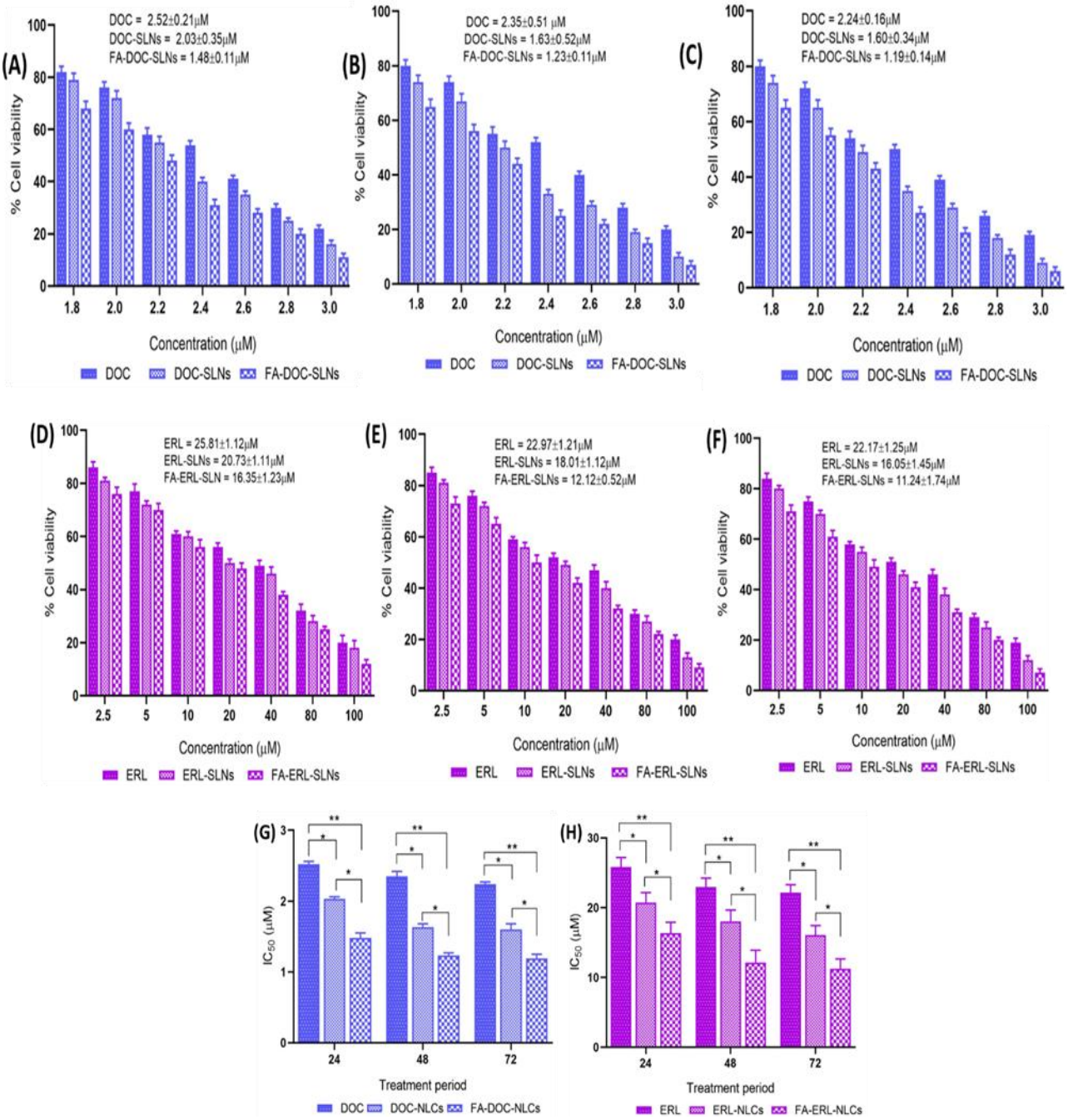

Figure 4. 18: Cell cytotoxicity assay of DOC, DOC–SLNs, and FA–DOC–SLNs in the 4T1 cell line at 24 (A), 48 (B), and 72 h (C), and ERL, ERL–SLNs, and FA–ERL–SLNs at 24 (D), 48 (E), and 72 h (F). IC_{50} values of DOC–loaded SLNs (G), and ERL–loaded SLNs (H). Data are presented as mean±SD (n=3). Statistical analysis was performed by one–way ANOVA followed by the Tukey P test with multiple comparisons and the significance level *p<0.05, and **p<0.01

4.3.5.2. Cellular uptake assay

In the qualitative uptake study, the fluorescent images (Figure 4. 19, and 4. 20) of cells showed significantly enhanced fluorescence with C6 loaded FA–SLNs compared to C6–SLNs, and free C6, which indicates efficient internalization of SLNs by TNBC cells. Once

uptake was confirmed, further quantitative uptake assays were performed. Following the treatment, the uptake increases in a time–dependent manner (Figure 4. 21), with conjugated SLNs showing enhanced uptake, compared to non–conjugated SLNs, followed by free drugs.

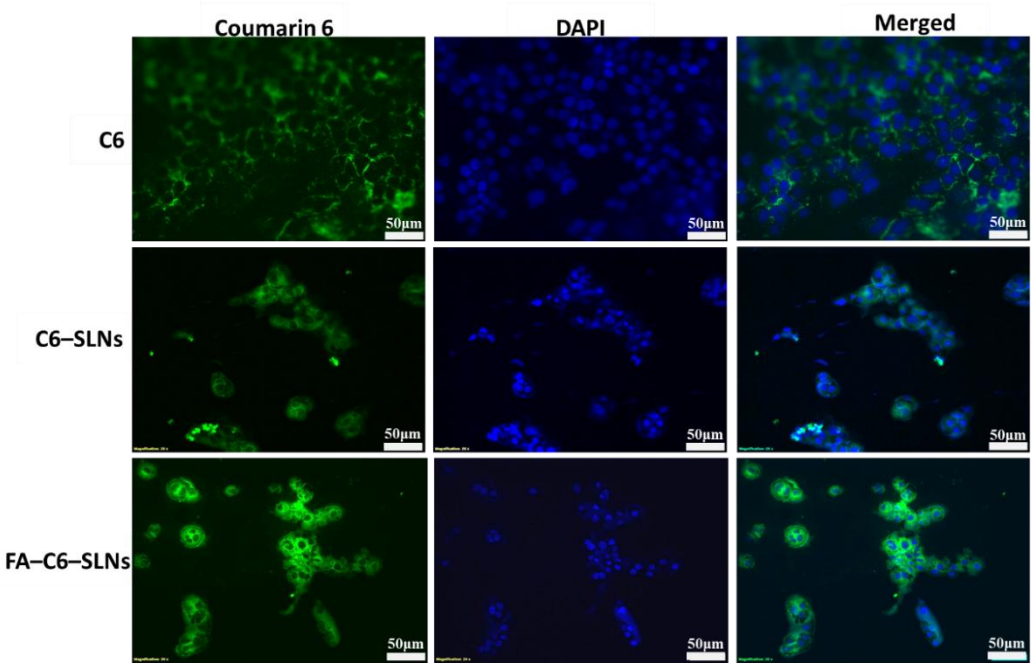

Figure 4. 19: Observation of the qualitative cellular internalization of Coumarin 6 (C6) and various C6 loaded SLNs in MDA–MB–231, as viewed under a fluorescence microscope

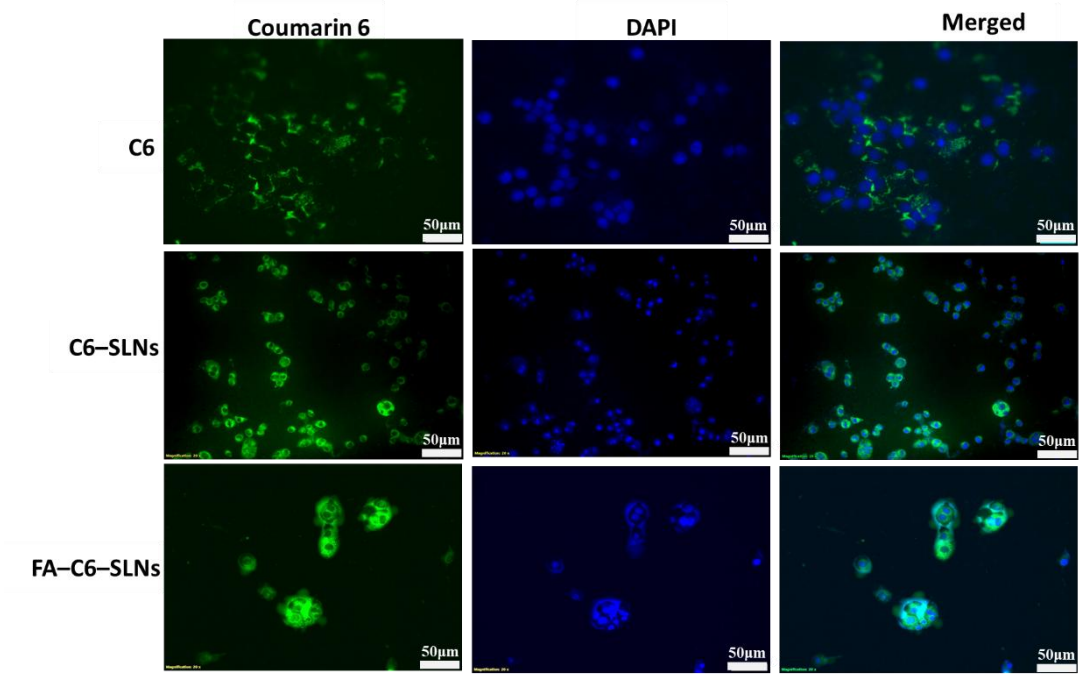

Figure 4. 20: Observation of the qualitative cellular internalization of Coumarin 6 (C6) and various C6 loaded SLNs in 4T1, as viewed under a fluorescence microscope

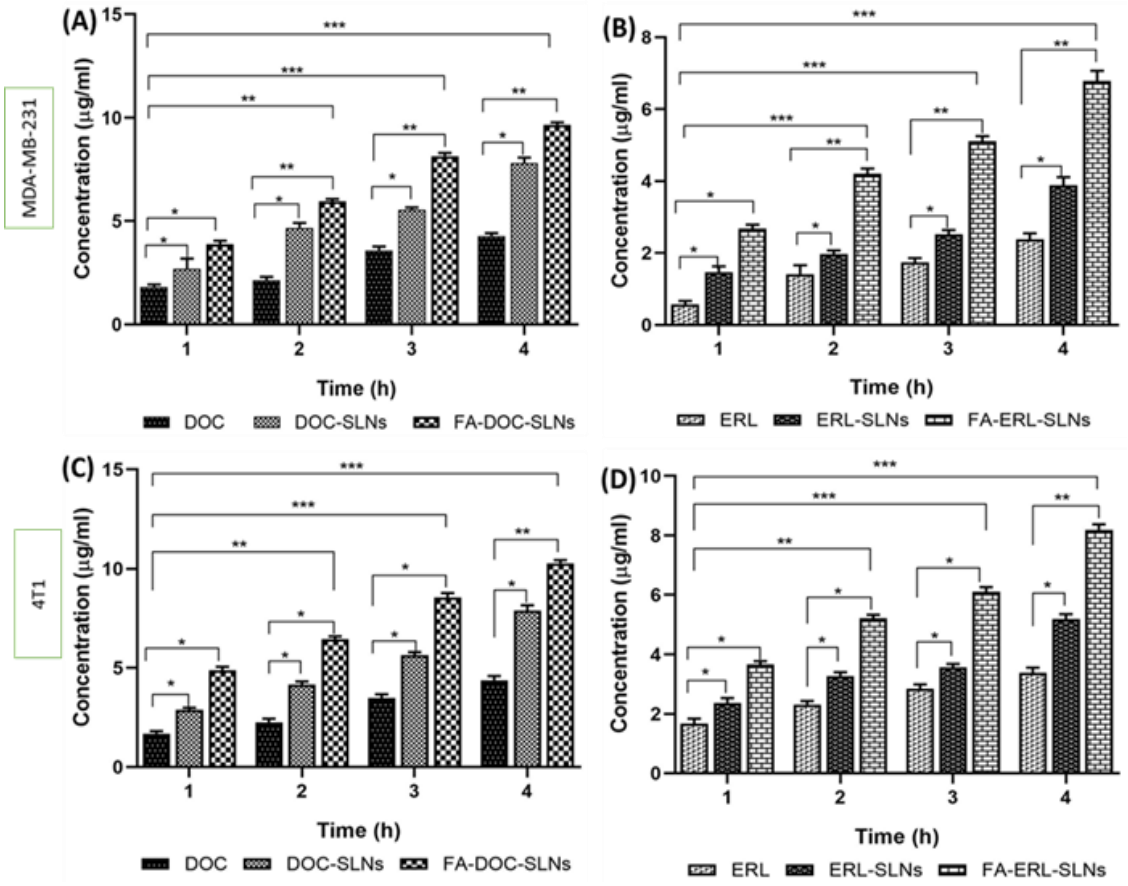

Figure 4. 21: Quantitative analysis of cellular uptake for free drugs, and different SLNs dispersions after an incubation time of 1, 2, 3, and 4 h in TNBC cells indicated statistical significance at *p<0.05, **p<0.01, and ***p<0.001. Data are presented as mean±SD (n=3)

A time–dependent cellular uptake was observed in SLNs for the cancer cells. As DOC, and ERL lack fluorescence properties, they have been substituted by coumarin 6 (C6), owing to its lipophilic nature, in qualitative uptake study. The cellular uptake showed enhanced internalization of FA–SLNs as compared to SLNs. The increased cellular uptake of SLNs compared to free C6 could be associated with their nano size and composition as they are composed of biocompatible and biodegradable solid lipids. Additionally, the augmented fluorescent intensity associated with FA–C6–SLNs in comparison to C6–SLNs is due to an increased cell membrane permeability, and receptor–mediated endocytosis. The findings were analogous to the findings of Garg *et al.,* 2016 [137].

4.3.5.3. Colony formation assay

As shown in figure 4. 22(I), and 4. 23(I), the cells treated with the FA–SLNs combination demonstrated a remarkable decrease in the formation of colonies, compared to other groups in MDA–MB–231, and 4T1 respectively. It was observed that the cells of the control groups were closely packed while in the treatment groups there existed gaps between the cells, with

smaller colonies. Further, the efficacy of treatments in inhibiting colony formation was calculated in terms of % colonies formed, as indicated in figure 4. 22(II), and 4. 23(II) for MDA–MB–231, and 4T1 cell respectively.

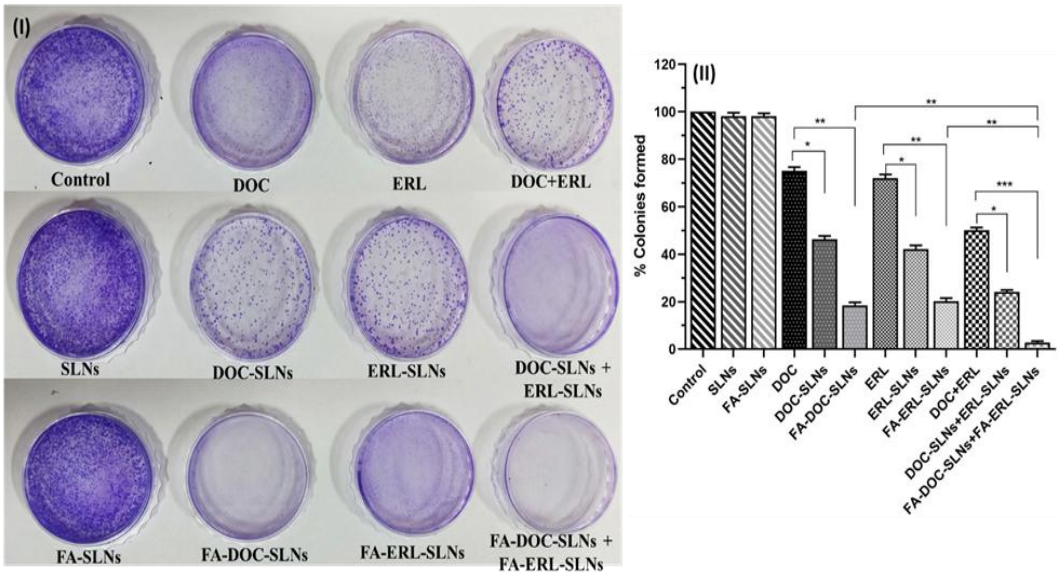

Figure 4. 22: (I) Images of colonies formed after administering various treatments in MDA–MB–231 cells. (II) The statistical data illustrates the proportion of colonies formed from various SLNs dispersions. Data are presented as mean±SD (n=3). Statistical analysis was executed utilizing one–way ANOVA, followed by the Tukey post hoc test for multiple comparisons. The significance levels were represented as follows: *p<0.05, **p<0.01, and ***p<0.001

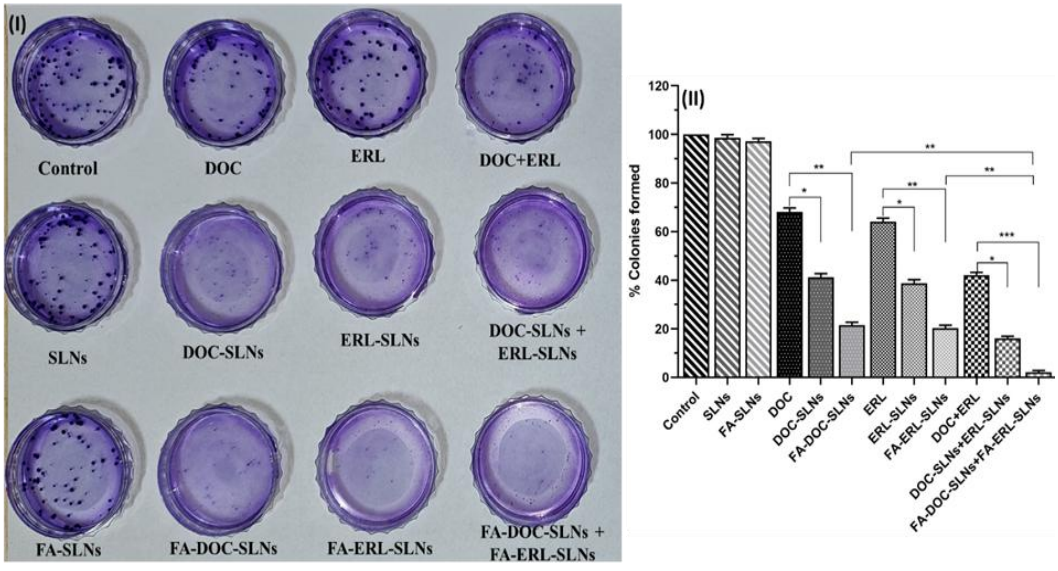

Figure 4. 23: (I) Images of colonies formed after administering various treatments in 4T1 cells. (II) The statistical data illustrates the proportion of colonies formed from various SLNs dispersions. Data are presented as mean±SD (n=3). Statistical analysis was executed utilizing one–way ANOVA, followed by the Tukey post hoc test for multiple comparisons. The significance levels were represented as follows: *p<0.05, **p<0.01, and ***p<0.001

The colony formation assay was performed to understand whether the developed formulations could reduce the colony–forming ability of the TNBC cells. The FA–SLNs combination remarkably inhibited colony formation, which revealed that the FA–SLNs not only offer cytotoxicity but also prevent colony formation in TNBC cells. The results were in accordance with the observations of Ayyanaar *et al.,* 2020 [138].

4.3.5.4. Mitochondrial membrane potential (MMP) assay

Mitochondrial functioning is a key indicator of apoptosis, which can be analyzed by observing alterations in MMP, as it reflects the status of the mitochondria. A reduction in MMP, as evident from reduced JC–1 aggregates (red fluorescence) is associated with apoptosis. Figures 4. 24 (A), and 4. 25(A) showed that the cells treated with FA–SLNs combination demonstrated weak red fluorescence, compared to single SLNs, and control. Figure 4. 24(B), and 4. 25(B) quantifies the fluorescence intensity in MDA–MB–231, and 4T1 respectively.

Depolarization of MMP and loss of electrochemical gradient during cell death contributes to the loss of JC–1 aggregates and accumulation of JC–1 monomers which consequently attenuates the red fluorescence and strengthens the green fluorescence. The FA–SLNs combination exhibited significantly decreased red fluorescence, demonstrating damage to the mitochondria's integrity, reducing the mitochondrial membrane potential, and causing apoptosis. The observations were found in harmony with the findings of Wang *et al.,* 2017 [139].

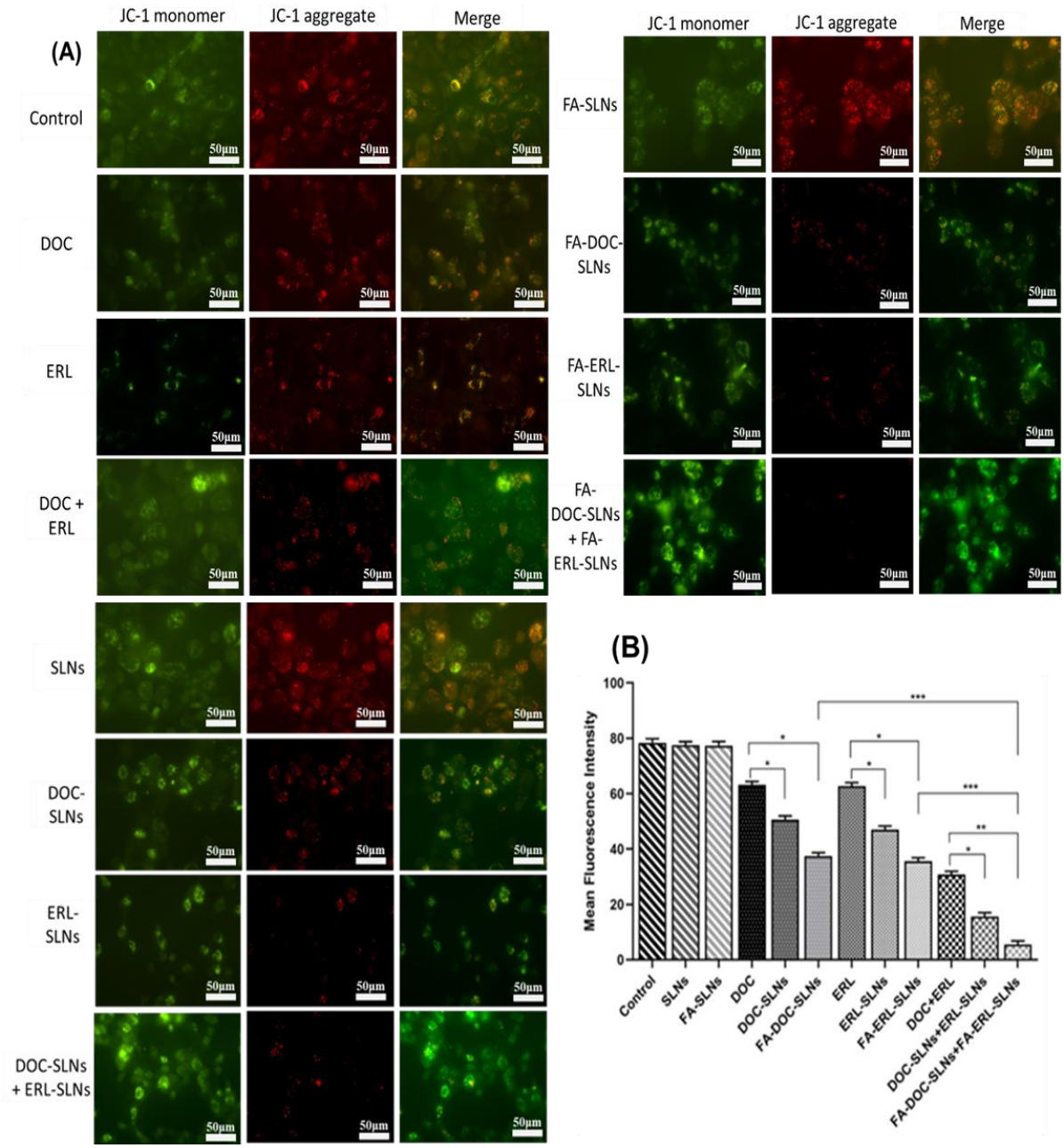

Figure 4. 24: (A) The mitochondrial membrane potential of MDA–MB–231 cells was evaluated subsequent to treatment with various formulations, (B) The mean fluorescence intensity (MFI) of various treatments was evaluated with respect to JC–1 aggregates. Data are presented as mean±SD (n=3). Statistical tests included a one–way ANOVA, complemented by Tukey's post hoc test for multiple comparisons. Significance levels were denoted as *p<0.05, **p<0.01, and ***p<0.001

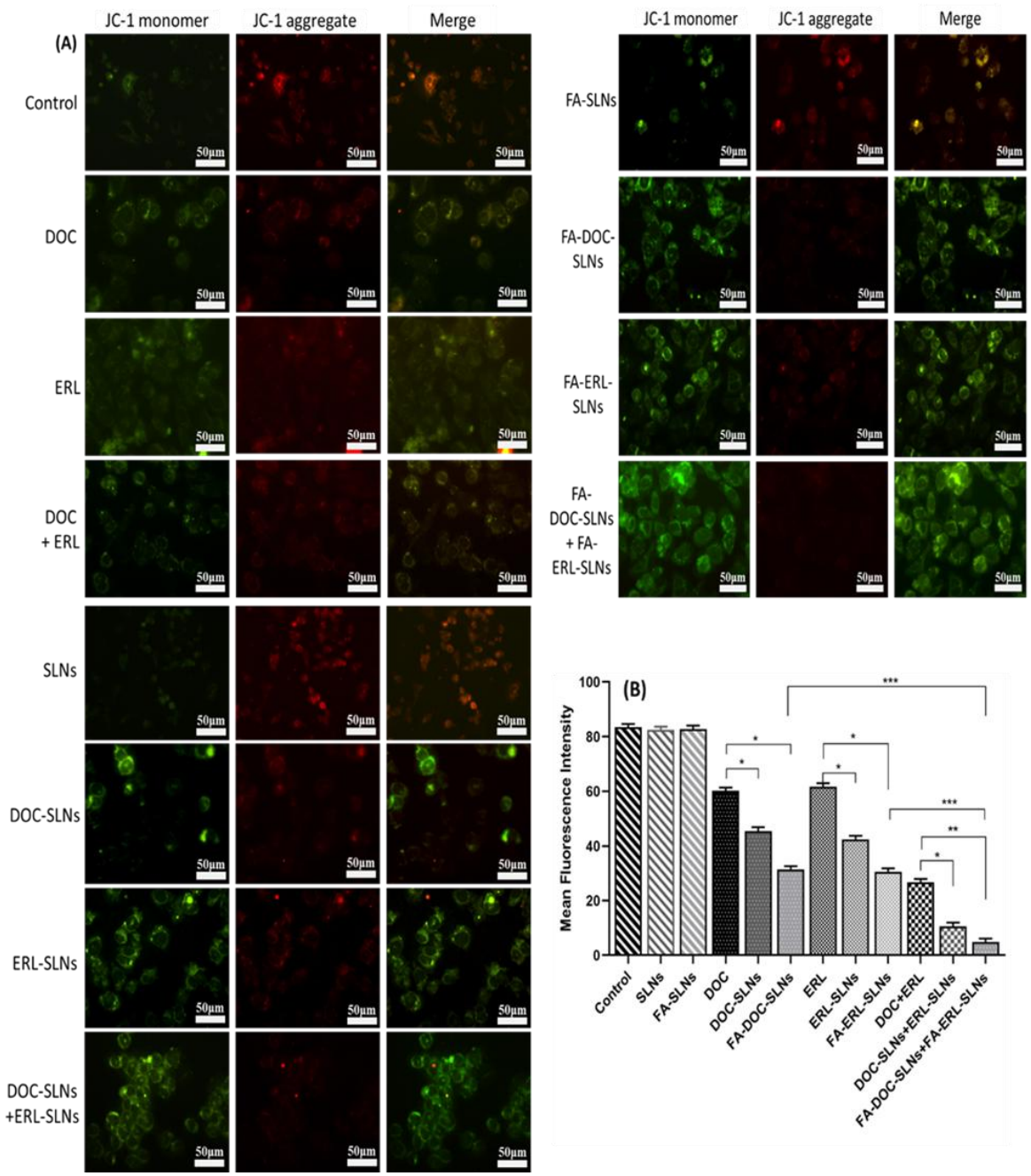

Figure 4. 25: (A) The mitochondrial membrane potential of 4T1 cells was evaluated subsequent to treatment with various formulations, (B) The mean fluorescence intensity (MFI) of various treatments was evaluated with respect to JC–1 aggregates. Data are presented as mean±SD (n=3). Statistical tests included a one–way ANOVA, complemented by Tukey's post hoc test for multiple comparisons. Significance levels were denoted as *p<0.05, **p<0.01, and ***p<0.001

4.3.5.5. Reactive oxygen species (ROS) assay

Drug-induced oxidative stress promotes ROS generation, which is associated with apoptosis, as analyzed by H_2DCFDA dye. H_2DCFDA dye is a non–fluorescent dye, but when exposed to endogenous ROS, primarily hydrogen peroxide (H_2O_2), it oxidizes to fluorescent dichlorofluorescein (DCF), which then emits green fluorescence. As shown in figure 4. 26,

and 4. 27, an enhanced ROS level was observed with FA–SLNs combination as evident from the strong green fluorescence of DCF, compared to SLNs, and control. Also, % ROS production was quantified using flow cytometry, as shown in figures 4. 28 and 4. 29, which supports the fluorescence microscopy results.

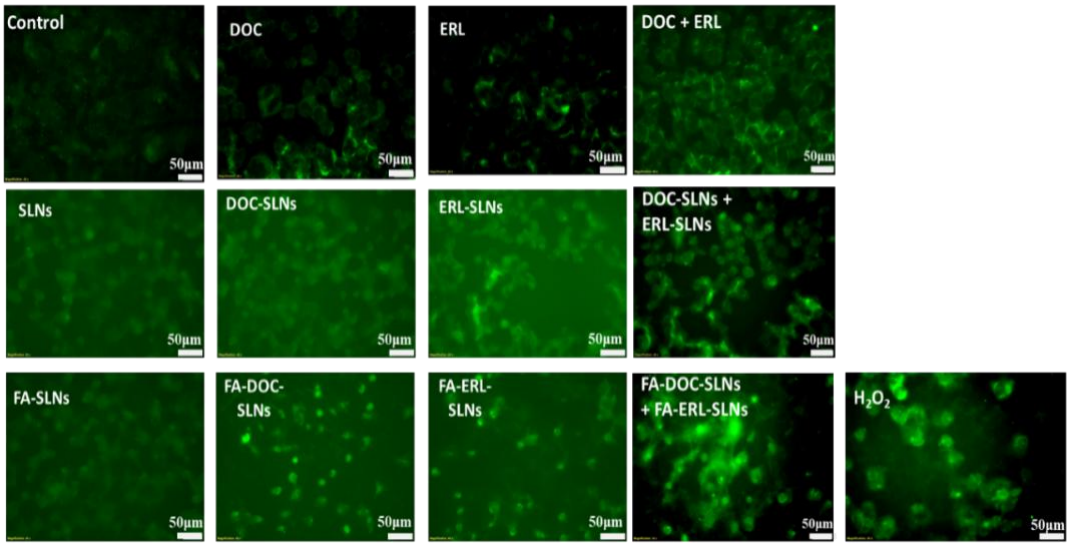

Figure 4. 26: The assessment of ROS was conducted using fluorescence microscopy with H_2DCFDA dye at a concentration of 10 µM. This was performed to evaluate the effects of various treatments in MDA–MB–231 cell lines

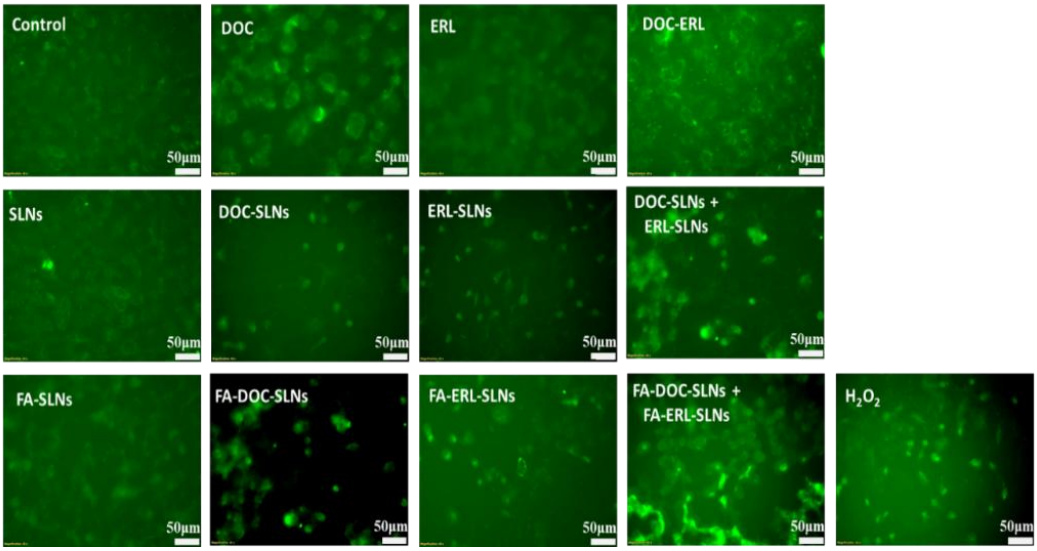

Figure 4. 27: The assessment of ROS was conducted using fluorescence microscopy with H_2DCFDA dye at a concentration of 10 µM. This was performed to evaluate the effects of various treatments in 4T1 cell lines

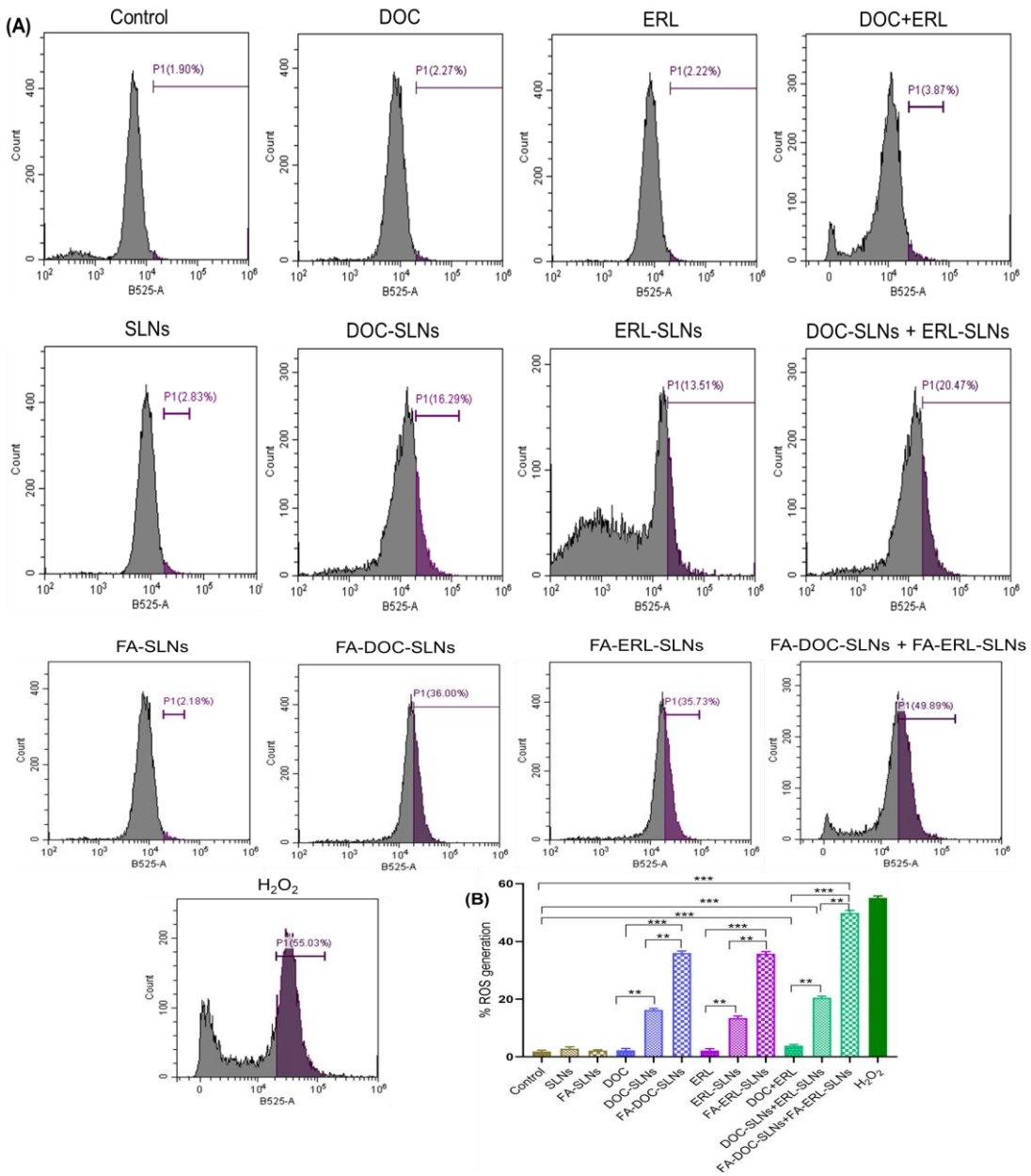

Figure 4. 28: (A) Flow cytometry analyzing the % ROS generation in MDA–MB–231 cell lines. (B) Statistical analysis involved one–way ANOVA followed by the Tukey post hoc test for multiple comparisons. *p<0.05, **p<0.01, and ***p<0.001 indicate significance. Data are presented as mean±SD (n=3).

ROS is a crucial indicator for analyzing cellular antioxidant activities. When ROS excels at the normal level, oxidative stress accumulates damaging the structural integrity of the cancer cells, which further leads to loss of cell functioning and ultimately apoptosis. With the treatment of SLNs, a strong green fluorescence was detected demonstrating that the SLNs accelerate the generation of ROS intracellularly. The findings further revealed that FA–SLNs combination induced massive generation of free radicals in cells, which later destroys the

mitochondrial membranes' integrity by restricting the MMP, thus facilitating the stimulation of the mitochondrial–mediated apoptosis pathway.

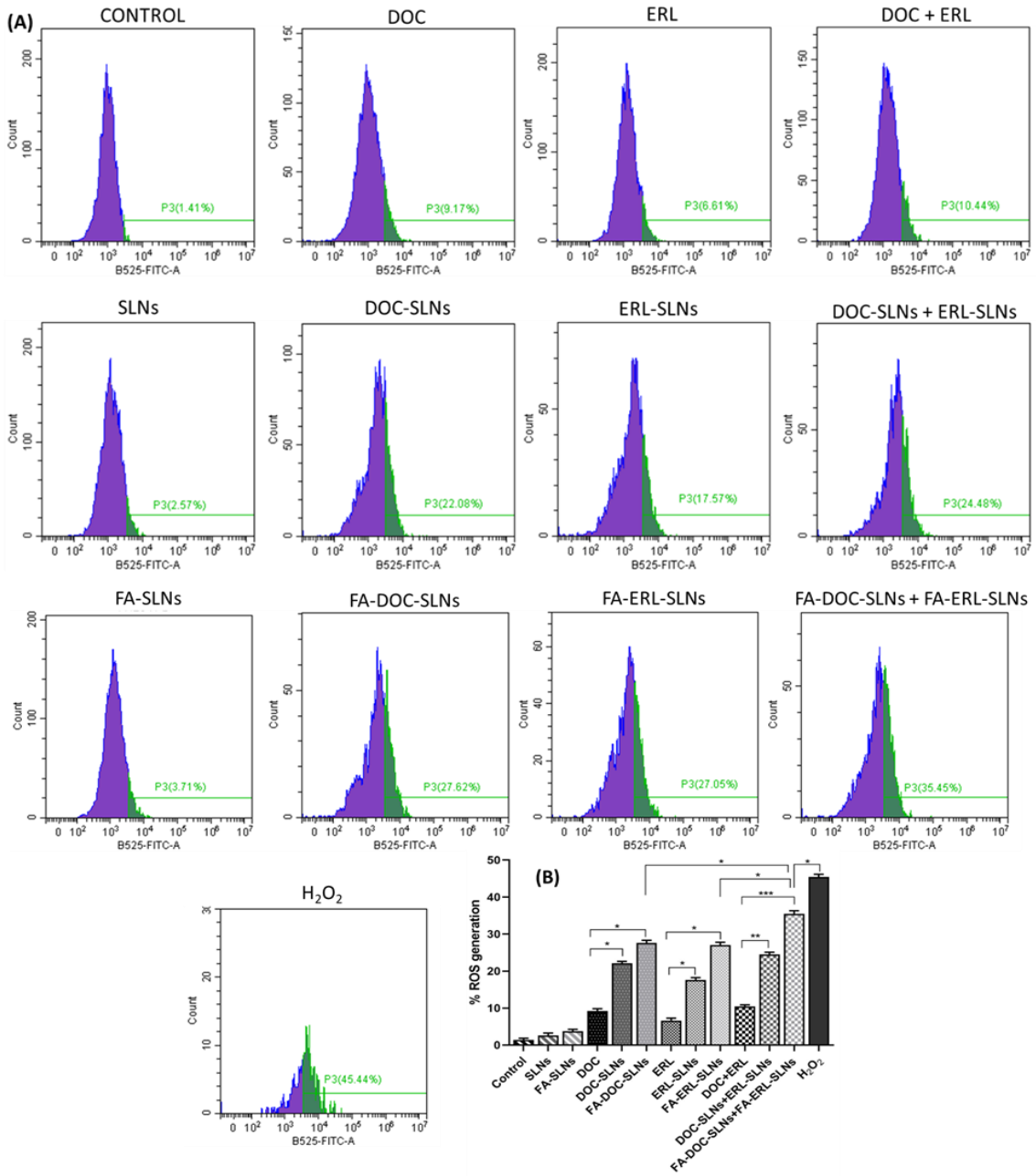

Figure 4. 29: (A) Flow cytometry analyzing the % ROS generation in 4T1 cell lines. (B) Statistical analysis involved one–way ANOVA followed by the Tukey post hoc test for multiple comparisons. *p<0.05, **p<0.01, and ***p<0.001 indicate significance. Data are presented as mean±SD (n=3).

4.3.5.6. Annexin V apoptosis assay

Figures 4. 30 and 4. 31 revealed that cells treated with the FA–conjugated combination treatment indicated increased intensity of red fluorescence as obtained from Annexin Cy3.18, compared to non–conjugated SLNs, and free drugs. Further, the increased apoptosis

by the FA–conjugated combination treatment was justified via a higher apoptosis index of 1.42 for MDA–MB–231, and 1.45 for 4T1 cells.

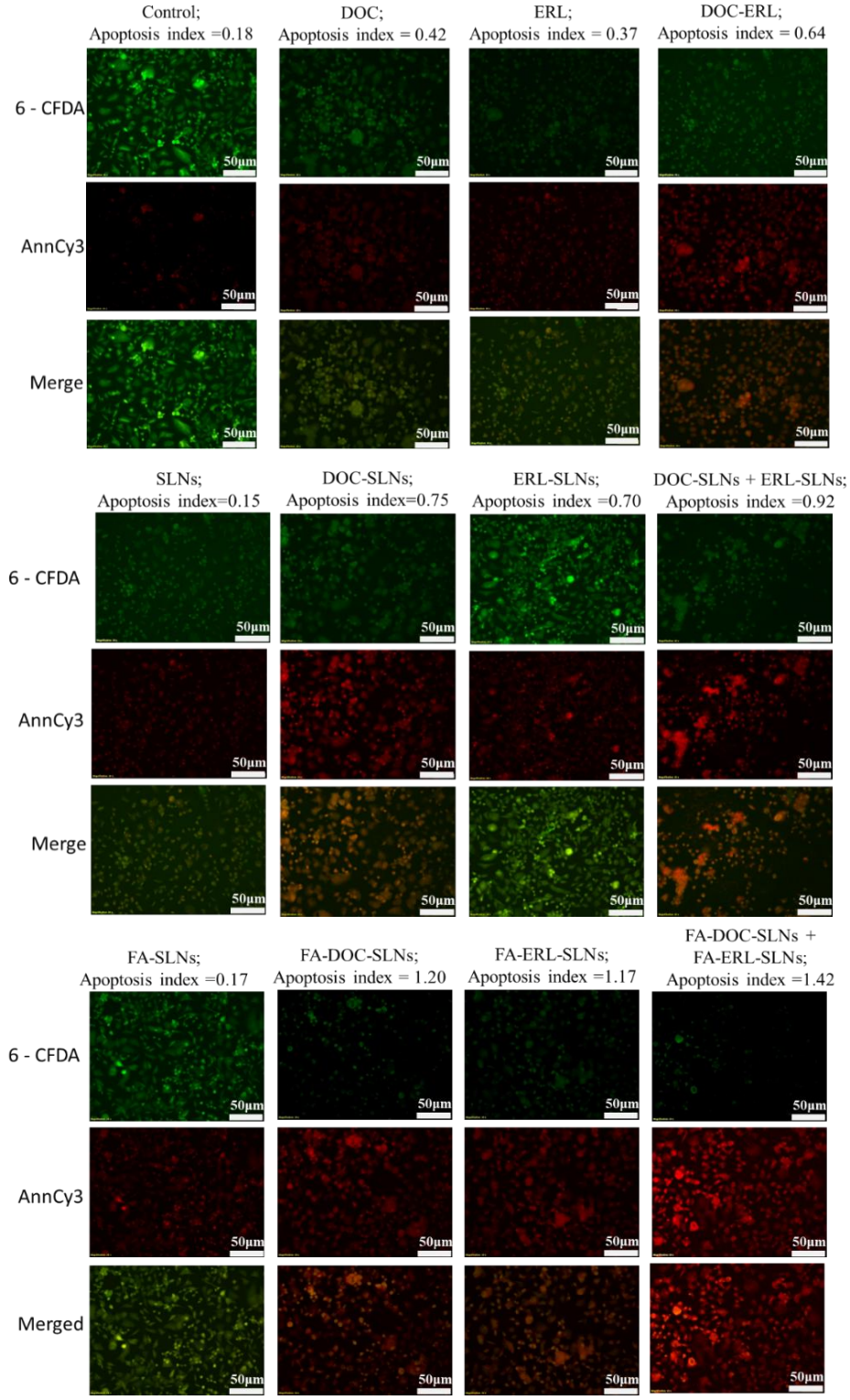

Figure 4. 30: Annexin V–Cy3 staining for detecting apoptosis in MDA–MB–231 cells by different SLNs dispersions

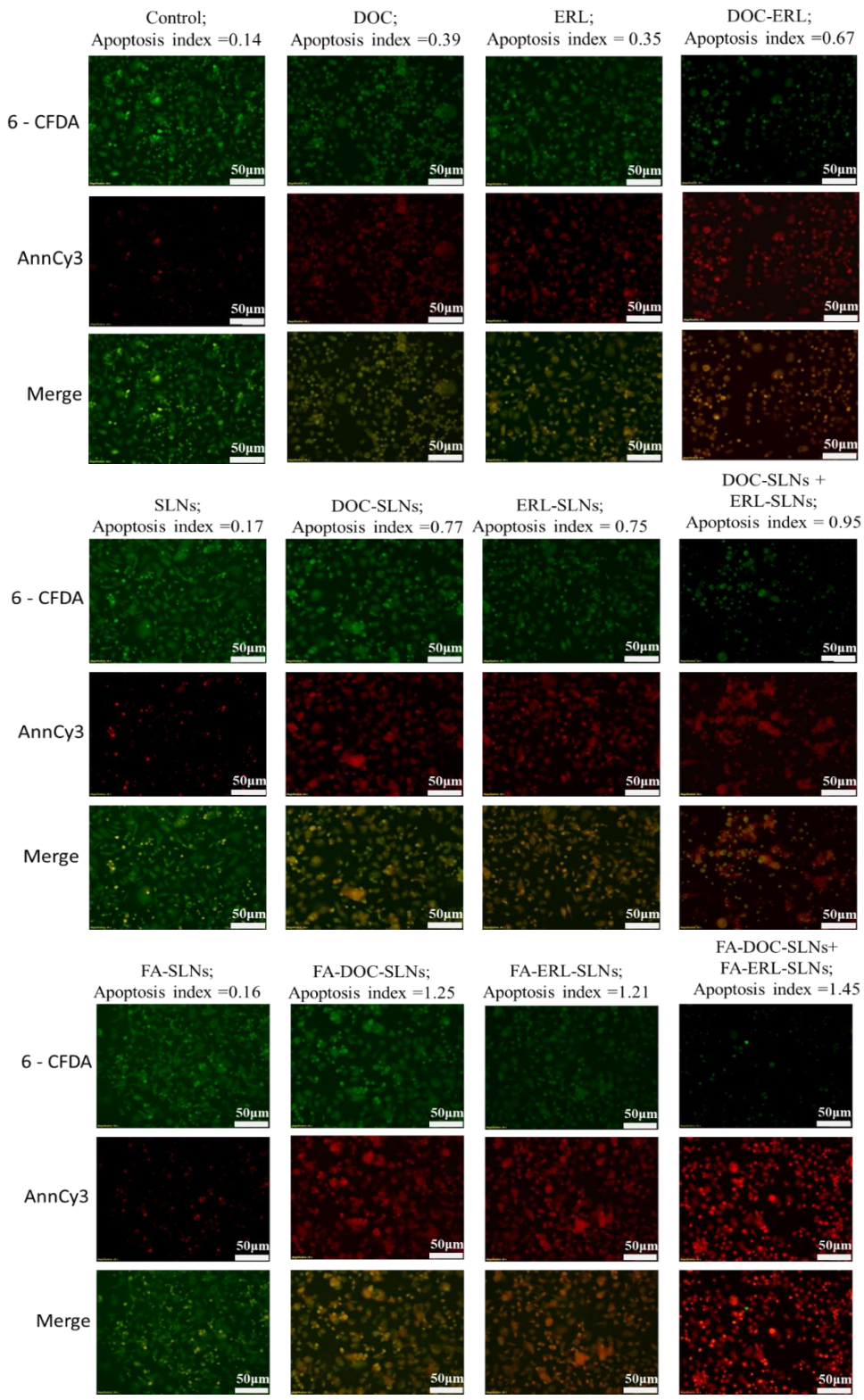

Figure 4. 31: Annexin V–Cy3 staining for detecting apoptosis in 4T1 cells by different SLNs dispersions

Upon apoptosis, the cell membrane gets disrupted, causing the exposure of the phosphatidylserine on the outer leaflet, which usually remains at the inner leaflet of the plasma membrane in healthy cells. The Annexin V–Cy3 binds to phosphatidylserine present in the outer leaflet of the cell's plasma membrane, starting the apoptotic process. The binding is observed as red fluorescence. On the contrary, 6–CFDA is used to measure viability. When this non–fluorescent compound enters living cells, esterases present hydrolyze it, producing the fluorescent compound, 6–carboxyfluorescein (6–CF). This appears as green fluorescence. FA–SLNs combinations exhibited strong red fluorescence, indicating increased binding of Annexin V–Cy3 with phosphatidylserine of the apoptotic cells

4.3.5.7. Wound healing assay

As can be seen in figure 4. 32(A), and 4. 33(A), at t=24 h, there is a complete closure of the wound in the control group, while the wound remained intact even after 24 h in FA–SLNs combination. Additionally, the rate of wound closure was significantly reduced in FA–SLNs combination compared to SLNs, and free drugs at 24 h post treatment (Figure 4. 32(B), and 4. 33(B)).

4.3.5.8. Transwell migration assay

Cell migration is one of the key characteristics of the progression of TNBC. The transwell migration assay revealed that the number of cells migrated was remarkably reduced in FA–SLNs combination, as compared to SLNs, and free drugs (Figure 4. 34(I), and 4. 35(I)). This is found to be consistent with the significantly reduced number of cells migrated through the transwell chamber when treated with FA–SLNs combination (Figure 4. 34(II), and 4. 35(II)).

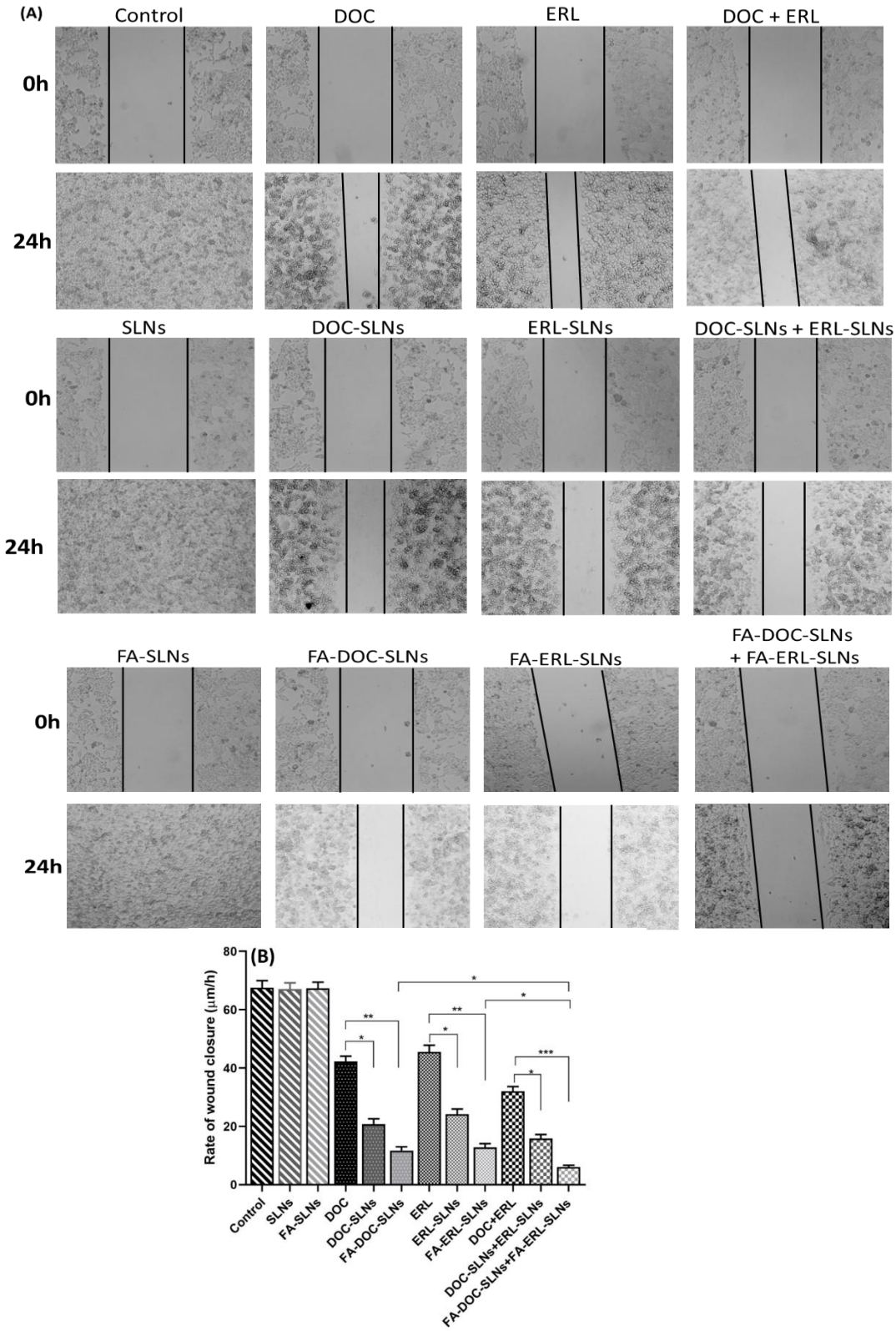

Figure 4. 32: (A) Photographs demonstrating the wound closing efficacy of various treatments in MDA–MB–231 cells, at 0 h, and 24 h. Photographs were taken at 10x magnification. (B) The rate of wound closure (µm/h) was measured for different treatments. Data are presented as mean±SD (n=3). Statistical analysis was executed using one–way ANOVA and the Tukey P test with multiple comparisons. The level of significance was recorded as *p<0.05, **p<0.01, and ***p<0.001

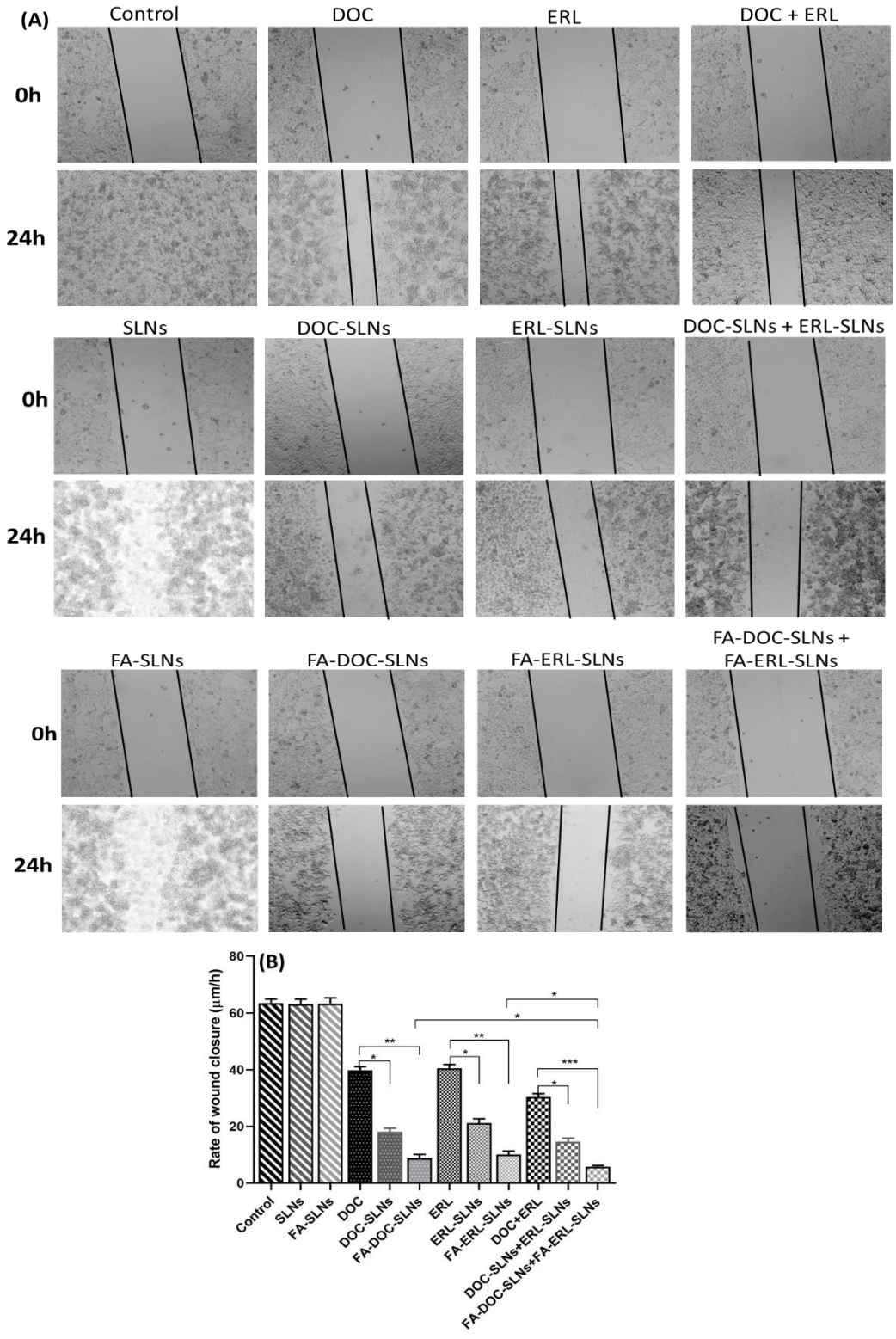

Figure 4. 33: (A) Photographs demonstrating the wound closing efficacy of various treatments in 4T1 cells, at 0 h, and 24 h. Photographs were taken at 10x magnification. (B) The rate of wound closure (µm/h) was measured for different treatments. Data are presented as mean±SD (n=3). Statistical analysis was executed using one–way ANOVA and the Tukey P test with multiple comparisons. The level of significance was recorded as *p<0.05, **p<0.01, and ***p<0.001

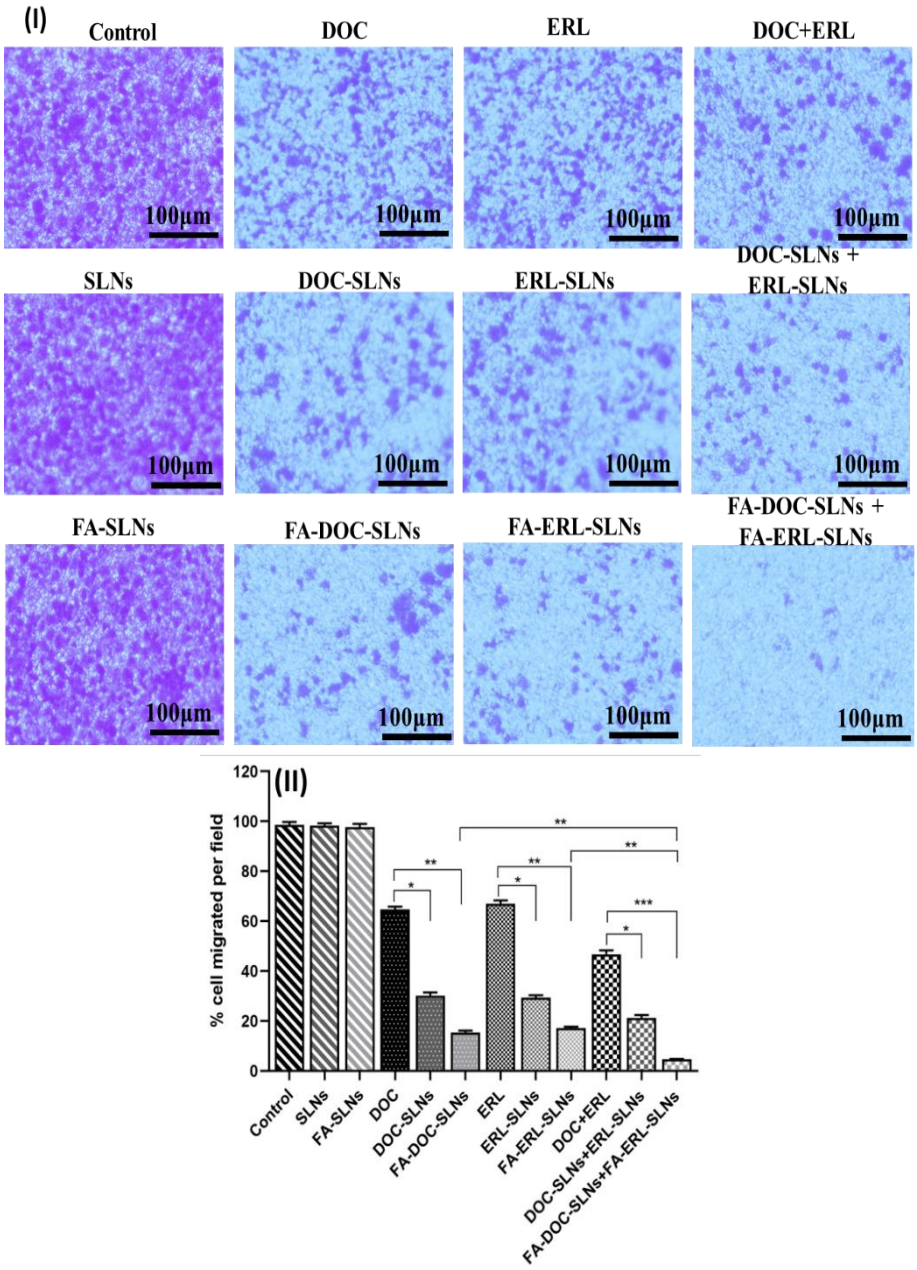

Figure 4. 34: (I) Effect of different treatments on the migration of MDA–MB–231 cells through the transwell chamber. (II) Quantitative analysis of transwell migration assay. Data are presented as mean±SD (n=3). Statistical analysis was executed utilizing one–way ANOVA, followed by the Tukey post hoc test for multiple comparisons. The significance levels were represented as follows: *p<0.05, **p<0.01, and ***p<0.001

Metastasis is one of the characteristics of TNBC, where the cells metastasize through the basement membrane and vasculature into other organs. Wound healing assay and transwell migration assay are widely used to analyze cell migration *in vitro*. Upon treatment with the combination of FA–SLNs, it was observed that the rate of wound closure, and percentage of cells migrated per field were reduced significantly, attributed to increased cellular uptake

and accumulation of the dual nanoformulations, accompanied by enhanced targeting by FA. A similar finding was procured by Kumari *et al.,* 2021 [140].

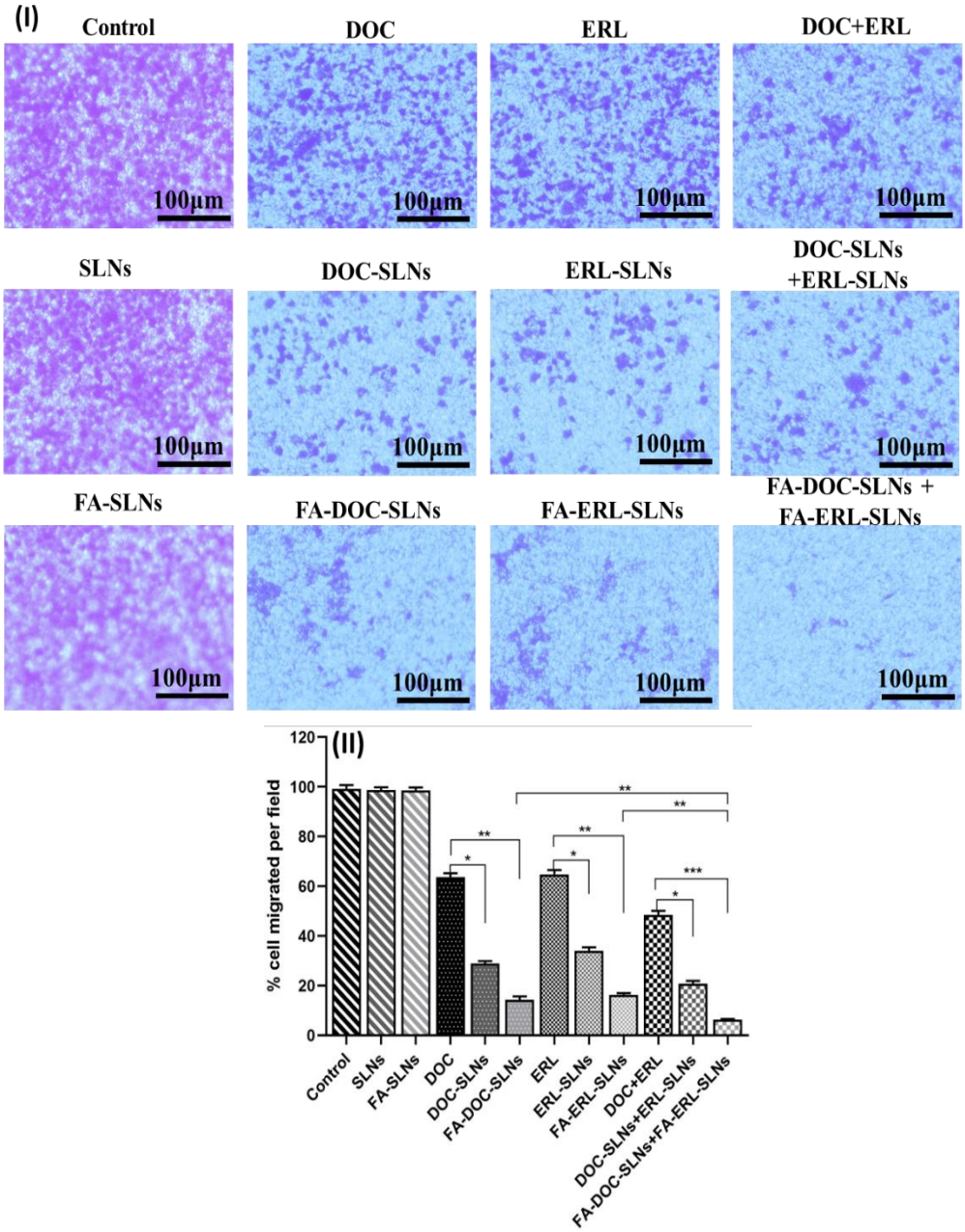

Figure 4. 35: (I) Effect of different treatments on the migration of 4T1 cells through the transwell chamber. (II) Quantitative analysis of transwell migration assay. Data are presented as mean±SD (n=3). Statistical analysis was executed utilizing one–way ANOVA, followed by the Tukey post hoc test for multiple comparisons. The significance levels were represented as follows: *p<0.05, **p<0.01, and ***p<0.001

4.3.6. *In vivo* anticancer studies

4.3.6.1. Pharmacokinetic study

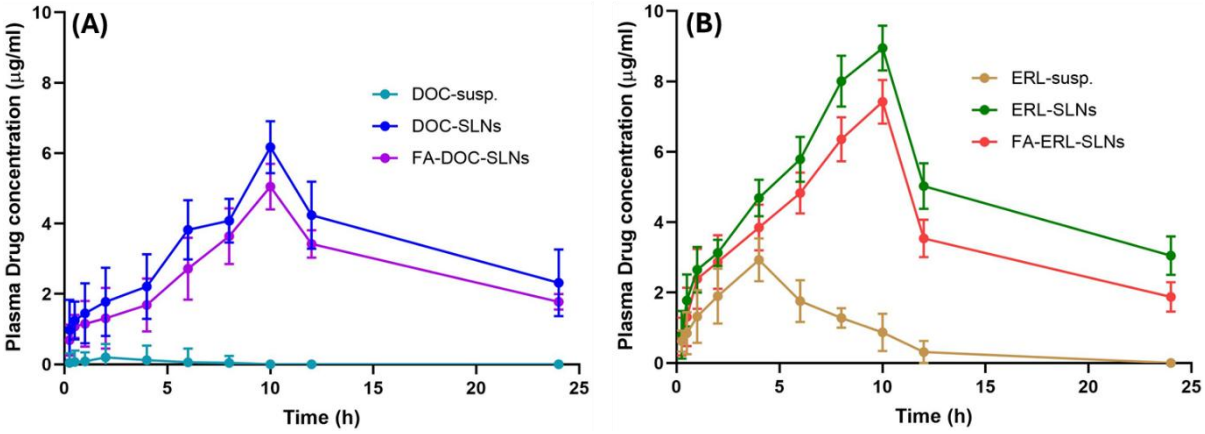

Figure 4. 36: Pharmacokinetic profile of DOC (A) and ERL (B) as suspensions, and their corresponding loaded SLNs and FA–SLNs after oral administration. DOC and ERL were administered equivalent to 10 mg/kg and 30 mg/kg respectively. 'susp' indicates suspension. Data are presented as mean±SD (n=5).

Figure 4. 36 showed the concentration of DOC, and ERL in rat plasma as a function of time after administration of respective suspension, SLNs, and FA–SLNs. The corresponding pharmacokinetic parameters are shown in table 4. 16.

Table 4. 16: Pharmacokinetic parameters of different formulations after oral administration in rats

Pharmacokinetic parameters	Formulations					
	DOC susp.	DOC–SLNs	FA–DOC–SLNs	ERL susp.	ERL–SLNs	FA–ERL–SLNs
T1/2 (h)	1.64± 0.40	11.65± 0.23**	10.27± 0.16*	2.67± 0.60	10.73± 0.28**	8.43± 0.33**
Tmax (h)	2	10**	10**	4	10**	10 **
Cmax (µg/ml)	0.20± 0.06	6.17± 0.54**	5.05± 0.27*	2.93± 0.15	8.95± 0.68**	7.42± 0.43**
AUC_{0-t} (µg/ml*h)	0.85± 0.04	70.63± 2.07**	64.23± 1.84**	18.30± 0.56	115.94± 2.42**	87.76± 1.48**
MRT_{0-t} (h)	3.72± 0.59	20.58± 0.51**	19.62± 0.68**	5.74± 0.35	19.31± 1.55**	15.77± 0.72**
CL/F ((mg/kg)/(µg/ml)/h))	23.24± 0.27	0.17± 0.08**	0.22± 0.16**	2.56± 0.21	0.31± 0.05**	0.45± 0.08**
Fr	-	83.06± 3.14	75.56± 1.45	-	6.33± 1.23	4.79± 1.16

Values are represented as Mean±SD, n=5. Statistical analysis was performed by one–way ANOVA followed by the Tukey P test with multiple comparisons and the level of significance *p<0.05 and **p<0.01 with respect to DOC susp., and ERL susp. Cmax: peak plasma concentration, Tmax: time to reach peak plasma concentration, AUC0−t: area under the plasma drug concentration−time curve from time 0 to 24 h, t1/2:

elimination half-life, MRT0−*t*: mean residence time from time 0−24 h, CL/F: apparent systemic clearance following an oral administration, and Fr: Relative bioavailability.

The bioavailability of drugs from SLNs, and FA–SLNs was evaluated to analyze the effect of the lipid matrix and surface functionalization over the circulation time and the plasma drug release profile. The maximum plasma drug concentration was seen in about 10 h for SLNs and FA–SLNs respectively and a decrease in drugs was noted at the end of 24 h after oral administration. The results inferred that the drugs are being released from the lipid matrix in a sustained manner as achieved by curbing the drug–diffusion, and increasing the mean residence time (MRT) of SLNs, and FA–SLNs (~5–fold) in circulation, as compared to pure drugs. It was further observed that the plasma concentration of drugs from FA–SLNs was slightly less than non–targeted SLNs due to the distribution of FA–SLNs in sites where folate receptors are overexpressed.

4.3.6.2. Quantitative biodistribution study

Further, to evaluate the biodistribution profile of the oral SLNs, the concentration of DOC, and ERL was analyzed in different organs including the brain, lungs, heart, spleen, kidneys, and liver (Figure 4. 37). The concentration of drugs in kidney, lungs, and liver was found to be increased after 12 h of oral administration of suspension, compared to SLNs, and FA–SLNs (Figure 4. 38).

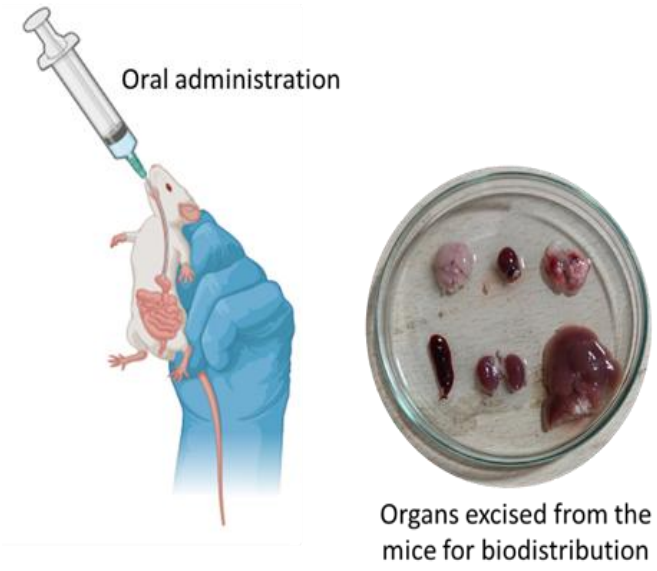

Figure 4. 37: The design for biodistribution study

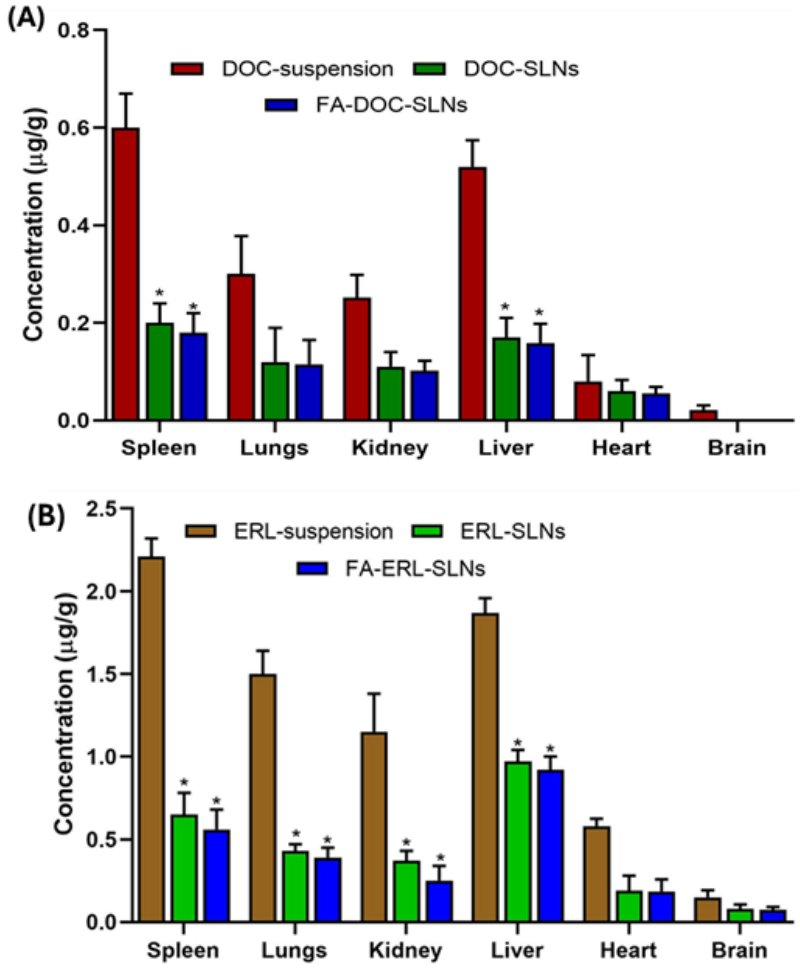

Figure 4. 38: Organs distribution profile of (A) DOC–loaded treatments, and (B) ERL–loaded treatments after oral administration in female Balb/c mice at an oral dose of 10 mg/kg for DOC, and 30 mg/kg for ERL. Data are presented as mean±SD (n=3). Statistical analysis was executed using one–way ANOVA and the Tukey P test with multiple comparisons. The level of significance was recorded as *p<0.05, and **p<0.01 with respect to DOC suspension and ERL suspension.

A higher amount of free drugs accumulated in the kidney and liver is suggestive of clearance of drug substances. However, the concentration of drugs from SLNs, and FA–SLNs was found less in the stated organs justifying the EPR in clamping the entry of SLNs in normal tissues and their increased prevalence to systemic circulation.

4.3.6.3. *In vivo* anticancer efficacy study

As shown figure 4. 39, the concurrent use of DOC and ERL–loaded FA–SLNs achieved unrestricted success in tumor growth inhibition, with improved tumor regression when compared to the efficacy of SLNs, and the control group. The FA–SLNs combination exhibited 1.5– and 2.5–times smaller tumor volume than that observed with the combination of SLNs and drugs, respectively. Similarly, FA–SLNs combination exhibited reduced tumor weight, compared to SLNs combination and control.

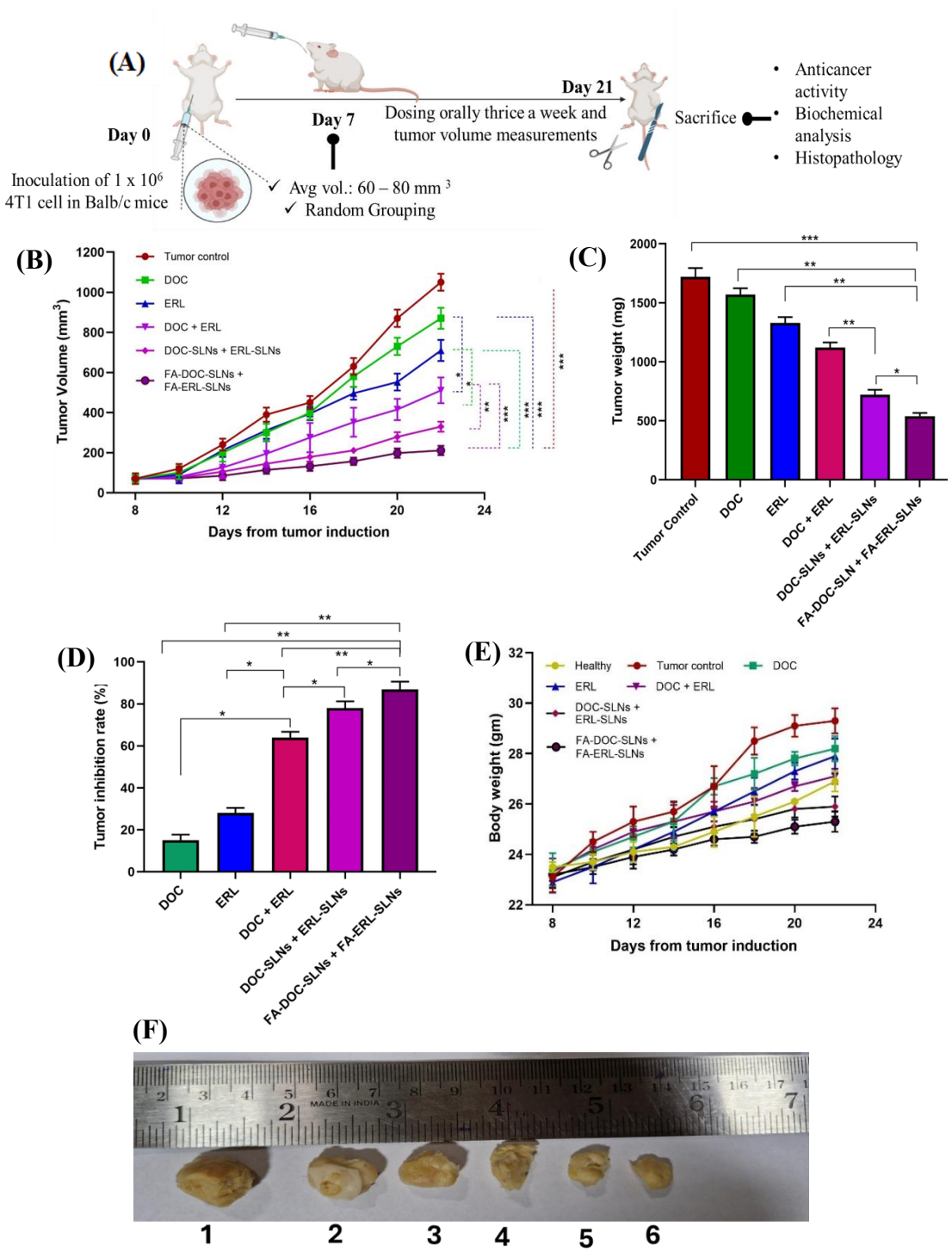

Figure 4. 39: *In vivo* anticancer efficacy of different SLNs in 4T1–induced TNBC in female Balb/c mice: (A) Illustration of the design for the *in vivo* anticancer study. Tumor regression analysis representing: (B) tumor volume in different treatment groups with respect to time, (C) tumor weight, (D) percent tumor growth inhibition, (E) body weight of the tumor–bearing mice. (F) Representative images of tumors from various groups: (**1**) control, (**2**) DOC, (**3**) ERL, (**4**) DOC + ERL, (**5**) DOC–SLNs + ERL–SLNs, and (**6**) FA–DOC–SLNs + FA–ERL–SLNs. Data are presented as mean±SD (n=5). One–way ANOVA was employed for establishing the statistical analysis followed by the Tukey P test with multiple comparisons. The level of significance recorded as *p<0.05, **p<0.01, and ***p<0.001

4.3.6.4. Hematological, biochemical, and histopathological study

Hematological markers are crucial for cancer diagnosis and cancer treatment. Red Blood Corpuscles (RBCs), Haemoglobin (HB), Haematocrit (HCT), and lymphocyte levels were found to be significantly decreased in tumor control, compared to the healthy group, whose levels have been improved when treated with the combination of FA–SLNs, compared to the combination of SLNs, and free drugs (Figure 4. 40A, D, E, and F). Conversely, compared to the healthy group, elevated levels of White Blood Corpuscles (WBCs), and platelets, were observed in tumor control groups. In FA–SLNs combination, the levels of platelets, WBCs, and neutrophils were significantly reverted to normal levels, compared to non–conjugated SLNs, and free drugs (Figure 4. 40B, and C).

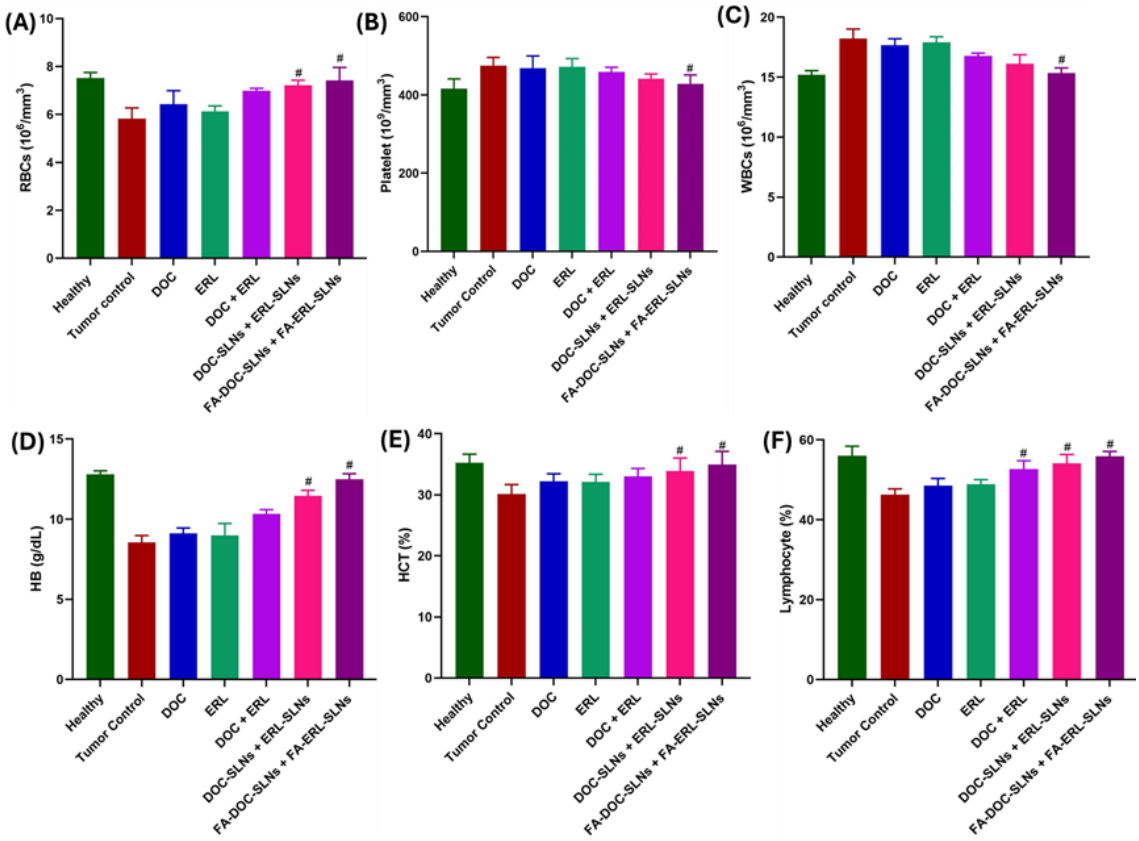

Figure 4. 40: Representative bar diagram indicating hematological profile: (A) RBCs, (B) WBCs, (C) platelet, (D) hemoglobin (HB), (E) Haematocrit (HCT), and (F) lymphocyte in different groups post-treatment. Data are presented as mean±SD (n=5). One–way ANOVA was employed for establishing the statistical analysis followed by the Tukey P test with multiple comparisons. The level of significance was recorded as #$p<0.05$, as compared to the tumor control group

The *in vivo* toxicity of the SLNs dispersions was evaluated by analyzing the functional liver parameters (ALT, AST, and ALB), and kidney parameters (urea, and creatinine) in healthy, tumor control, and treated groups (Figure 4. 41). Results indicated that there was ~ 1.5–fold

increase in AST for the tumor-induced group (205.77±3.12 U/L), compared to healthy group (126.77±3.35 U/L), and a significant decrease for the animals treated with the combination of FA-SLNs (138.62±2.45 U/L). A comparable trend was observed in the levels of ALT. On the contrary, there was a ~1.5–fold decrease in ALB level in the tumor control group (3.04±0.20 g/dL), compared to the healthy group (4.56±0.18 g/dL), which then got elevated and close to normal, when treated with the FA–SLNs combination (3.78±0.12 g/dL). Similarly, the level of urea and creatinine was increased in tumor control groups, compared to healthy groups, which were then significantly reduced on treatment with FA–SLNs combination, compared SLNs combination and pure drugs.

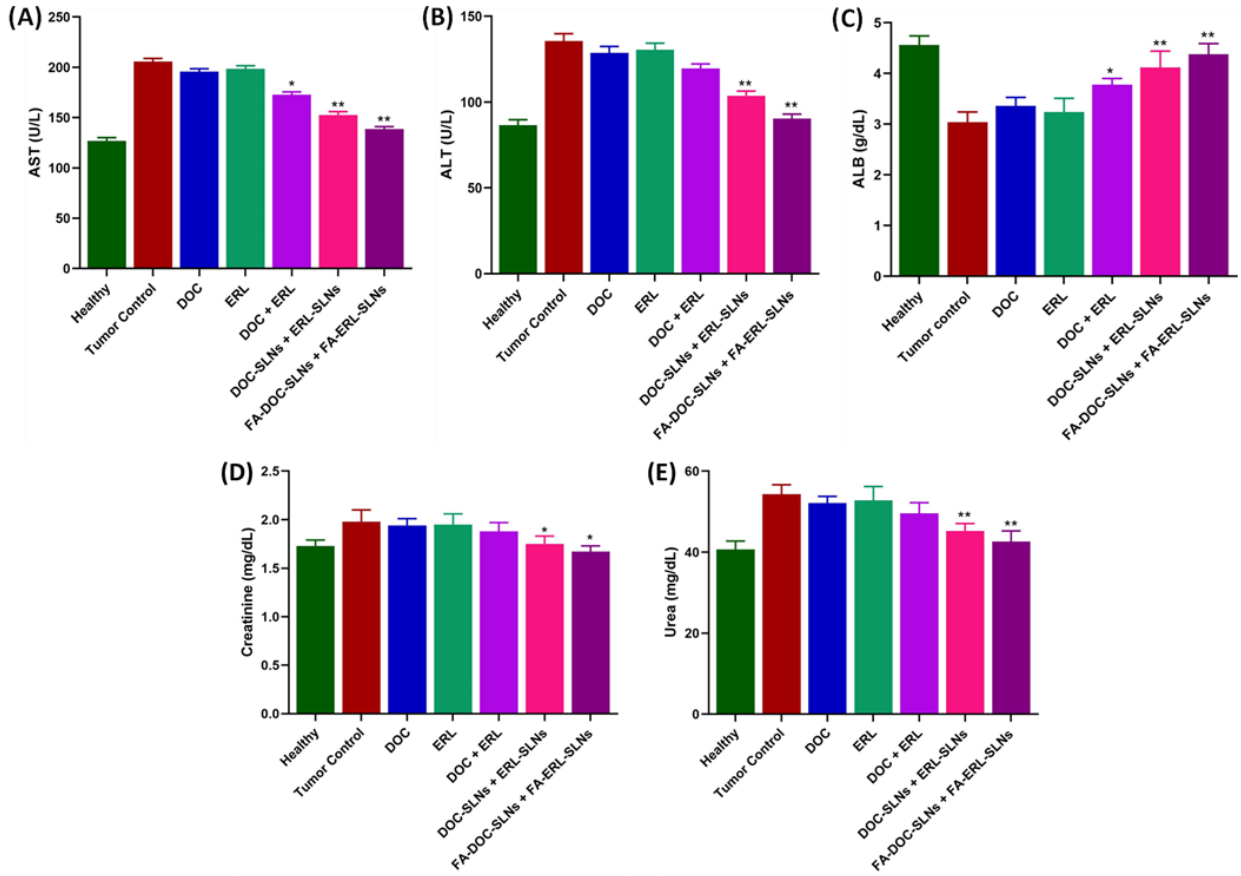

Figure 4. 41: Illustration of the assessment of biochemical parameters in plasma after oral administration of different formulations including (A) AST, (B) ALT, (C) ALB, (D) creatinine, and (E) urea. Data are presented as mean±SD (n=5). Statistical one–way ANOVA was employed for establishing the statistical analysis followed by the Tukey P test with multiple comparisons The significance levels are indicated as *p<0.05, and **p<0.01, on compared with the tumor control group.

All H&E–stained heart, lung, liver, spleen, and kidney sections from the experimental group were evaluated histologically (Figure 4. 42). In the DOC treatment group, metastatic nodules in lungs (green arrow), ballooning degeneration of hepatocytes (red arrows), and glomerular

atrophy (blue arrow) were observed. Similarly, in the ERL treatment group, cardiomyolysis (black arrow), ballooning degeneration of hepatocytes (red arrows), and renal peritubular congestion (maroon arrow) were seen. The histopathological micrographs from the spleen samples were normal without any alterations for all the treatment groups. The results further revealed that no major histological changes in the indicated organs were observed for the combination of FA–SLNs suggesting the site-targeting nature of FA–conjugated SLNs with reduced systemic toxicity, compared to naïve drugs.

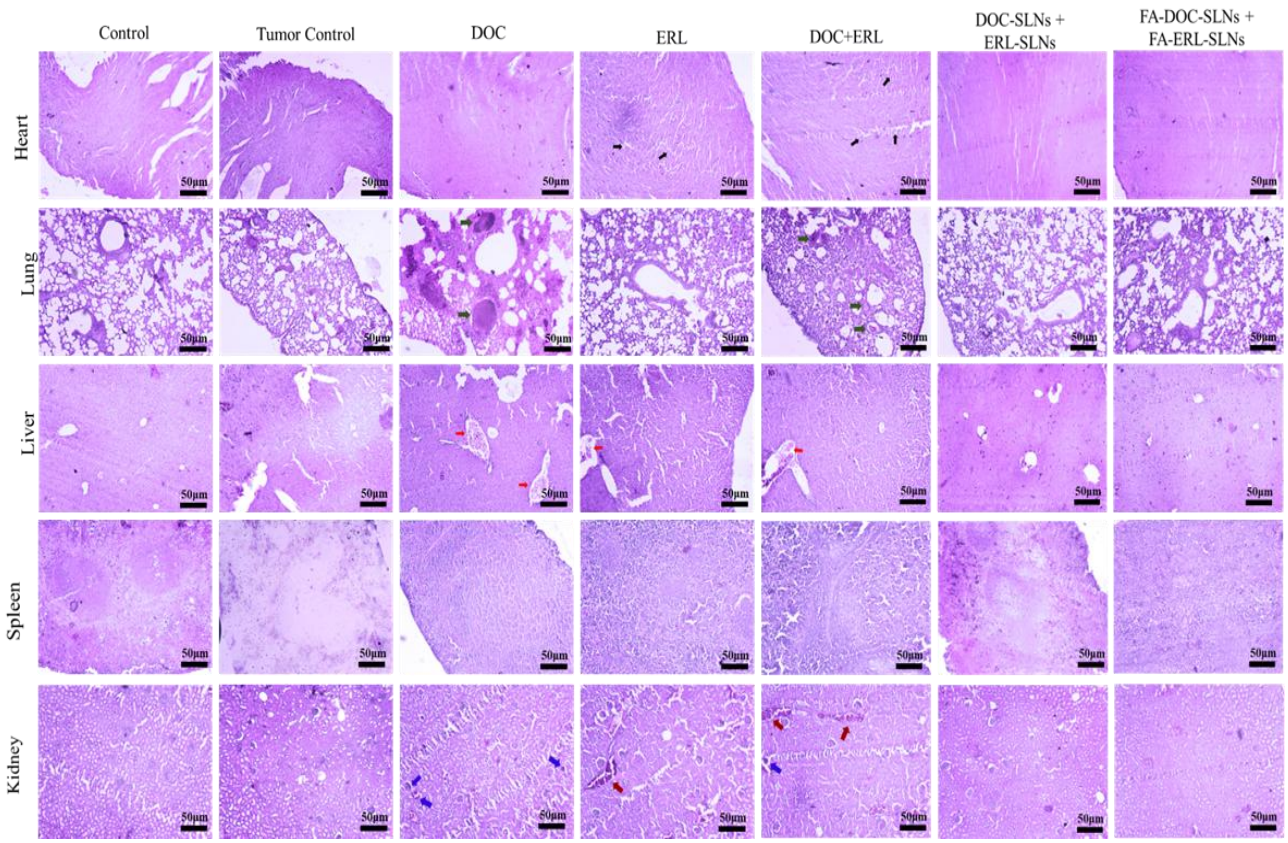

Figure 4. 42: Histopathology of different vital organs was performed by H&E staining; organs were isolated from tumor–bearing mice after the treatment

The administration of FA–SLNs combination demonstrated a significant inhibition of tumor volume and tumor weight compared to other treatment groups ($p < 0.001$). The enhanced *in vivo* antitumor efficacy of FA–SLNs is correlated with better cellular uptake, cell cytotoxicity, and active targeting to the TNBC site. The overexpressed folate receptors at the tumor specifically bind to the FA anchored on the SLNs surface, resulting in increased deposition of the drugs in the target site with improved therapeutic efficacy. Moreover, no major changes were observed in the body weight mice for all groups, indicating the absence of acute toxicity. The liver and kidney are crucial for the metabolic transformation of drugs.

Plasma levels of various liver enzymes like ALT, AST, and ALB, and serum levels of creatinine and urea are considered useful markers for hepatotoxicity and nephrotoxicity respectively. Our results demonstrated the non–hepatotoxic and non–nephrotoxic properties of FA–SLNs combination, as they restored the levels of ALT, AST, ALB, creatinine, and urea to normal range, indicating its increased targeting in the tumor site and bypassing its biodistribution to non–diseased site, thus minimizing the toxicity of the free drugs to healthy cells. WBCs and platelet levels were increased in inflammation and diseased conditions. In the same context, the RBCs become susceptible to toxicity and oxidative stress in TNBC. Like that of the biochemical study, the FA conjugated combination SLNs proved to be the non–haematotoxin also. Similar results were obtained by Askar *et al.,* 2022 [141]. Drug–related toxicity to vital organs was further analyzed using H&E staining. Free DOC resulted in tissue damage to the liver, lungs, and kidneys. The free DOC exhibited cellular swelling of hepatocytes, and tumor nodules in lungs. Cardiac H&E of free ERL demonstrated disrupted cardiac muscle fibers, along with hepatotoxicity and nephrotoxicity. No such disruption or sign of toxicity was observed in animals treated with FA–conjugated combination SLNs, suggesting the competence of FA–SLNs due to increased targeting and accumulation of drugs at the TNBC cells. The fabrication of a delivery system that reduces organ damage and enhances anticancer efficacy has great implications [142].

4.4. Conclusion

The study concluded that an augmented synergistic ratio between DOC and ERL was established from the synergy analysis at a 1:3 molar ratio by determining the combination index, which was found to be 0.35 from MDA–MB–231, and 0.37 for 4T1. The DOC and ERL–loaded SLNs were successfully developed using high–shear homogenizer and probe sonication method and further optimized using QbD approach. The QbD approach includes PBD as a screening model, and BBD as an optimizing model. The optimized SLNs were then surface functionalized using folic acid (FA–SLNs) as the targeting ligand. The developed nanoformulations were characterized, where PS, PDI, ZP, % EE, and % DL were found to be <200nm, <0.35, negative surface charge, ~80 %, and ~4 % respectively. Further, TEM and AFM revealed the spherical morphology of the developed nanoformulations. The *in vitro* release study revealed that the developed nanoformulations ensured low drug release in gastric fluid (~10 %), with the majority being released in circulation, and a small amount released on physiological intestinal medium, leaving around 10–15 % of drugs to be delivered on cancer site by FA functionalization. *In vitro* digestion indicated the stability of

FA–SLNs in intestinal pH conditions, as compared to SLNs. Moreover, the combination of FA–SLNs exhibited increased *in vitro* cytotoxicity, as compared to SLNs, and free drugs, with increased cellular uptake, causing enhanced apoptosis, as justified by MMP assay, ROS assay, and annexin V apoptosis assay. Further, the FA–SLNs revealed their remarkably enhanced anti–metastatic property against TNBC cells, compared to SLNs, and free drugs, as demonstrated by wound healing assay and migration assay. The pharmacokinetic results demonstrated an improved performance of FA–SLNs, and SLNs over free drugs. Further, from the biodistribution study, it was inferred that free drugs were preferentially accumulated in the liver, and kidney, with less accumulation observed for FA–SLNs, and SLNs in all the organs excised due to their greater prevalence in the systemic circulation. Despite the quantitative biodistribution studies were conducted in healthy Balb/c mice, the observations disclosed the efficiency of FA–SLNs, and SLNs in bypassing normal tissues. Furthermore, *in vivo* antitumorigenic activity in 4T1 tumor–induced Balb/c mouse model displayed the potency of FA–SLNs combination in killing tumor cells and significantly suppressing the tumor growth following oral administration without any detectable side effects, as revealed by hematological, biochemical, and histopathology studies.

In conclusion, the present study exhibited that surface functionalization of SLNs with FA improved the pharmaceutical attributes of the drugs, along with sustained and ratiometric drug release, tumor–specific targeting, and increased anticancer efficacy, and may be considered the encouraging platforms for the delivery of diverse drugs in the treatment of TNBC.